

**University of Alberta**

Effects of manufacturing method on surface  
mineralization of bioactive glasses

by

Hamidreza Pirayesh

A thesis submitted to the Faculty of Graduate Studies and Research  
in partial fulfillment of the requirements for the degree of

Master of Science

in

Materials Engineering

Chemical and Materials department

©Hamidreza Pirayesh

Fall 2010

Edmonton, Alberta

Permission is hereby granted to the University of Alberta Libraries to reproduce single copies of this thesis and to lend or sell such copies for private, scholarly or scientific research purposes only. Where the thesis is converted to, or otherwise made available in digital form, the University of Alberta will advise potential users of the thesis of these terms.

The author reserves all other publication and other rights in association with the copyright in the thesis and, except as herein before provided, neither the thesis nor any substantial portion thereof may be printed or otherwise reproduced in any material form whatsoever without the author's prior written permission.

## **Examining Committee:**

Dr. John A. Nychka, Chemical and Materials engineering (Supervisor)

Dr. Dave Mitlin, Chemical and Materials engineering

Dr. Mark McDermott, Chemistry

## **Abstract**

Amorphous bioactive glass powders are used as bone-filling materials in many medical applications. Bioactivity is achieved through ion exchange with bodily fluids, leading to surface apatite mineral formation – a necessity for tissue development. Traditional fabrication is by melt-casting and grinding, however sol-gel synthesis is another method which directly produces powders with higher specific surface area and potential for increased ion exchange rates. In this study sol-gel derived powders were manufactured and compared with melt-cast powders to determine the effects of crystallinity, composition, and specific surface area on apatite formation. Powders were immersed in simulated body fluid as a function of time and the evolution of apatite minerals was characterized.

Apatite formation was most significantly affected by powder composition, followed by specific surface area; merely having sodium in the powder was more influential than altering the surface area and/or atomic structure, yet high specific surface area was found to enhance reactions on crystalline powders.

## Acknowledgments

It is often said that it is the journey that is more important than the final destination. After completing my degree, I am at the vantage point to look at both, the journey and people who helped me in this way as well as the destination. Quoting names of people who assisted me in this journey might be the least way I can show my respect to them.

I would like begin by expressing my appreciation to Prof. John A. Nychka who instilled the spirit of adventure and enthusiasm with regard to scientific research. He taught me to perform research not only for what we get, but for how we achieve it. It was such a great honor for me to be guided by him.

I would also like to thank my committee members, Dr. Dave Mitlin and Dr. Mark McDermott for agreeing to review my work and Dr. Anastasia Elias for being the chair of my examining committee.

Many others have contributed to the accomplishment of this work. I would like to acknowledge the Chemical and Materials engineering department and Natural Sciences and Engineering Research Council of Canada for financial support of this research. I am also grateful to Shiraz Merali for assistance with XRD, George Braybrook and De-ann Rollings for SEM and EDX and Wayne Moffat for FTIR, my friends Ali Torabi for ball-milling, Babak Shalchi for helping me on BET tests, Mohammadreza Salehi for particle size distribution and Dr. Nemanja Danilovic for DSC-TGA. Finally, thanks to my research group Jadid Samad and Satadru Kashyap for their help during research and Kasra Nikooyeh for useful notes whilst writing thesis.

## Table of content

List of figures.....	7
List of tables.....	10
1 Introduction:.....	1
1.1 Objectives .....	3
2 Literature review:.....	4
2.1 Bioactivity.....	4
2.2 Cell cycle and effect of HA .....	6
2.3 Interfacial reaction kinetics.....	7
2.4 45S5 composition .....	13
2.5 Manufacturing bioglasses by casting.....	16
2.6 Manufacturing bioglasses by sol-gel method .....	18
2.6.1 Sol-Gel Mechanism .....	20
2.7 Effect of crystallization.....	34
2.8 Preparation of crystalline 45S5 by the sol-gel method .....	38
2.9 In vitro test .....	39
2.10 Summary .....	40
3 Experimental procedure .....	41
Objectives .....	41
Experiments .....	41
Anticipated outcomes.....	41
3.1 Materials .....	42
3.2 In vitro bioactivity testing.....	44
3.3 Characterization .....	45
3.3.1 Particle size distribution (PSDA).....	45
3.3.2 <i>BET</i> .....	46
3.3.3 <i>DSC-TGA</i> .....	47
3.3.4 <i>XRD</i> .....	48
3.3.5 <i>FTIR</i> .....	48
3.3.6 <i>SEM-EDS</i> .....	49

4	Results and discussion .....	51
4.1	Crystallization and stabilization of gel-derived 45S5 .....	51
4.1.1	<i>DSC-TGA</i> .....	51
4.1.2	<i>XRD</i> .....	53
4.1.3	<i>FTIR</i> .....	58
4.1.4	<i>EDS mapping</i> .....	60
4.2	Particle size distribution.....	61
4.2.1	SEM .....	64
4.3	Surface area.....	65
4.3.1	<i>BET</i> .....	65
4.3.2	<i>SEM</i> .....	65
4.4	In vitro test .....	65
4.4.1	XRD .....	67
4.4.2	FTIR.....	72
4.4.3	SEM .....	76
4.4.4	EDS.....	84
5	Conclusions.....	91

## List of figures

Figure 2-1 Effect of age on strength of bone and probability of fracture [3].	5
Figure 2-2 Glass and glass ceramic in clinical use: A. Intervertebral discs, B. Artificial vertebrae C. Spinal spacer, D. Iliac crests, E. Porous spacer, F. Bone filler [6].	6
Figure 2-3 Schematic illustration of cell cycle [1, 5].	7
Figure 2-4 Reaction stages of class A bioactive material with bone [2].	9
Figure 2-5 Schematic illustration of interfacial reaction between bone and implant which result in HA formation [16].	12
Figure 2-6 Compositional dependence (in wt%) of bone and soft tissue bonding bioactive glasses and glass ceramics [1, 3, 4].	14
Figure 2-7 Schematic molecular structure of amorphous 45S5 bioactive glass; showing fast ion exchange of $\text{Na}^+$ with $\text{H}^+$ from body fluid [5].	16
Figure 2-8 Graphical representation of ion distribution, bioglass 45S5 in a, b and c axis [20].	17
Figure 2-9 Particle shape using acidic (left) and basic (right) catalyst.	22
<b>Figure 2-10 Schematic diagram of (A) elasticity and (B) viscosity for on material at sol-gel process, after [31].</b>	25
Figure 2-11 Variation of the gelation time with R ratio, after [30].	25
Figure 2-12 The 2-D models of silica tetrahedra a)ring b)chain, after [31]	26
Figure 2-13 Simulation of hydrolysis, condensation and gelation in the sol-gel method [24].	27
Figure 2-14 a. Polycondensation b. Syneresis c. Coarsening during aging [24].	29
Figure 2-15 Plot of rate of water loss vs. water in the gel [30].	30
Figure 2-16 TEM images of 70S30C a. 24hrs reagent mixing of sol b. dried gel c. stabilized gel [20].	33
Figure 2-17 Schematic illustration of evolution of ion distribution during a. gelation b. drying c. stabilization [20].	34
Figure 2-18 TGA-TDA of 45S5 bioglass [13].	37

Figure 2-19 Effect of temperature on volume of a crystal and a glass cooled with two cooling rates a. slow b. fast [39].	38
Figure 4-1 DSC-TGA of unsterilized 45S5 prepared by sol gel method.	52
Figure 4-2 X-ray diffraction pattern of 45S5 prepared by the sol-gel method as function of stabilization temperature.	55
Figure 4-3 XRD pattern of raw 45S5 stabilized: a. 6 hrs at 600°C b. 18hrs at 500°C and 6 hrs at 500°C. b shows lower intensity of peaks but still formation of combeite could be seen (▼: combeite and ●: nitrate).	57
Figure 4-4 XRD of gel-derived 45S5, a. stabilized at 700°C b. stabilized 12hrs at 550°C for phase separation and then kept at 900°C for 12hrs. Peaks are related to combeite phase.	58
Figure 4-5 FTIR spectra of gel-derived 45S5 with $T_{stab}=800^{\circ}C$ .	59
Figure 4-6 EDS mapping of gel-derived 45S5. Color points are related to elements. Calcium and silicon were not detected in phosphorous rich regions.	61
Figure 4-7 Particle size distribution of a. gel and b. cast derived 45S5 and c. gel-derived 58S.	63
Figure 4-8 SEM micrograph of particle distribution of gel and melt-derived 45S5 powders.	64
Figure 4-9 SEM micrograph of gel-derived and melt-cast 45S5 before immersion in SBF.	66
Figure 4-10 XRD spectra of immersed 45S5 prepared by a. sol-gel and b. casting in SBF as function of time.	69
Figure 4-11 Brief comparison of melt and gel-derived 45S5 hydroxyapatite formation rate. After one day immersion, combeite peaks are not detectable in gel-derived 45S5 and after 18 days both samples show similar amount of apatite formation.	70
Figure 4-12 XRD spectra of gel-derived 58S, immersed in SBF as function of time.	71
Figure 4-13 FTIR spectra for gel and melt derived 45S5 after immersion in SBF for various times.	75

Figure 4-14 Melt-cast 45S5 immersed in SBF for 12 hrs.....	77
Figure 4-15 High porosity structure of gel derived 45S5 after 1 day immersion in SBF. ....	79
Figure 4-16 SEM micrograph of gel derived 45S5 immersed in SBF for 7 days.	80
Figure 4-17 SEM micrograph of gel-derived and melt-cast 45S5 after a. 1 day b. 14 days c. 21 days immersion in simulated body fluid.....	81
Figure 4-18 SEM micrograph of gel-derived 58S after a. 1 day b. 7 days c. 14 days and d. 21 days immersion in SBF.....	82
Figure 4-19 Schematic illustration of the effect of presence of sodium on the morphology of bioglass, HA forms on itself more in 58S than 45S5.	83
Figure 4-20 EDS analysis of melt-cast and gel-derived 45S5.....	86
Figure 4-21 Schematic illustration of the dept of electrons could be detected. Before immersion, interaction volume just detect 45S5 as expected, after 7 days both 45S5 and HA will be detected and finally after 21 days, the thickness of HA will be as thick as interaction volume that only HA could be detected.....	87
Figure 4-22 Schematic illustration of Surface with low roughness which shows less nucleation sites than surface with more roughness.....	90

## List of tables

<b>Table 2-1 Bioactive materials [2, 3].</b> .....	8
Table 2-2 Mechanical properties of bioactive ceramics and human cortical and cancellous bones [6].	35
Table 2-3 [40] .....	40
Table 4-1 Brief explanation of DSC-TGA curve of gel-derived 45S5 .....	52
Table 4-2 Particle size distribution analysis of 45S5 and 58S bioactive glasses..	62
Table 4-3 Correlation of energy peaks achieved by FTIR.....	72
Table 4-4 Absorbance Intensity ratio of P-O bending at $560\text{ cm}^{-1}$ over Si-O bending at $470\text{ cm}^{-1}$ .....	76
Table 4-5 EDS analysis of melt cast powder immersed in SBF for 12 hrs. ....	76
Table 4-6 EDS results of immersed 45S5 prepared by sol-gel method in SBF (mol%).....	85
Table 4-7 EDS results of immersed 45S5 prepared by melt-casting technique in SBF (mol%).....	85

## **List of abbreviations:**

HA: Hydroxyapatite

HCA: Hydroxycarbonate apatite

SBF: Simulated body fluid

DSC: Differential scanning calorimetry

TGA: Thermogravimetric analysis

PSDA: Particle size distribution analysis

SEM: Scanning electron microscopy

EDS: Energy dispersive X-ray analysis

XRD: X-ray diffraction

FTIR: Fourier transform infrared spectroscopy

BET: Brunauer, Emmet and Teller (Specific surface area measurement)

TEM: Transmission electron microscopy

DTA: Differential thermal analysis

# 1 Introduction:

Bioglasses are a group of materials which exhibit high bioactivity and are used successfully for bone-filling in certain medical applications. These materials are made from glasses with high bioactivity. Most of bioglasses contain silicon for network formation and calcium as a network modifier. Bioactive glass 45S5 which includes silicon, calcium, sodium and phosphorous oxides is one of the main bioglasses used widely in medical applications. Although bioglasses show higher bioactivity than other implants such as those made from metal, their poor mechanical properties prohibit their wide use in medical applications. One of the main goals of recent research has been focused on improvement of bioglass mechanical properties. One of the most efficient ways to achieve this, is to crystallize the bioglass to form a glass ceramic. Reports show that although transformation of bioglass to glass ceramic increases mechanical properties, reduces bioactivity. So, trying to develop bioactive glasses with high bioactivity and acceptable mechanical properties is desirable.

Bioglasses are traditionally manufactured by melt casting. In this method primary materials melt and then mix at high temperature in the molten state. Eventually the liquid is quenched to form an amorphous structure at room temperature.

Increasing the rate of reaction with body tissues and reducing the temperature of synthesis were two main reasons of working on sol-gel derived bioglasses instead of cast glasses. This technique has been studied for more than 20 years and shows beneficial properties. Some other advantages of this method are: better homogeneity, better control on composition, less impurity in resultant sample and material in form of powder instead of a bulk monolith.

Many bioactive glasses have been formed by sol-gel method. But since 45S5 becomes crystalline during sol-gel procedure, characterization of gel-

derived 45S5 still needs more study. The presence of sodium as a network modifier improves bioactivity but results in crystallization at low temperatures (~650°C) and makes it impossible to prepare amorphous 45S5 via the sol-gel method.

Although it is believed that crystalline structure alters or degrades the bioactivity of bioglasses, the high surface area of gel-derived glasses could be a saving grace. If the high surface area of the sol-gel powder could overcome the lower bioactivity of crystalline bioglass ceramics, it could be possible to produce a material with satisfactory mechanical properties, high homogeneity, and high bioactivity while using less costly fabrication method than casting.

As mentioned, although the presence of sodium as a network modifier increases bioactivity, it might reduce bioactivity in 45S5 prepared by the sol-gel method because of its effect on combeite formation. Therefore, studying the effect of sodium of gel-derived 45S5 was another goal of this project. For this reason, bioglass with same composition of 45S5 but without sodium oxide was produced by sol-gel method. This bioglass called is 58S, and it displays an amorphous structure after production via sol-gel technique. Bioactivity and apatite formation rate of this glass was studied before, but comparison of it with crystalline gel-derived 45S5 has not been carried out yet.

Three different parameters of a well-known bioactive glass have been studied in this research. Effect of composition (with vs. without sodium), structure (crystalline vs. amorphous) and morphology (rough vs. flat) which can all be affected by the processing method, and play important roles on bioactivity of manufactured biomaterials will be studied in this research.

The dissolution rate of crystalline gel-derived 45S5, amorphous melt-cast 45S5 and amorphous gel-derived 58S in the form of powders with diameters less than 10  $\mu\text{m}$  was tested by immersion in simulated body fluid (SBF) solution for various periods of time. Analysis followed through XRD, SEM, EDX and DSC/TGA and FTIR qualitatively determine interfacial reaction kinetics of samples.

## ***1.1 Objectives***

1. Manufacture and characterization of 45S5 bioactive glass via sol-gel method and.
  - a. Optimize stabilization temperature for gel-derived 45S5
2. Manufacture and characterization of bioglass 58S by sol-gel method.
3. *In vitro* study of manufactured biomaterials by immersion in simulated body fluid.
  - a. Comparing *in vitro* results between melt-cast 45S5, gel-derived 45S5 and gel-derived 58S to understand the effect of powder composition, morphology and structure on apatite composition, morphology and formation rate.

## **2 Literature review:**

Biomaterials are needed to ease pain and restore diseased or damaged parts of the body. As shown in Figure 2-1, increasing the age of humans will reduce the strength and density of bones. This effect is more severe in women because of hormonal changes associated with menopause. Such phenomena result in bone fracture or collapse in the elderly. Using materials that can replace these old and weakened bones whilst having safe function for the remaining years of patients lives is desirable. Different kinds of biomaterials have been use as bone filling alternatives. Metals such as 316L stainless steel and titanium, ceramics such as alumina, hydroxyapatite and bioglasses and polymers such as polyethylene are some of these examples [1-3].

Bioactive glasses were the first generation of materials which provided interfacial bond between implant and hard and soft host tissues. These materials were first prepared by L. L. Hench in 1969 [4]. Bioglasses show better compatibility with the body compared with other external materials such as metal implants due to the possibility of controlling the range of chemical properties and rate of bonding to tissues [4]. They have been widely used since 1985 in clinical applications (e.g. middle ear prostheses and for maintenance of edentulous alveolar ridge) [1, 3, 5]. Figure 2-2 shows some types of bioglass and glass ceramics and their application [6].

### ***2.1 Bioactivity***

L. L. Hench defined a biomaterial “as a material that elicits a specific biological response at the interface of material which results in a formation of a bond between the tissue and that material”. Usually a bioactive material forms a bond with strength equal or more that the original bone, and can be made of metal, glass or ceramic.

The level of bioactivity of a biomaterial can be measured by calculating the time needed for more than 50% of the interface to bond to bone ( $t_{0.5bb}$ ):

$$\text{Bioactivity index, } I_b = 100/t_{0.5bb}$$

It is necessary to impose a 50% bonding criterion since the interface between implant and bone is irregular. The larger the bioactivity index, the higher the bioactivity and solubility of the biomaterial reacted with bone tissue. Materials with a bioactivity index equal to zero are called inert [7].

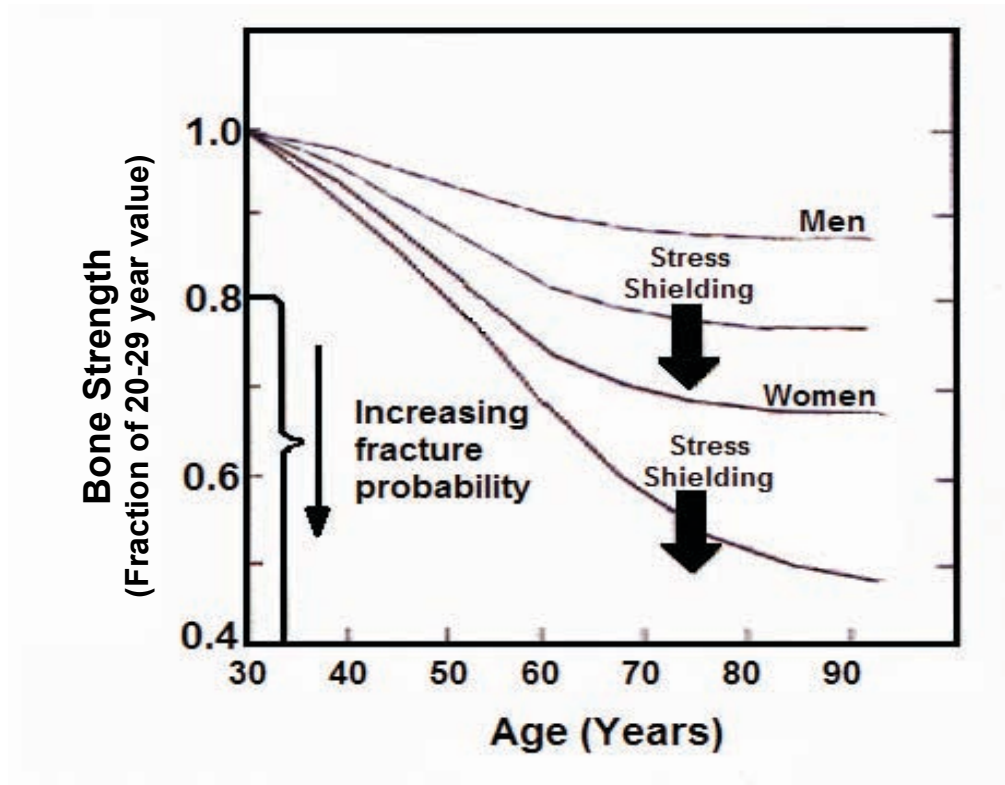
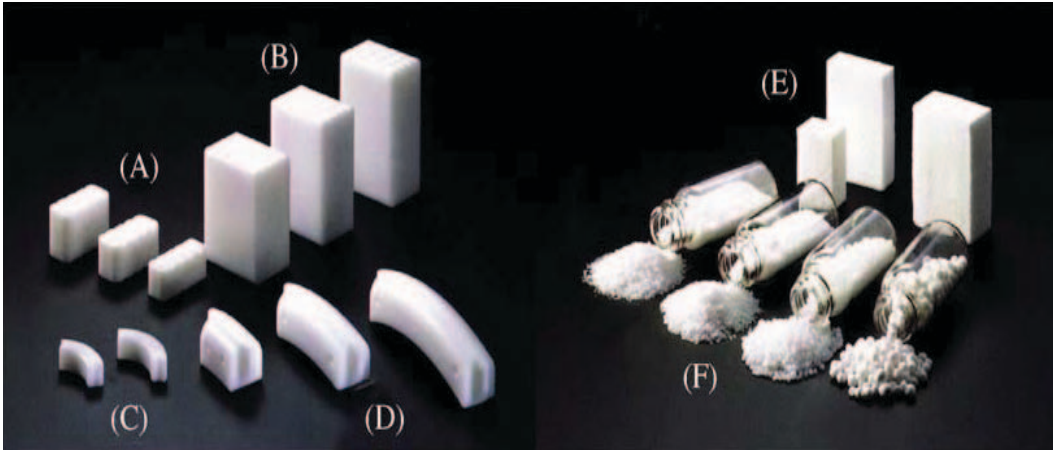


Figure 2-1 Effect of age on strength of bone and probability of fracture [3].



**Figure 2-2 Glass and glass ceramic in clinical use: A. Intervertebral discs, B. Artificial vertebrae C. Spinal spacer, D. Iliac crests, E. Porous spacer, F. Bone filler [6].**

## ***2.2 Cell cycle and effect of HA***

Cell division and its rate is a complicated process which depends on many factors like medium which this procedure is occurred. Figure 2-3 briefly describes cell cycle procedure in body. During different stages of cell division and chromosome nucleation, there are protein inhibitors which act as check points for replication, chromosome condensation and presence of suitable area for this procedure. Bone cells which are capable of dividing are called osteoblasts. Osteocytes are bone cells that are unable to divide after they are entrapped in the bed of mineralised collagenous matrix [1, 5].

Hydroxyapatite (HA) and hydroxycarbonate apatite (HCA) are main minerals which initiate appropriate place for the cell cycle process. Formation of HA or HCA or other types of apatite containing  $F^-$  and  $Cl^-$ , depends of the media of reaction [8]. These minerals form a crystalline layer between implant and collagen which produces an interface for osteoblasts. The chemical bonding of HA layer to collagen creates the strongly bonded interface. Quantitative evolution of interfacial shear strength has shown that the strength of the interfacial bond was equal to or greater than the strength of the host bond. Generally HA, which forms between bone and implant shows higher compressive and bending strength as will briefly be discussed later [1, 3].

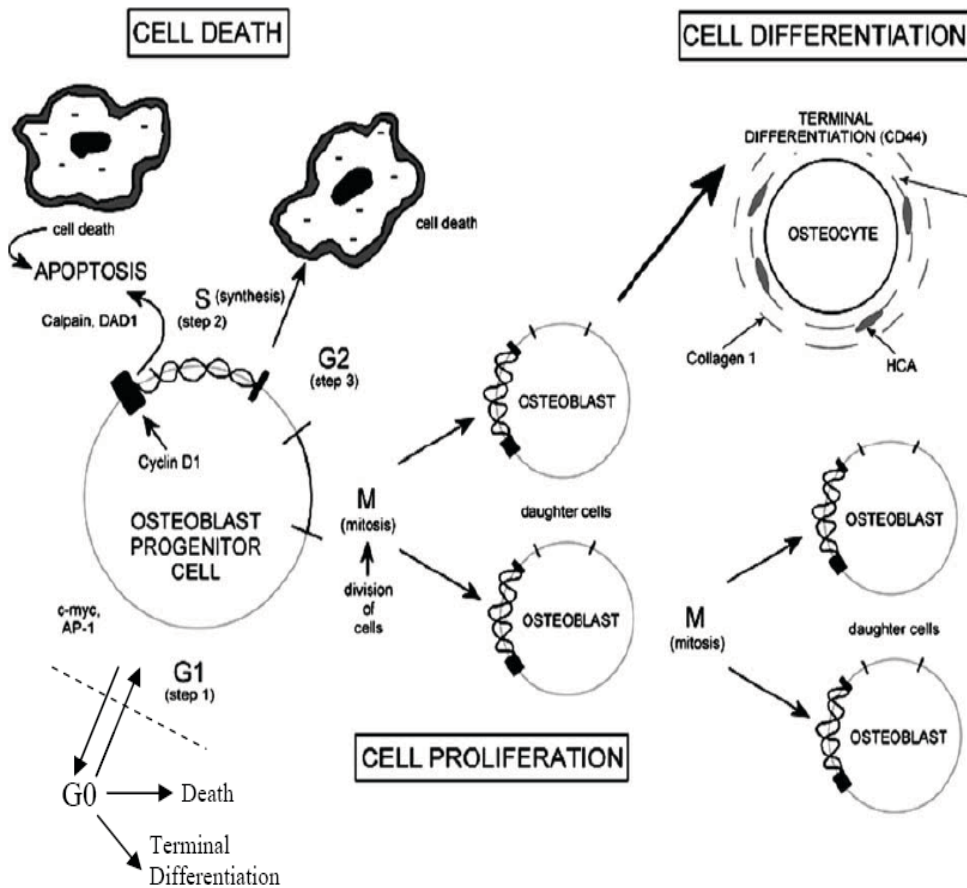


Figure 2-3 Schematic illustration of cell cycle [1, 5].

The rate of HA formation might be a good sign showing bioactivity of an implant, but studies show that this rate cannot be a critical stage of reaction for bone regeneration. Controlled rate of ionic dissolution product release is the main effective phenomenon that shows true bioactivity of a material [1]. Ion release indicates that as hydroxyapatite forms faster, it could be expected that bioactivity be higher, but this rule is not applicable all situations.

### 2.3 Interfacial reaction kinetics

As mentioned before, the main parameter that affects bioactivity is controlled chemical release kinetics. Rapid dissolution rate leads to high

concentration of ions, so they cannot be effective enough. Besides, slow rate of dissolution makes the concentration too low to stimulate cellular proliferation and differentiation. Regarding this explanation, two classes of bioactivity exist. Class A refers to biomaterials which contain both osteoproliferative (proliferation of bone distant from an implantation site) and osteoconductive (growth of the bone along the surface of the material) properties [1, 3]. These materials exhibit  $I_b$  value more than 8. But class B occurs while only osteoconduction happens due to slower interfacial reaction, so only extracellular responses occur on the surface. Class B materials have bioactivity index less than 8, but greater than zero. Table 2-1 shows some characteristics of classes A and B of bioactivity [1-3, 5, 9].

**Table 2-1 Bioactive materials [2, 3].**

<b>Class A</b>	<b>Class B</b>
Osteoproliferative and Osteoconductive	Only osteoconductive
Rapid bonding to bone	Slow bonding to bone
Enhanced bone proliferation	No enhancement of bone proliferation
Bonding to soft connective tissues	No bonding to soft connective tissues

Generally class A bioactive materials show 12 stages of interfacial reaction during insertion in the body. Figure 2-4 briefly illustrates these 12 stages with reaction time. Generally stages 1-5 occur on the material side of the interface (which are most rapid for implants) with the highest level of bioactivity, but stages 6-12 happen on tissue side of interface [2, 9, 10]. The first five stages happen rapidly on the surface of most bioactive glasses because of fast ion exchange of alkali ions with hydrogen ions from body fluid to form Si-OH silanols (stage 1) network dissolution (stage 2) silica-gel polymerization (stage 3) and chemisorption and crystallization of HCA layer (stage 4 and 5). The surface reactions lead to the biochemical adsorption of growth factors (stage 6) and the synchronized sequence of cellular events (stages 7-12) that result in rapid formation of new bone. Generally, the rapid attachment, proliferation and differentiation of osteoblast progenitor cells are the critical steps of new bone

formation [3, 5, 9, 11]. In this research, surface reactions on the material side of interface and during first five stages have been studied. The following stages should usually be studied by using live samples (*in vivo*), but are not the focus herein.

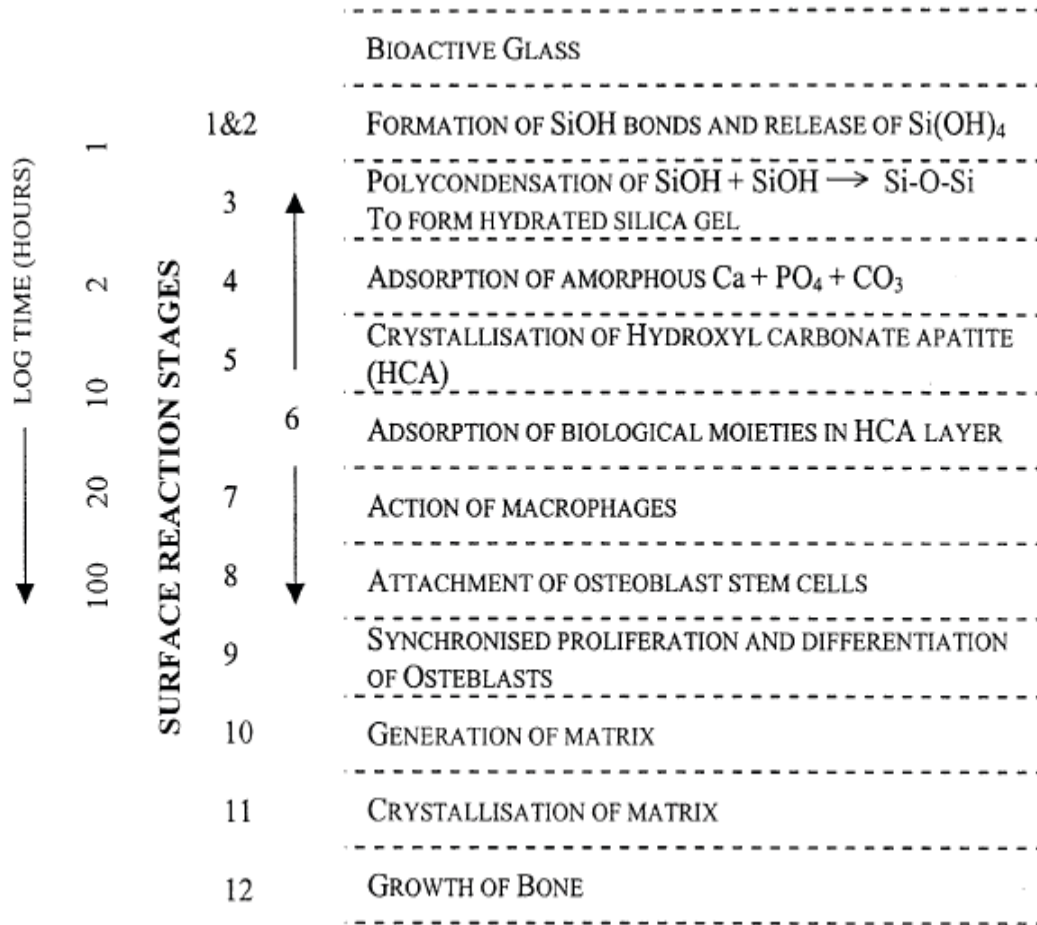


**Figure 2-4 Reaction stages of class A bioactive material with bone [2].**

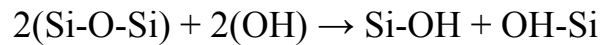
A brief explanation of the primary five stages is that the bioactive glass first dissolves to form a silica gel layer, then amorphous calcium phosphate forms from a hydrated silica gel and finally apatite crystals of HA (which are a prerequisite of bond formation) nucleus and grow from calcium phosphates [2, 10]. Surface reaction stages 1-5 are summarized below:

*Stage 1:* Rapid exchange of Na<sup>+</sup> or K<sup>+</sup> with H<sup>+</sup> or H<sub>3</sub>O<sup>+</sup> from solution:



Stage 1 is usually controlled by diffusion and exhibits a  $t^{-1/2}$  dependence on time. The weak ionic bonding, especially of the alkali ions gives rise to a very rapid ion exchange. Cation exchange at this stage increases the hydroxyl concentration of the solution which leads to attack of the silica glass network producing additional silanol formation and controlled interfacial dissolution [12]. Eventually the pH of solution increases as a result of  $\text{H}^+$  consumption in the solution [7].

*Stage 2:* Cation exchange increases hydroxyl concentration of the solution, which leads to attack of the silica glass network. This stage is related to a loss of soluble  $\text{SiO}_2$  in the form of  $\text{Si}(\text{OH})_4$  in the solution, resulting from breaking Si-O-Si bonds and formation of Si-OH (silanols) in amorphous silica gel formation at the interface:



This stage is usually controlled by interfacial reactions and exhibits linear time dependence [11].

*Stage 3:* SiOH repolymerizes and forms a Si-O network [11]. This Si-O network is depleted in alkaline earth cations:



*Stage 4:*  $\text{Ca}^{+2}$  and  $\text{PO}_4^{-3}$  migrate to the surface through the  $\text{SiO}_2$ -rich layer forming a CaO- $\text{P}_2\text{O}_5$ -rich film on top of  $\text{SiO}_2$ -rich layer followed by growth of amorphous CaO- $\text{P}_2\text{O}_5$ -rich film through incorporation of soluble calcium and phosphate from solution.

*Stage 5:* Incorporation of OH<sup>-</sup> and CO<sub>3</sub><sup>-2</sup> or F<sup>-</sup> anions from solution forms mixed crystalline hydroxyl, carbonate, and fluorapatite layer from the amorphous CaO-P<sub>2</sub>O<sub>5</sub>-rich film. The HA layer formed is equivalent to the extremely small 100-600Å platelets of the mineral phase of normal bone with large surface area [3, 5, 11, 13].

In class B bioglasses, usually the rate of Si ion exchange or network dissolution is low or zero [11].

Figure 2-5 schematically represents five stages for formation of HA or HCA as mentioned above.

The theoretical composition of stoichiometric HA is: Ca<sub>10</sub>(PO<sub>4</sub>)<sub>6</sub>(OH)<sub>2</sub> with a corresponding Ca to P ratio of 1.67 [8, 14-16]. It has been shown that new HA will form not only directly on the surface of silica gel, but also on the surfaces or interfaces of other growing apatite. This indicates that the front of a growing apatite can also become a nucleating site of another [17].

After these five steps, the next seven stages, which lead to formation of bone cells, begin. These stages will be described briefly below [7]:

*Stage 6:* Adsorption and desorption of biological growth factors in HA layer to activate differentiation of stem cells (this stage will continue throughout the process).

*Stage 7:* Action of macrophages to remove debris from the site and allowing cells to occupy the space

*Stage 8:* Attachment of stem cells on the bioactive surface

*Stage 9:* Differentiation of stem cells to form bone growing cells, osteoblasts

*Stage 10:* Generation of extracellular matrix by osteoblasts to form the bone

*Stage 11:* Crystallization of inorganic calcium phosphate matrix to enclose bone cells in a living structure

*Stage 12:* Growth of the bone

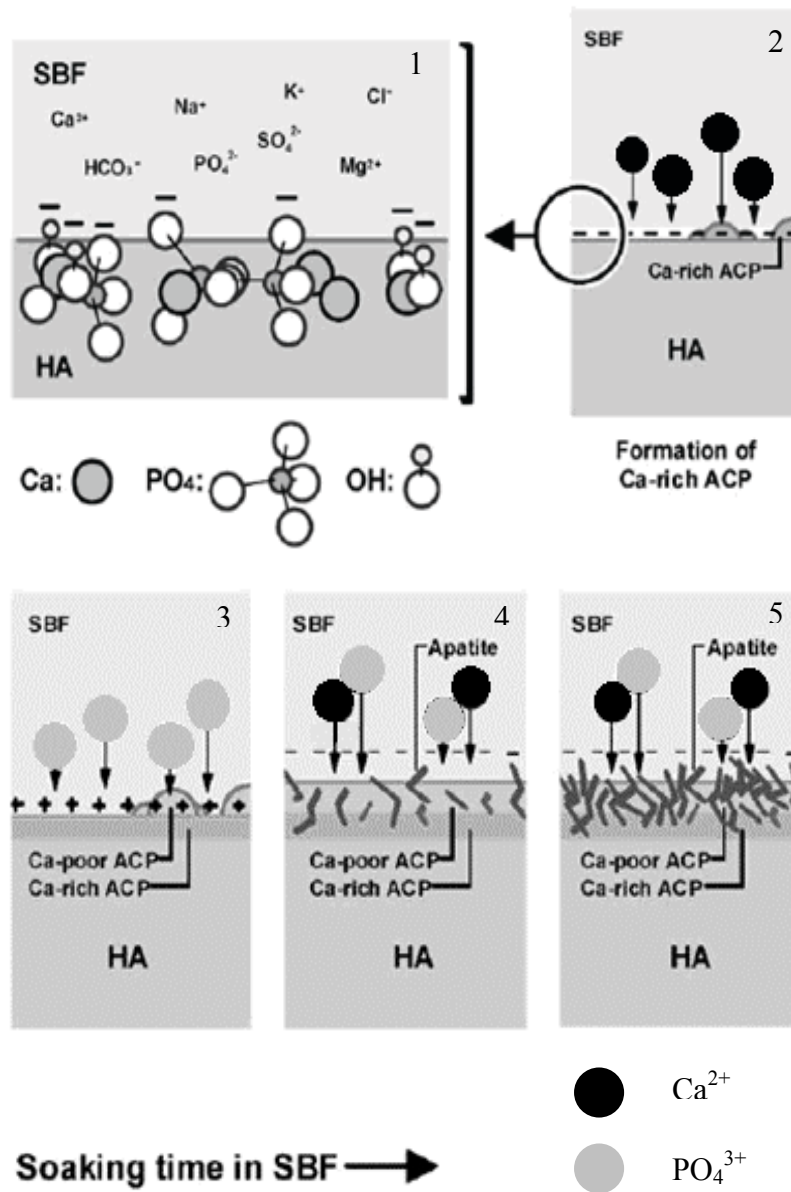
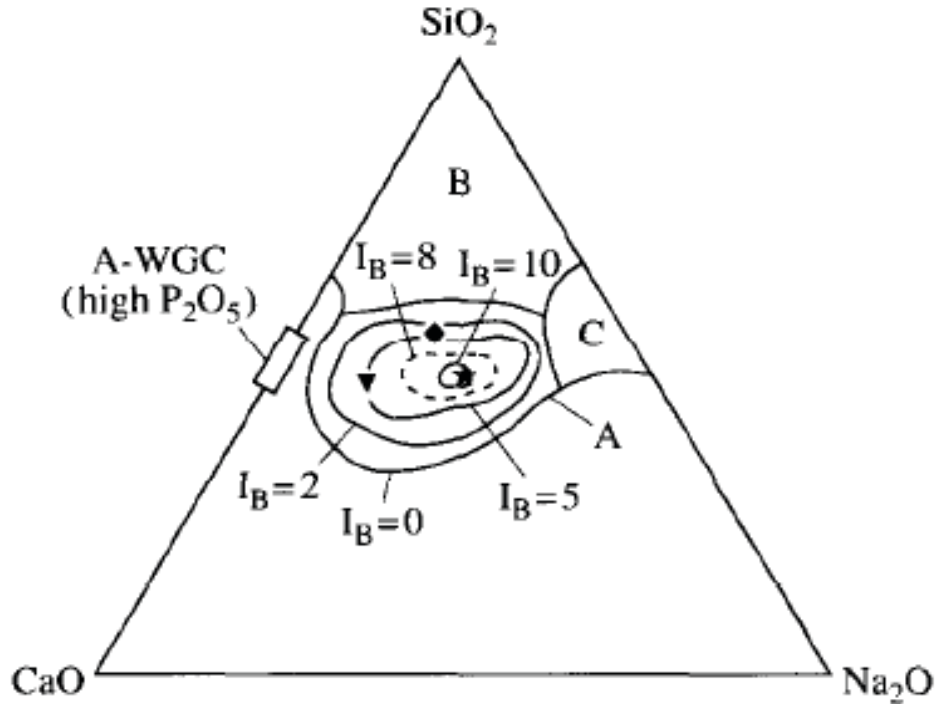


Figure 2-5 Schematic illustration of interfacial reaction between bone and implant which result in HA formation [16].

## 2.4 45S5 composition

First bioactive glass prepared was 45S5 with composition: 45% SiO<sub>2</sub>-24.5% Na<sub>2</sub>O-24.5% CaO-6%P<sub>2</sub>O<sub>5</sub> (wt %) provided a large amount of CaO with some P<sub>2</sub>O<sub>5</sub> in a Na<sub>2</sub>O-SiO<sub>2</sub> matrix [1]. Origin of “45S5” is that it contains 45 wt% of silicon (45S), and molar ratio of Ca/P is 5 and represents the second part of the name. This composition was achieved by considering the compositional diagram for bone bonding shown in Figure 2-6 [1, 3, 4]. In this diagram all glasses contain 6 wt% of P<sub>2</sub>O<sub>5</sub>. Different regions in this figure refer to different amounts of bioactivity. Silicate glasses within region A form a bond with bone. As the composition gets closer to the center of region A, bioactivity increases. Compositions close to center of region A, region E, which refers to bioglasses with I<sub>b</sub>>8 form a suitable bond between the implant and host tissue. 45S5 has the composition in center of region A (E) with bioactivity index equal to 10. Compositions in region B behave as almost inert materials. Bottle glasses and windows are some examples of glasses in this region. Glasses within region C are resorbable and disappear in 10-30 days of implantation. Region D refers to glasses which are not technically practical and have not been tested as implants [3].

Silicon is the main element presented in 45S5 and all other glasses. This element acts as a strong network former. Si maintains the structure of glass by having four bonds with neighbor atoms. Figure 2-6 shows that glasses with less than 52 wt% SiO<sub>2</sub> bond to both hard and soft tissues, but the ones with 52 to 60 wt% do not bond to soft tissues, and glasses with more than 60 wt% SiO<sub>2</sub> do not even bond and are bio-inert [1]. At these percentages the rates of surface reactions are sufficiently slow that the material is biologically inert [3]. However, increasing the surface area by other manufacturing methods instead of casting, like using sol-gel method can increase this value to 90wt% SiO<sub>2</sub> whilst maintaining bioactivity [5, 14].



**Figure 2-6 Compositional dependence (in wt%) of bone and soft tissue bonding bioactive glasses and glass ceramics [1, 3, 4].**

The main structural characteristics of the bioactive glasses are related to their open structure which allows the incorporation of cations ( $\text{Na}^+$  and  $\text{Ca}^{2+}$ ) into the glass matrix. This phenomenon is due to the presence of chemicals called network modifiers which induce network disruption and consequent formation of non-bridging oxygens (NBO). Non-bridging oxygen is the oxygen that is not shared with two  $\text{SiO}_4$  tetrahedral, whereas bridging oxygen is shared with two tetrahedral. Thus, these cations deeply affect the connectivity of the glass structure [18]. The presence of network modifiers such as  $\text{Na}^+$ , is not necessary but is helpful for increasing dissolution rate in body fluid. In addition,  $\text{Ca}^{2+}$  has another important effect, which makes the presence of this cation more important than others. Calcium is one of two main elements presented in HA composition, so existence of  $\text{Ca}^{2+}$  in bioglass increases the rate of dissolution with both increasing  $\text{Ca}^{2+}$  concentration and acting as a network modifier. High  $\text{Na}_2\text{O}$  and  $\text{CaO}$  content and high  $\text{CaO} : \text{P}_2\text{O}_5$  ratio can make the surface highly reactive [3]. Generally the presence of  $\text{Na}_2\text{O}$  or other alkali cations in the glass composition increases the solution pH at the implant-tissue interface and thereby enhances the precipitation and crystallization of HA [14].

The presence of phosphorous in the glass or glass-ceramic increases the rate of HA formation because they are much more soluble and also raise the rate of calcium release, especially in reaction stages 1 and 2. This happens because presence of phosphorous makes the surface of the implant more negative as shown in Figure 2-5 [11].

A way to denote the network connectivity is through the structural unit usually represented as  $Q^n$ , where Q represents the tetrahedral unit and n the number of bridging oxygen (BO) per tetrahedron. For silicon compounds, n varies between 0 and 4 where Si is a central tetrahedral atom ranging from  $Q^0$ , which represents orthosilicates ( $SiO_4^{4-}$ ), to  $Q^4$  (tectosilicates) and  $Q^3$ ,  $Q^2$  and  $Q^1$  representing intermediate silicate structures with concentrations of modifiers [18].

The schematic molecular structure of amorphous 45S5 is demonstrated in Figure 2-7. As shown, weak ionic bonding especially of alkali ions raises ion exchange rate of  $H^+$  or  $H_3O^+$  ions at the glass surface.

Computational analysis of amorphous materials like 45S5 was carried out by Malavasti et al. [19]. They calculated the density of 45S5 equal to  $2.82 \text{ g/cm}^3$  which is close to experimental value of  $2.72 \text{ g/cm}^3$ . They represented the ion distribution of amorphous 45S5 as shown in Figure 2-8. The unit cell shown contains 78 atoms with  $Na_{12}Ca_7P_2Si_{13}O_{44}$  composition. They showed that phosphate groups in 45S5 are in two different states inside the unit cell as shown in Figure 2-8 by number (1) and (2). The first is an isolated phosphate while the second group is linked to  $SiO_4$  tetrahedron. It is understood that the number of Si-O-P bonds is strongly dependent on the annealing procedure used to obtain the glass structure [19, 20].

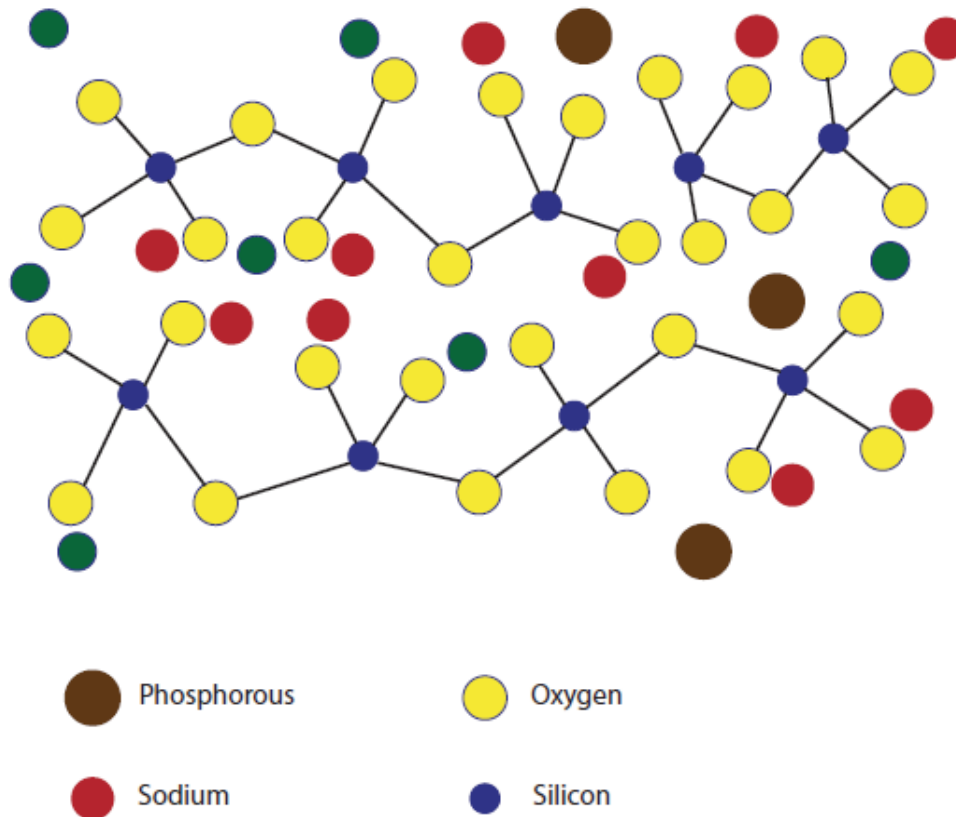


Figure 2-7 Schematic molecular structure of amorphous 45S5 bioactive glass; showing fast ion exchange of  $\text{Na}^+$  with  $\text{H}^+$  from body fluid [5].

## 2.5 Manufacturing bioglasses by casting

Usually bioglasses and glass ceramics are prepared by melt-casting. Traditionally, melting and mixing material together is the method which is used widely for manufacturing different kinds of glasses and glass ceramics. For example 45S5 is a bioglass with melting point:  $T_m=1450^\circ\text{C}$  and needs to reach higher temperatures for production. Mixing different kinds of oxides and carbonates at high temperature in a crucible, removing carbon in the form of  $\text{CO}_2$  and  $\text{CO}$ , quenching in water, and finally annealing is the usual glass formation process [21]. Cooling rate should be that much high that crystals do not have enough time to form. Annealing and heat treating are needed for stress relieving and achieving a more uniform structure [1, 22].

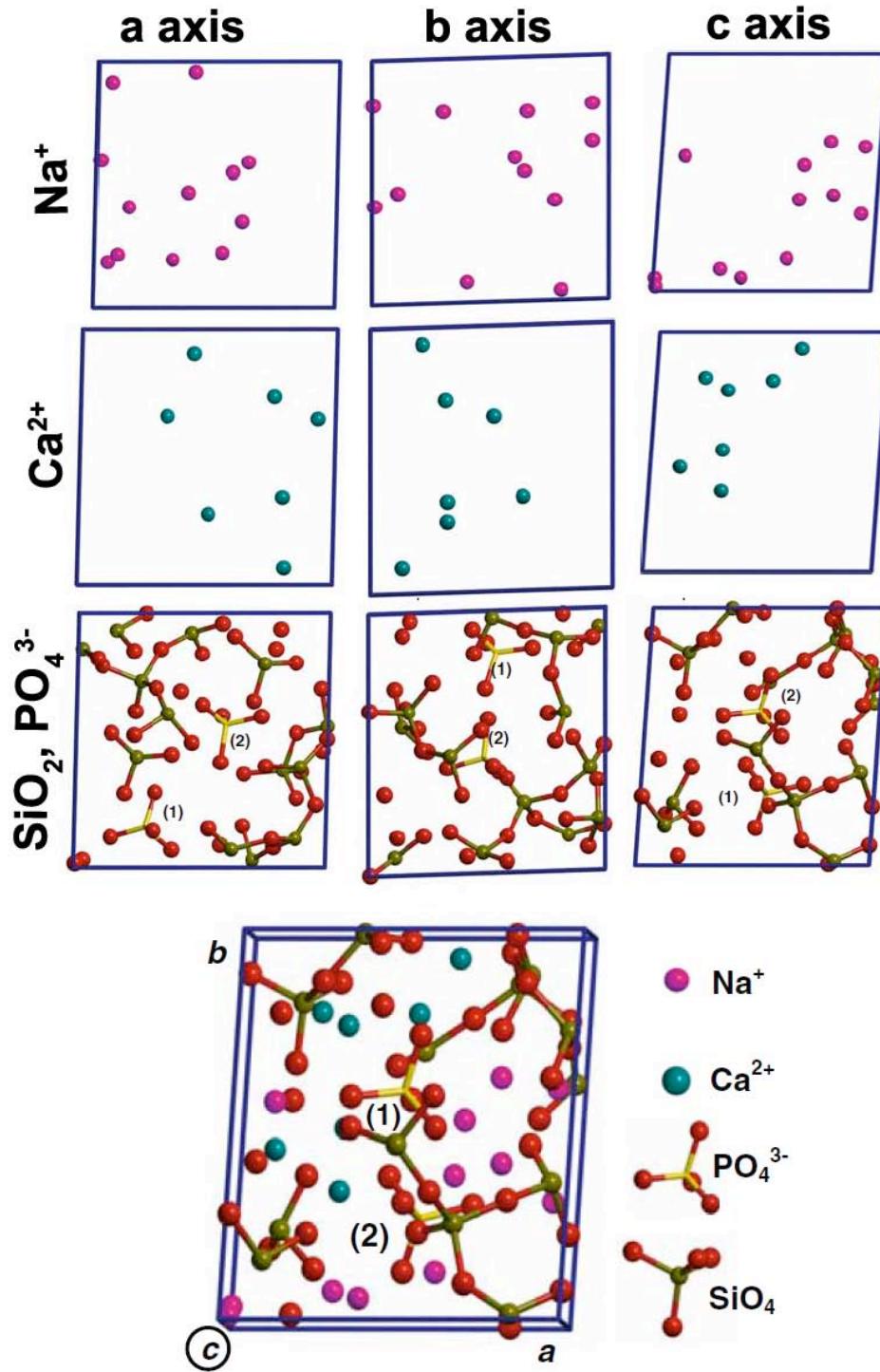


Figure 2-8 Graphical representation of ion distribution, bioglass 45S5 in a, b and c axis [20].

## **2.6 Manufacturing bioglasses by sol-gel method**

This is another method of manufacturing bioactive glasses. Sol-gel is a chemical solution precipitation method (wet chemical) for preparing different kinds of materials. This procedure started with processing of oxide materials more than 50 years ago. Since then, this technique has been used not only for oxide materials, but also non-oxides such as nitrides and carbides [23, 24].

In 1991, Li *et al.* showed that a stable bioactive glass could be prepared by the sol-gel method [1, 14]. Materials made by this technique showed better properties (discussed more later). After that, many studies characterized bioglasses prepared by the sol-gel method [25-29]. Most of this work showed higher bioactivity of materials prepared by this technique. The glass prepared by this procedure has higher surface area because of the porous 3D network of the gel which is completely interpenetrated with a liquid. A wide range of organic and biological molecules can be incorporated within the pore networks. Small pores (nanoporosity) in the structure leads to increasing surface area by two orders of magnitude and higher bioactivity compared to the melt-derived glasses. By varying the processing conditions, very wide ranges of porosity have been obtained [2, 9, 14, 20]. Also the chemical composition and stabilization temperature are the main synthesis conditions that will define the network connectivity, the textural properties and the glassy conformational structure [18]. The important thing about this method is that the final product properties depend strongly on many factors. For instance, the final size of the powder is a function of the initial concentration of water and catalyst, the type of precursor used, the reaction media and reactor temperature [30]. So, controlling the processing condition seems very important that can considerably affect the final product.

Some of main characteristic of gel-derived samples are [2, 16, 18]:

1. Most organic or biomolecules can be entrapped in sol-gel network.
2. Entrapped molecules generally retain their physical characteristics.
3. Entrapped molecules retain many of their chemical and biological properties.
4. Particulates can be made with controlled size and shape, distribution and connectivity of porosity.

5. Porous bioactive sol-gel glasses have a broader range of compositions and exhibit an *in vitro* and *in vivo* bioactivity equivalent to or greater than melt-derived bioactive glasses, ceramics and glass-ceramics.
6. High homogeneity.
7. Greater ease of powder production.
8. Presence of residual hydroxyl ions.

Generally the rate of HA formation and index of bioactivity is higher for sol-gel glasses when compared with melt-derived glasses due to high surface area of gel-derived bioglass [2]. As mentioned before, glasses made by sol-gel method (even 90% SiO<sub>2</sub>) show high bioactivity due to extremely high surface area [5, 14].

Another important result of sol-gel method is the formation of glass in the form of powder. For some clinical applications such as treatment of periodontal lesions and urinary incontinence, powders of the bioactive glasses are required.

Preparing powder from melt-cast samples has some disadvantages like [14]:

1. It is difficult to maintain the very high purity required for optimal bioactivity. This is primarily because of high temperatures associated with melting, but also related to high activity of silica and alkali composition which tend to dissolve in the platinum crucible during melting.
2. Grinding, polishing and sieving exposes powder to potential contaminants which have a negative effect on bioactivity.
3. There is a compositional limitation imposed on bioactive glasses made by conventional high temperature process. This is due to extremely high equilibrium liquidus temperature of SiO<sub>2</sub>, 1713°C, and extremely high viscosity of silicate melts with high SiO<sub>2</sub> content.
4. High temperature processing and using platinum crucibles considerably increase production cost.

So, finally it is expected that bioglasses prepared by the sol-gel method, show higher bioactivity due to higher surface area, higher degree of homogeneity, fewer impurity and lower manufacturing cost when compared with melt cast powder.

### 2.6.1 Sol-Gel Mechanism

**Sol:** Molecules and atoms can form conglomerates under the influence of intermolecular forces. If these conglomerates remain stable, they are referred to as colloids (usually in the size range of 1-100nm in diameter). The state of colloidal suspension of solid in a liquid is called sol. The suspension of the sol particles in the solvent is best thought of as a dynamic process in equilibrium [30-32].

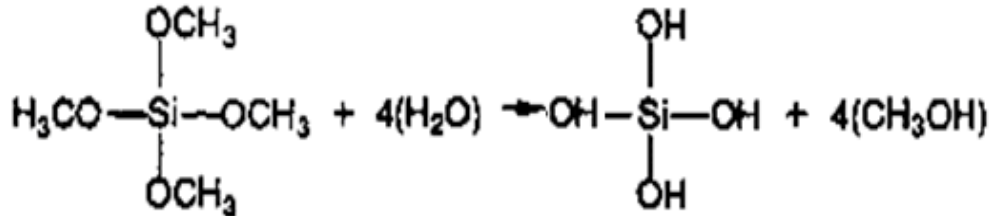
Generally sol-gel process could be categorized in six stages:

1. *Hydrolysis:* In this stage, the initial silicon alkoxide (precursor) hydrolyses by an acid or base catalyst. It is important that in this stage precipitation is prohibited. The general reaction can be demonstrated as:



\*Where R is the alkyl group

For example when R=CH<sub>3</sub> the alkoxide is called TMOS (Tetramethyl orthosilicate) the reaction is:

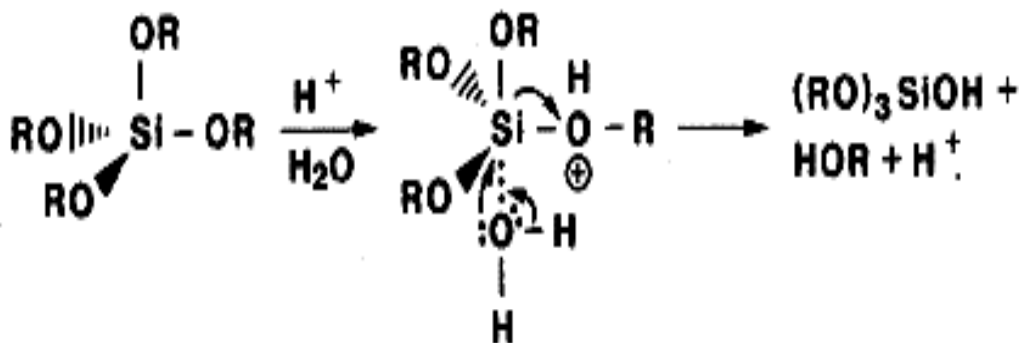


TEOS or Tetraethyl orthosilicate Si(OC<sub>2</sub>H<sub>5</sub>)<sub>4</sub> is one of the main alkoxides used in silica systems. Small alkyl groups in this component lead to fast hydrolysis. TEP or Triethyl phosphate PO(C<sub>2</sub>H<sub>5</sub>O)<sub>3</sub> is the other precursor which provides phosphorous in 45S5. The formation of multicomponent gels like 45S5 can be achieved without the use of all alkoxides and for economic reasons it is often desirable to reduce the number of alkoxides in the system. In many cases it is possible to use metal salts such as nitrates for the first and second group of elements in the periodic table instead of alkoxide precursors [4, 23, 24, 30].

*Effect of catalyst:* Catalyst is used to improve hydrolysis reaction rate. Many kinds of acids and bases such as HNO<sub>3</sub> and HCl and NaOH are used as

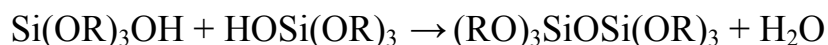
catalyst during sol-gel process. Aelion et al. showed that the rate and extent of hydrolysis is most affected by strength and concentration of acidic or basic catalyst. Temperature and solvent were of secondary importance [24, 33]. All strong acids behave similarly and react rapidly but weaker ones need more time for hydrolysis. Further, the mechanism of acidic catalyst reaction with alkoxides will be discussed.

The presence of acid as a catalyst will remove electron from silicon making it more electrophilic and more susceptible to attack by water. Water will acquire positive charge after attacking. This will result in reducing the positive charge of alkoxide, correspondingly, makes the reaction occur more rapid [24].



2. *Condensation*: After hydrolysis, silica tetrahedra interact and repolymerize.

Water condensation occurs:



Catalysts form the interconnection between linear molecules during hydrolysis. In silicon systems and at low pH, hydrolysis and polymerization occur by nucleophilic attack on the silicon ion ( $\text{Si}^{4+}$ ). This will result in formation of a three dimensional polymer form which is not a true colloidal dispersion. It is only when we go to very high pH and excess water content that a true colloidal dispersion forms. Under this condition, the linear chain molecules (siloxanes) become soluble. So during this, the small chains will depolymerize and deposit on a larger chain, so will result in growth of large molecules. This effect leads to the formation of colloidal silica particles [12, 30]. Using a basic or acidic catalyst has

great effect on final shape of achieved particles. Figure 2-9 shows final structure gained by acid and base catalysts.

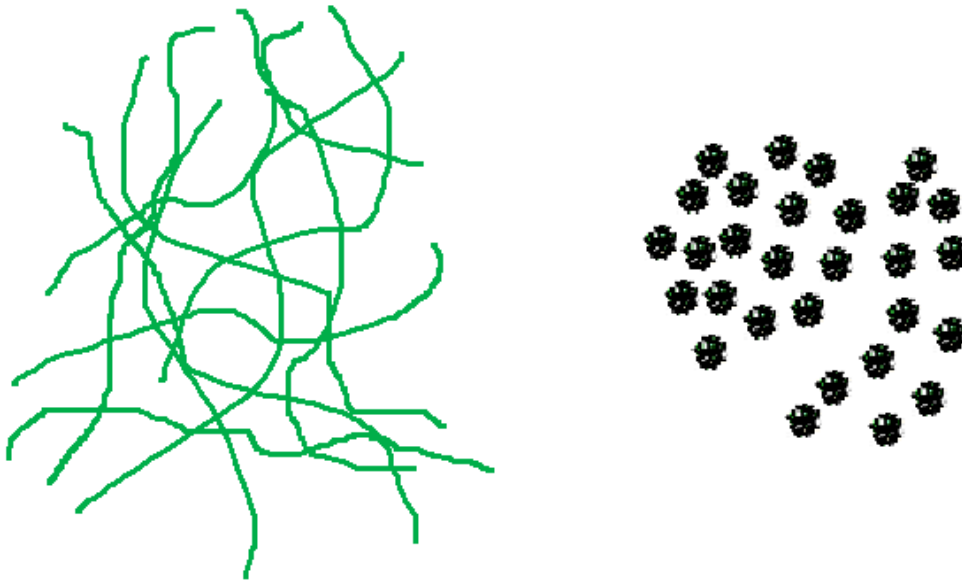
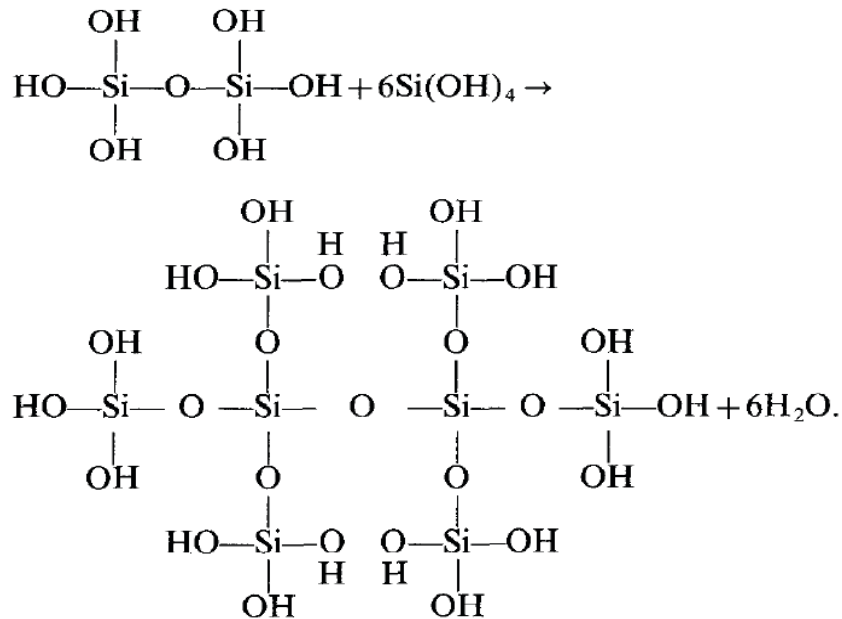


**Figure 2-9 Particle shape using acidic (left) and basic (right) catalyst.**

After this condensation, additional Si-OH tetrahedral will join together and form a polycondensation structure, and finally will result in SiO<sub>2</sub> network formation. Water which is removed from the reaction remains in the pores of the network. The network of polycondensation for water and OH<sup>-</sup> is shown below [24, 30, 31].



At the end of this stage, when sufficient interconnected Si-O-Si bonds are formed, they produce a colloid structure called sol. These colloidal particles have Brownian motion when they are dispersed in a liquid. It was shown that the sol was a suspension of colloidal particles with particle size of approximately 5nm [20].

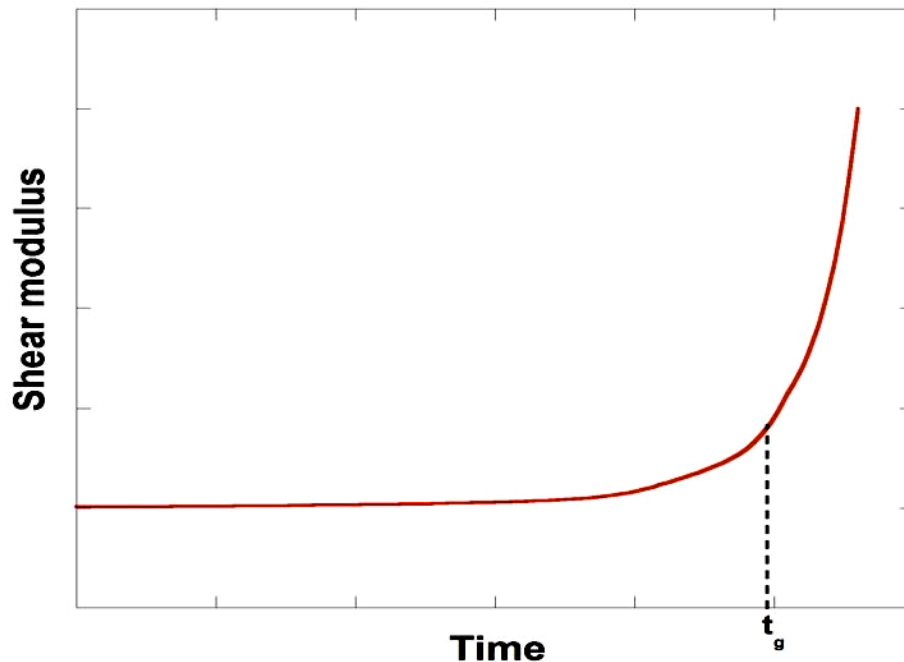
As discussed before, many factors influence the kinetics of hydrolysis and condensation. In general, the variables which influence on kinetics are temperature, nature and concentration of catalyst, nature of the solvent and the type of the alkoxide precursor [30, 31]. For example, the size of sol particles depend on the pH and R ratio ( $R=[\text{H}_2\text{O}]/[\text{Si}(\text{OR})_4]$ ). So by controlling this R value, colloidal particles size will change [24, 30].

3. *Gelation*: A gel is an interconnected, rigid network with submicrometer pores and polymeric chains with average length greater than a micrometer. More condensation of colloids and aggregation of particles, produce a single giant cluster which often exhibits the visco-elastic properties of a gelatinous mass called a gel [24, 30, 32]. Generally, gelation occurs when silica tetrahedra particles or macromolecules produced by hydrolysis and condensation have cross-linked and formed a three-dimensional network which is capable of immobilizing the

remaining solvent. This leads to the formation of a spanning cluster, so density and elasticity will increase rapidly as shown in Figure 2-10. The mechanical state of this gel depends very much upon the number of cross-links in the network. It is obvious that the greater the degree of cross-linking, the more rigid the structure will become [4].

At the beginning of the gelation process, viscosity rises suddenly and the resultant mass takes the shape of the mold, but the elasticity is still low. Following gelation, further adding of sol particles to the spanning cluster, leads to an increase in the elastic and shear modulus [30, 31].

The point that sol becomes a gel and can support stress elasticity is called gelation point or gelation time,  $t_g$ . Figure 2-10, schematically shows effect of  $t_g$  on shear modulus and fluidity [30, 31]. Reports show that  $t_g$  depends on many factors like nature of precursor and catalyst and even the size of container [30]. The effect of R ratio on  $t_g$  is represented in Figure 2-11. So high and low R ration will drastically reduce gelation time.



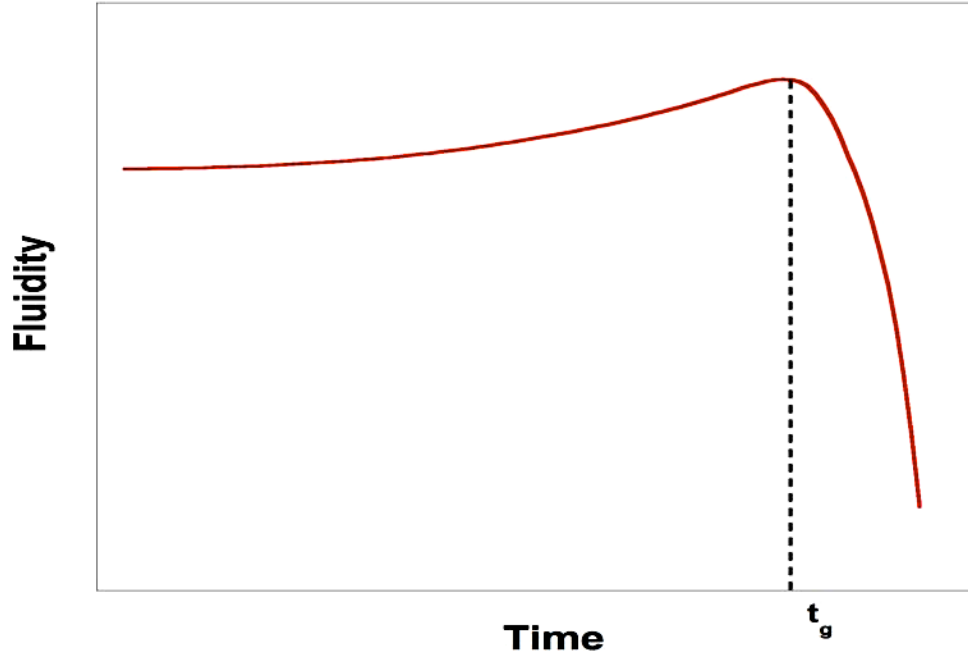


Figure 2-10 Schematic diagram of (A) elasticity and (B) viscosity for on material at sol-gel process, after [31].

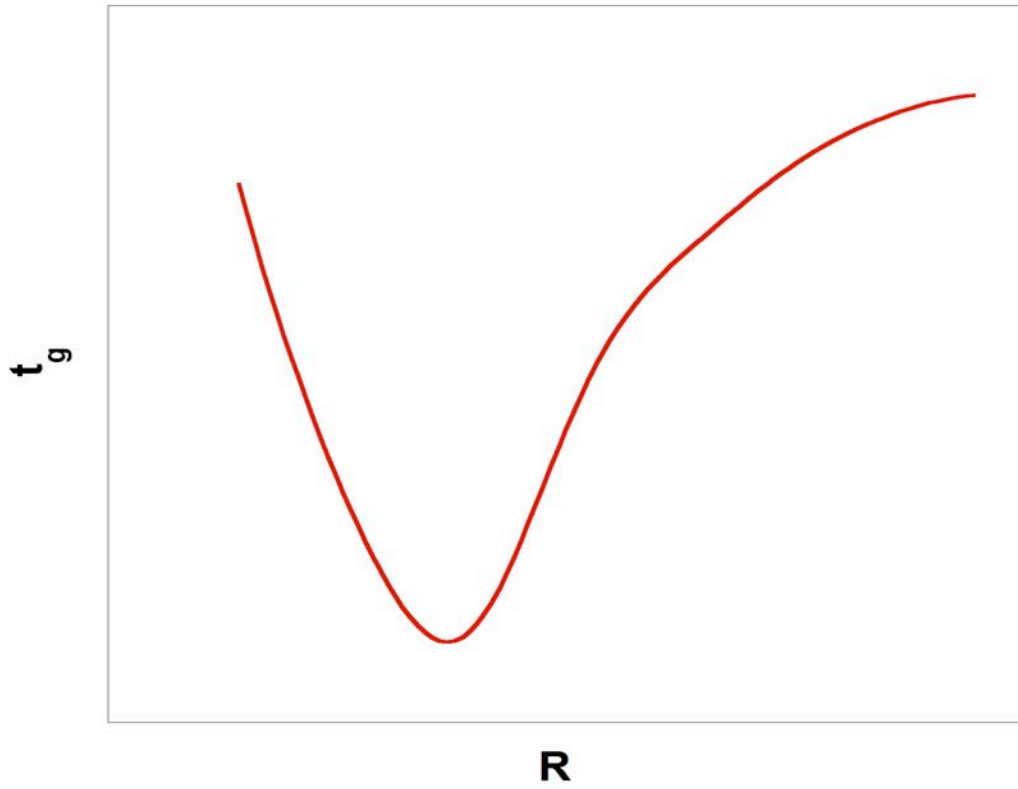


Figure 2-11 Variation of the gelation time with R ratio, after [30].

The form of the prepared gel depends on factors such as pH of solution. At low pH levels the silica tends to form linear molecules which are occasionally cross-linked. Linear chains have low density of crosslinks. This leads to creation of a soft gel which can be redispersed in solution. As we increase the pH value we increase the number of cross links between polymer chains. Also, it makes the linear polymers become more branched and that the number of cross links increases [30, 32]. Figure 2-12 illustrates two shapes of molecules discussed above.

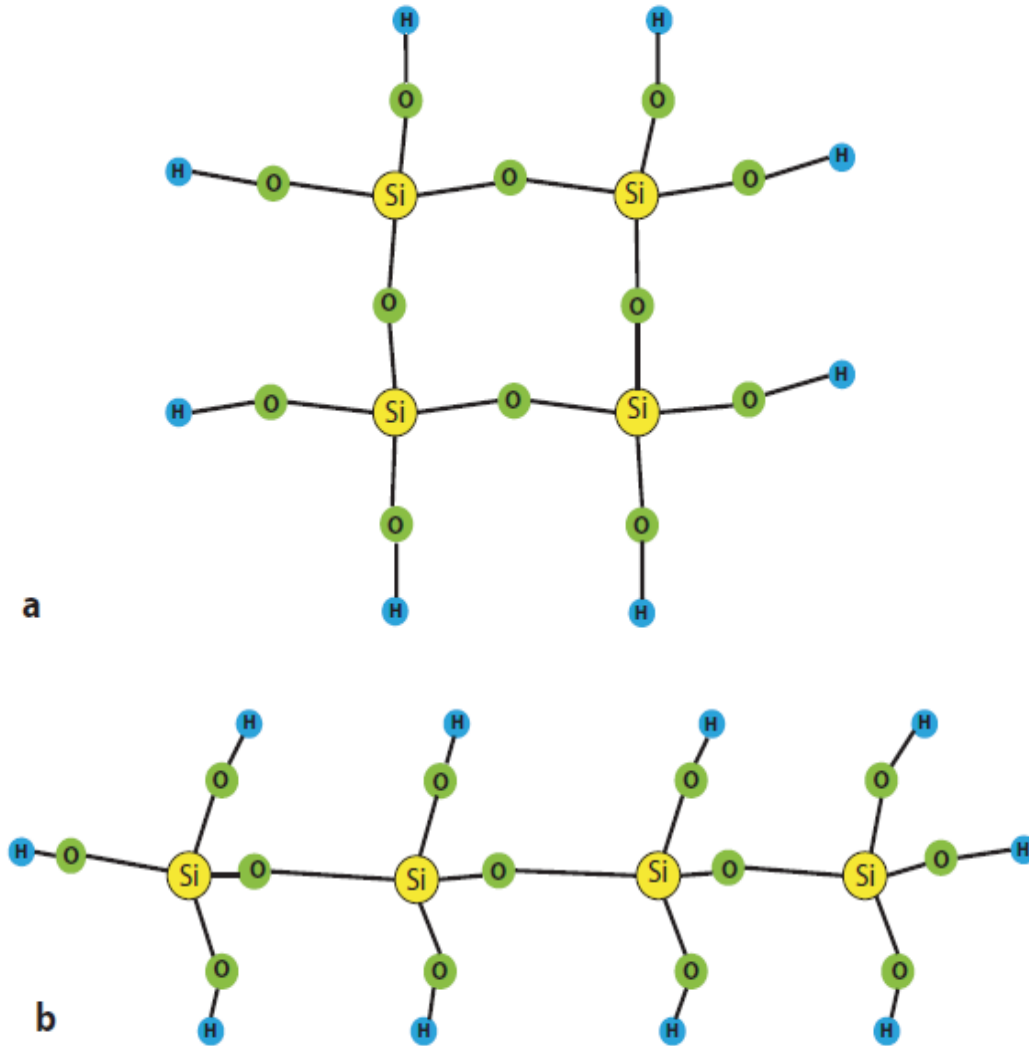


Figure 2-12 The 2-D models of silica tetrahedra a)ring b)chain, after [31]

In computer simulation of cluster aggregation shown in

Figure 2-13, the process of hydrolysis, condensation and gelation is represented. This simulation shows that in the first minutes, molecules start to join together to form micromolecules called colloids. These colloids form a sol which is a suspension of colloids in solution. Then, during gelation, the colloids continue to join together to form larger particles. Finally the connection between colloids increases so that one big cluster forms after a while [24, 31].

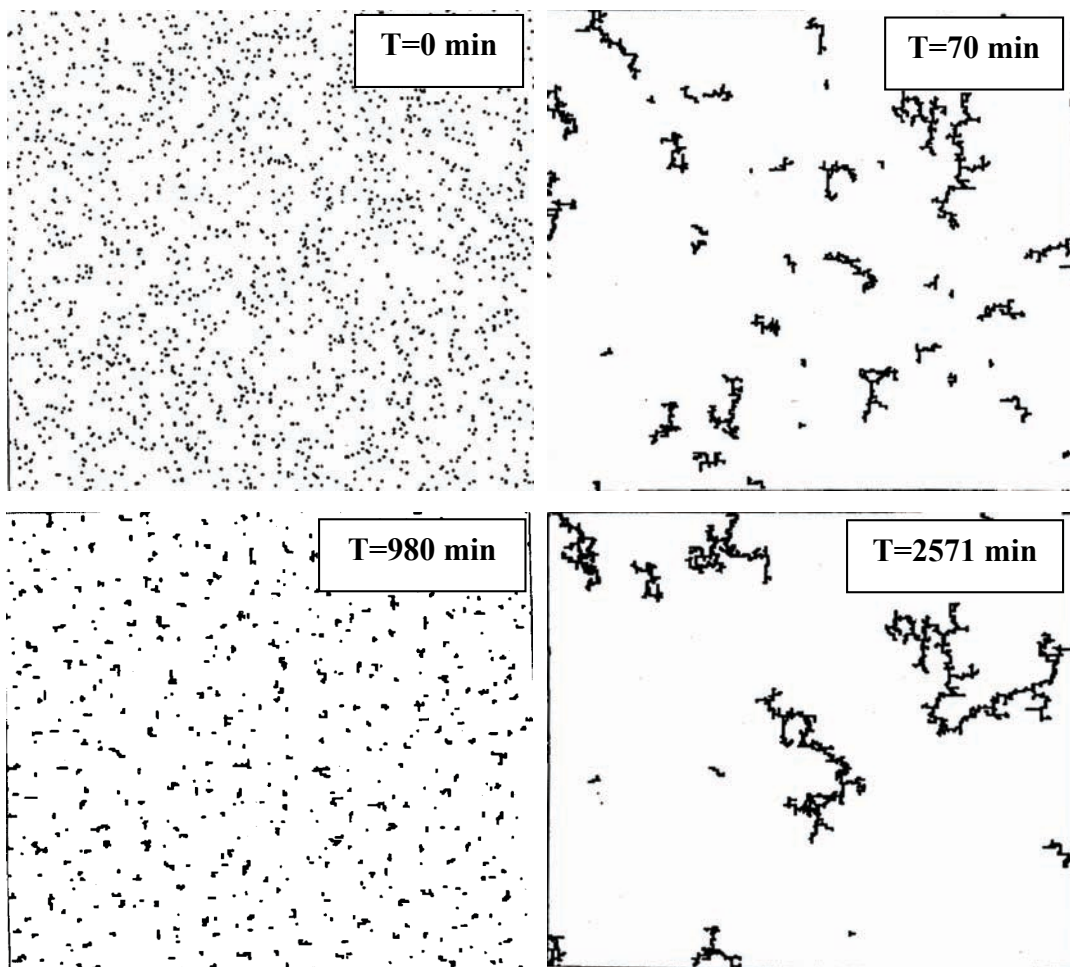


Figure 2-13 Simulation of hydrolysis, condensation and gelation in the sol-gel method [24].

4. *Aging*: The aging process involves maintaining the product for a period of time at relatively high temperatures ( $\sim 70-100^\circ\text{C}$ ), depending on pH, temperature, and gel composition. This stage will change structure and properties of gel. In this step four processes can occur singly or simultaneously including polycondensation, syneresis, coarsening, and phase transformation [30, 31].

The net effect of this stage is stiffening and shrinkage of the gel. These occur because new bonds are formed due to polycondensation instead of previous weak interactions between surface hydroxyl and alkoxy groups. Polycondensation (in this stage) involves the number of bridging bonds increasing long after gelation; large concentration of SiOH leads to condensation. Eventually the liquids will abandon the pore of the gel. By reducing hydroxyls during aging, new bonds will form and a more cross-linked structure will be created [24, 30].

Polycondensation causes the shrinkage of homogeneous gels and expulsion of liquid from the pores to occur. This process happens in a small period of time and is called syneresis. In aqueous systems and during shrinkage, the structure is controlled by the balance between electrostatic repulsion and attractive van der Waals forces. Therefore the amount of shrinkage is controlled by extent of electrolytes. Scherer suggested that driving force of contraction was the tendency to reduce the huge solid-liquid interfacial area [24, 30-32]. Ponomareva *et al.* showed that at higher temperatures, the gel becomes stiff faster, so the shrinkage will be prevented. Also, at higher temperature liquid repulsion occurs faster, so there should be an optimum temperature for this process [30, 34]. Syneresis resultant particles are called primary particles and are  $\sim 2\text{nm}$  diameter [30].

After syneresis, another important process is coarsening and ripening. Usually convex surfaces are more soluble than concave ones, so the gel which is immersed in liquid will show more dissolution in regions with negative curvature. Therefore, the neck between particles will grow and small pores will be filled. In this process, materials dissolve from the surface of large particles and deposit on the initially narrow necks which join particles to each other. This leads small particles (primary) to join larger ones and form secondary particles with diameters

of ~6-10nm. Coarsening and ripening strengthen the solid and make some changes in the pore size and shapes which is important to resist cracking during the next stage (drying) [30, 31].

Figure 2-14 schematically shows the three main steps of aging. As shown, shrinkage and coarsening occur and lead to the separation of liquid from clusters. This sequence results in physical and especially mechanical property changes in gel.

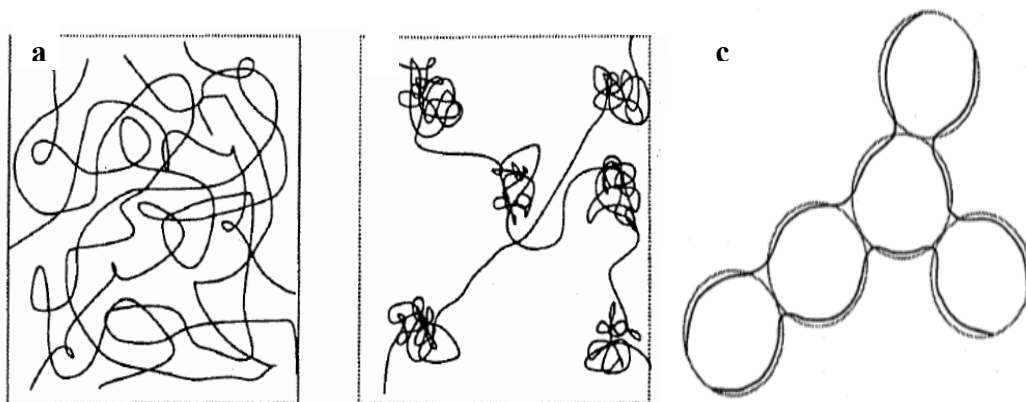


**Figure 2-14 a. Polycondensation b. Syneresis c. Coarsening during aging [24].**

5. *Drying*: During drying the solvent liquid which, in the case of alkoxide derived gels will be mainly alcohol and water is removed from the interconnected pore network. The porous solid remaining after evaporation of residual liquid is called xerogel. The heating rate during drying will affect cracking in the final solid. Faster heating increases cracks due to capillary forces [4].

Generally, drying has four main steps as shown in Figure 2-15:

1. The constant rate period: At this initial stage, the gel will shrink by an amount equal to the volume of liquid which evaporated. In this stage deformation of the network occurs by large capillary forces which cause shrinkage of the object. During constant rate period, evaporation rate per unit area of the drying surface is independent of time as illustrated in Figure 2-15. Usually the greatest changes in volume, weight, density and structure happen throughout this stage. Constant rate period ends when shrinkage stops [24, 30, 31].

2. The critical point: at this point, the gel becomes sufficiently stiff due to greater packing density of solid phase. So it will resist further shrinkage as the

liquid continues to evaporate. At this point, the liquid starts to go to the pores of the gel. Due to the small size of the porous structure, a very large pressure is generated across the interfaces of liquid in the pores. Eventually the highest capillary pressure is created and the gel can not be compressed any more. This will aid in emptying the pores and stage 3 will start accordingly [30, 31].

3. First falling rate period (transition zone): in this stage, liquid transport occurs by flow through the surface films that coat partially empty pores. In many gels, as the liquid recedes into pores, a thin liquid film remains on the pore walls. This film flows to the surface followed by evaporation, so further drying occurs. In this stage, cracking may happen due to extremely high capillary forces [30, 31]. This region is shown in Figure 2-15 as the transition zone.

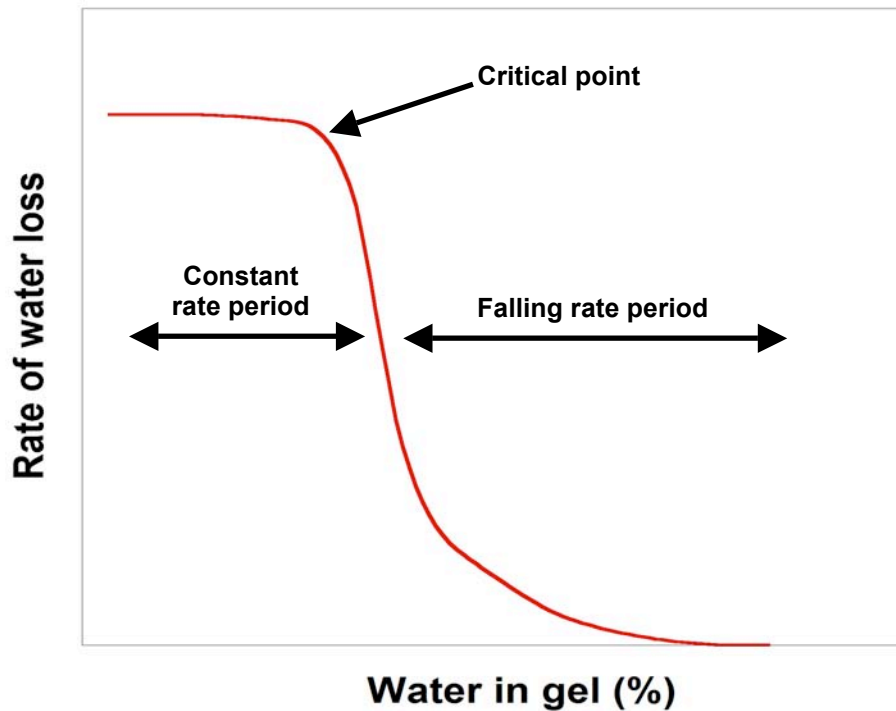


Figure 2-15 Plot of rate of water loss vs. water in the gel [30].

4. Second falling rate period: By progressing the evaporation, it becomes difficult to maintain the liquid film on the pores wall. So, this film breaks and further liquid transportation must involve a vaporization step and diffusion of vapor to the surface, before the liquid reaches the surface. In this period, there is just a small weight change without concomitant dimensional.

The main problem of this stage refers to the large capillary stress produced when pores are small (<20 nm) and leads to crack formation. For controlling this problem different methods have been developed: decreasing liquid surface energy by adding surfactants, hypercritical evaporation which avoids the solid-liquid interface, or controlling the rate of hydrolysis and condensation [23, 31].

TEM images taken by Lin *et al.* reveal that the dried gel before stabilizing consisted of 5-8 nm nanoparticles [20]. Comparing with the size of colloidal particles in sol (5nm), this indicates that although the whole gel shrinks significantly while drying (about 50vol %) the secondary particle size changes very little during gelling, aging and drying. This happens due to low temperature of drying as Hench and Wang expressed. They stated that viscous flow takes place at high temperatures and suggested irreversible sintering happens when heat treatment is higher than 400°C [20, 24].

5. *Stabilization and densification:* Although there are many applications of silica gels prepared at or near room temperature, heat treatment is necessary for the production of dense glasses and ceramics by this method. Most of times, by increasing temperature up to 700°C, the product will lose about 15% of its weight and 20% shrinkage will occur [31].

The main reason for a stabilization treatment is the very large concentration of silanols on the surface of the pores of the prepared materials. The main goal is to reduce these silanols to the level that the surface does not rehydroxylate during use. Stabilization reduces surface area, so optimum temperature is needed for removing all these silanols and compounds such as catalyst compositions, and minimum structural transformation and surface area reduction. It should be considered that dried gel contains water in two forms: free water within ultraporous gel structure and hydroxyl groups associated with the gel surface. Heat treating below 400°C leads to reversible removing of hydroxyl groups. For removing these groups irreversibly, heat treatment should be carried out at temperatures more than 400°C [30, 31].

After stabilizing, the particles are in the range of 10-30 nm size which is believed to occur from the fusion of dried particles via viscous flow due to the relatively high temperature heat treatment during this stage. Due to random packing and fusion between these particles, nanopores have totally irregular shapes and a wide size distribution compared to those in the dried gel [20, 31].

Stabilization occurs to remove the undesired compounds which form during hydrolysis and condensation. 45S5 will have sodium nitrate in the non-stabilized samples, which is related to the use of nitric acid as catalyst. For sodium free glass called 58S another phase called calcium nitrate forms. The existence of these nitrate crystals implies that the nitrate was dissolved in the aqueous solution before drying since if calcium or sodium is incorporated into the silica network as the modifier, the nitrate crystals would not form. This is due to the ionic nature of the calcium and sodium precursor and excess  $\text{HNO}_3$ , which leads to the pH value of the sol (less than 2) being below the isoelectric point ( $\sim 5$ ) and thus HO-Si bonds are dominant instead of  $\text{Ca}^+$ ,  $\text{Na}^+$  -O-Si bonds. After drying, the surface of the silica particles will be covered by nitrates. Thermal decomposition of nitrate takes place at 350-450°C during stabilization. As a result, nitrogen will be removed in the form of  $\text{N}_2$ . The remaining calcium or sodium helps fusion of secondary particles to form stabilized particles. Therefore calcium or sodium adopts the role as a nanoparticle fuser in sol-gel derived bioactive glass production. Nitrate deposited on the surface of particles, covers the surface of nano-texture silica before stabilization which decreased the surface area, so decomposition the particle size is reduced and the surface area increased. This leads to increase in pore volume and surface area instead of a decrease [20].

Figure 2-16 illustrates TEM images of 70S30C bioglass in different stages of preparation. It shows that the size of the colloids and particles after condensation and drying does not change significantly and it remains in the range of 5-8nm. But after stabilization, the size will increase to 10-30 nm due to fusion of dried particles. Figure 2-17 shows the evolution of bioglass 70S30C (70 mol%  $\text{SiO}_2$  and 30 mol%  $\text{CaO}$ ) ion distribution during sol-gel process. As shown, it could be understood that after gelation, the surface is covered with silanols. After

drying, the nitrate ions which were dissolved in liquid, deposit on the surface of particles and finally after stabilization, all nitrate ions removed from the particle surfaces and a few silanols bonds remain. This shows that stabilization is necessary for removing all these undesired components out of sample [20, 30].

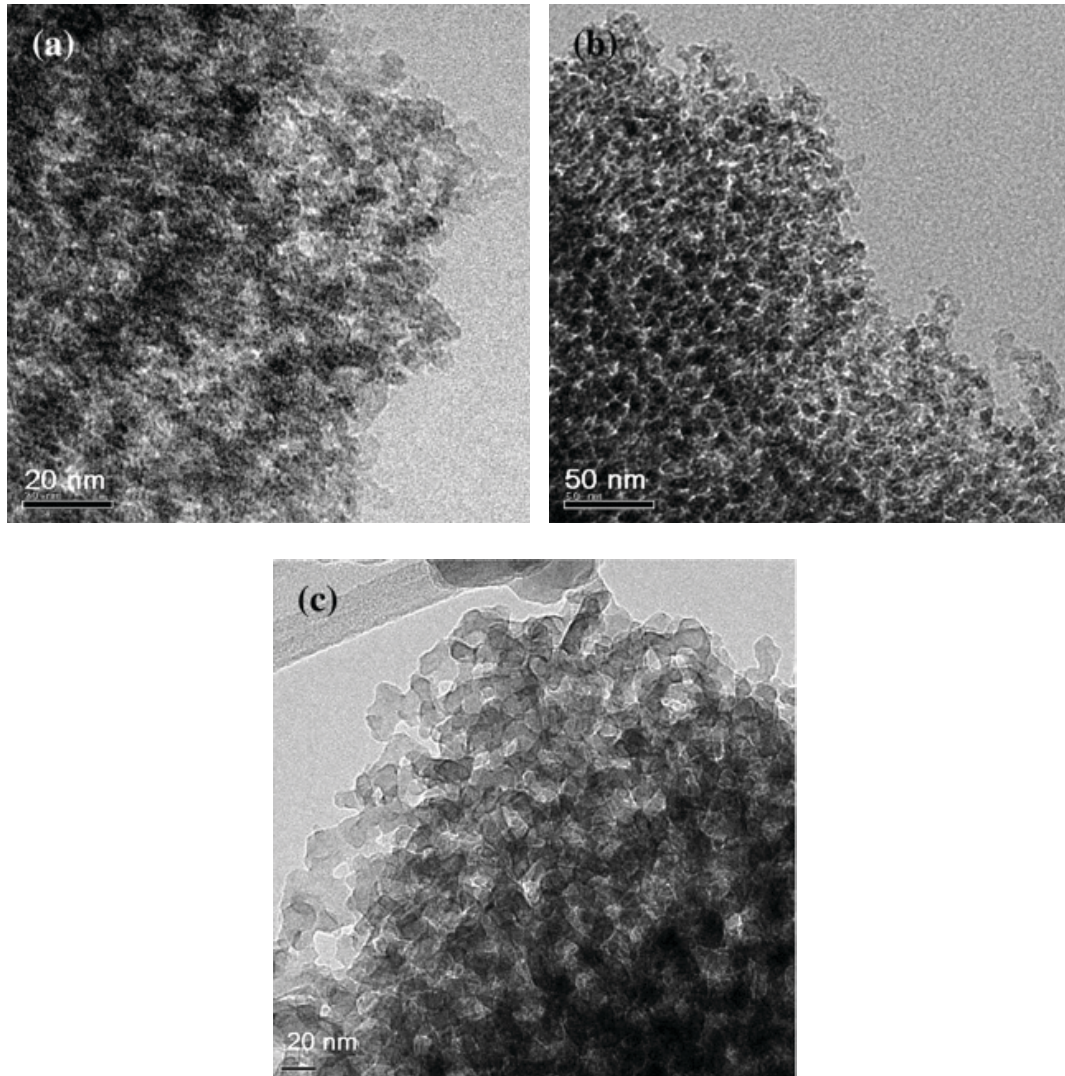


**Figure 2-16 TEM images of 70S30C a. 24hrs reagent mixing of sol b. dried gel c. stabilized gel [20].**

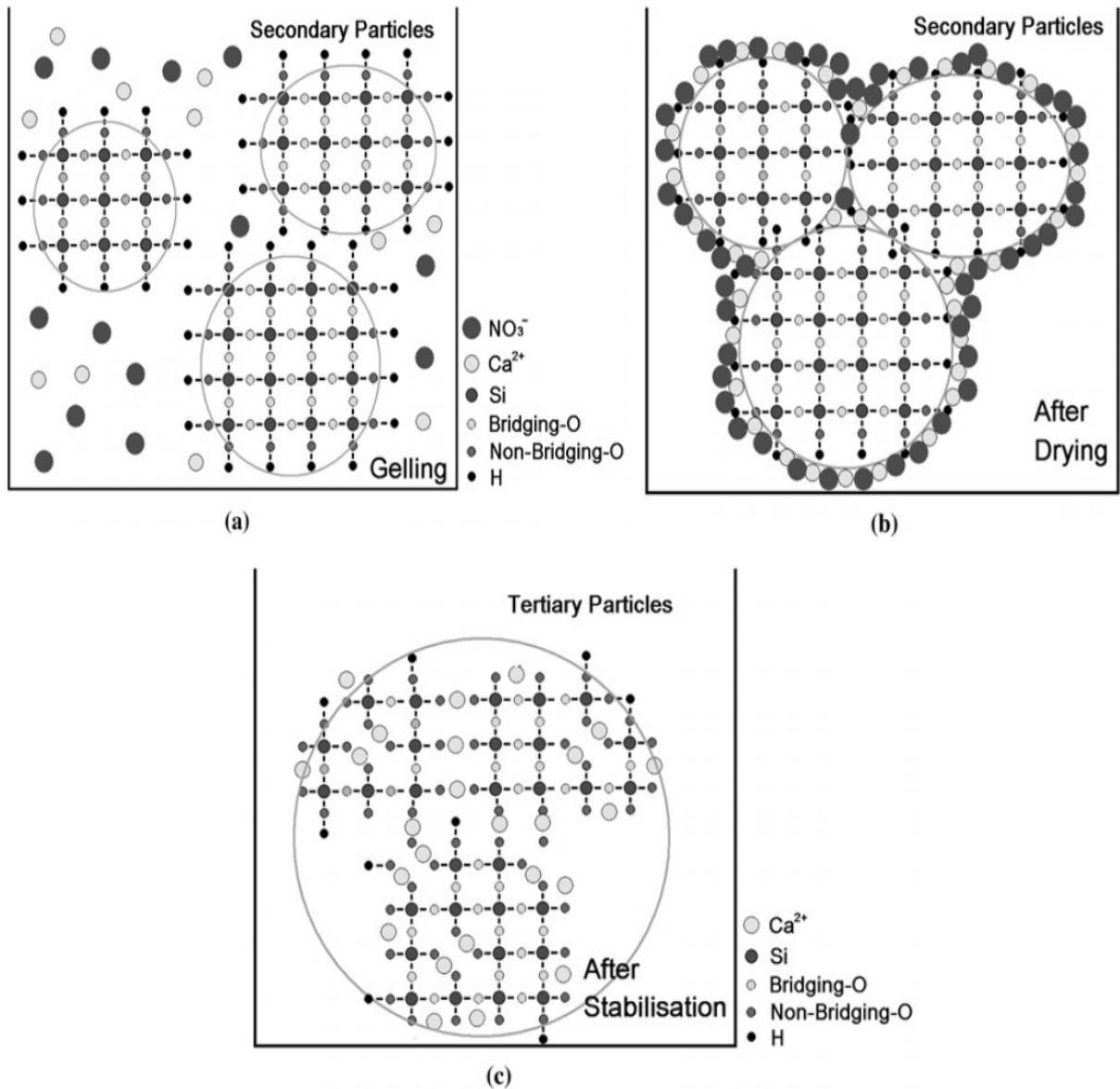


Figure 2-17 Schematic illustration of evolution of ion distribution during a. gelation b. drying c. stabilization [20].

## 2.7 Effect of crystallization

Bioactive glasses are a kind of material which shows the highest amount of bioactivity compared with other materials. As their clinical applications grow, their limited mechanical properties are becoming apparent. They can be used instead of other implants like titanium alloys as bone replacement, but as

mentioned the main shortcoming is related to poor mechanical properties of bioglasses. Table 2-2 represents mechanical properties of some biomaterials and compares it with human cortical bone. This shows that low strength and fracture toughness of bioglass 45S5 prove that improving mechanical properties is desirable. Glass ceramic shows better mechanical properties compared with glass. This has led to many studies to provide a bioceramic with the bioactivity as bioglass. Although glass ceramics show better mechanical properties, the relatively low fracture toughness prohibits using them to repair bone defects in high load bones like femoral and tibial bones [6].

**Table 2-2 Mechanical properties of bioactive ceramics and human cortical and cancellous bones [6].**

	Strength (MPa)		Young's modulus (GPa)	Fracture toughness, $K_{Ic}$ (MPa m <sup>1/2</sup> )
	Compressive	Bending		
Bioglass® (45S5)	—	42	35	—
HA	500–1000	115–200	80–110	1.0
Glass-ceramic A-W	1080	220	118	2.0
Human bone	Cancellous	2–12	0.05–0.5	—
	Cortical	100–230	50–150	2–12

As mentioned before mechanical properties could be improved by using glass ceramics instead of glass implants. Stabilized samples prepared by sol-gel method can be used in amorphous form, or could be sintered to gain a denser and stronger implant. The main drawback of crystallization is that it decreases the level of bioactivity and can even turn a bioactive glass into an inert material [11, 13, 35]. 45S5 will transform to a crystalline phase  $\text{Na}_2\text{Ca}_2\text{Si}_3\text{O}_9$  (combeite) temperatures around 650°C.

Li *et al.* showed that when 45S5 is transformed to glass-ceramic, the formation of surface apatite layer depends on the relative amount of residual glassy phase in the glass ceramic. They showed that a glass-ceramic with 5% or less residual glassy phase exhibited no formation of HA layer [10, 11, 36]. Other results demonstrate that the crystalline phase combeite (PDF#22.1455), slightly decreases the formation kinetics of an apatite layer on the bioglass sample surface but it did not totally suppress the formation of such layer [10, 37]. Reduction of bioactivity refers to a more stable crystalline structure compared with an amorphous material bioglass.

It is obvious that the crystallinity of sintered 45S5 cannot be 100%. From the components of 45S5 and Combeite, one can find that the combeite phase would demand too much CaO to fully crystallize from bioglass. Eventually CaO is depleted when the crystallinity reaches 80.7 mol% (i. e. 77.4 wt %), which is due to maximum crystallinity achieved by 45S5 composition [37].

Some reports suggest the presence of calcium phosphate crystals with a structure similar to hydroxyapatite after rising the temperature to 800°C for a long period [13]. 6 wt% of phosphorous seems not enough for precipitation of a phosphorus rich crystal phase such as  $\text{Ca}_{10}(\text{PO}_4)_6$  which has been reported in some papers at more than 800°C. So if this crystalline phase does not form, the phosphorous ions will stay in solid solution and probably in glassy grain boundary phase. Phosphorous ions can substitute for silicon ions in tetrahedral coordination in the glasses. Generally phosphorous rich crystalline phase will form after additional thermal treatment carried out for long time at high temperature. Also if phosphorous content is increased to 9 wt%, this apatite-like phase will start to form. The state of the phosphorous ions affects the bioactivity. Glass-ceramics containing an apatite-like phase are several times less reactive than materials containing phosphorous in solid solution [11].

Figure 2-18 demonstrates TGA-DTA (Thermogravimetric analysis-Differential Thermal Analysis) graph of 45S5 which shows an endothermic peak at  $T_g=550^\circ\text{C}$  caused by glass transition. Glass transition temperature is defined as the temperature of intersection between glassy state and supercooled liquid in specific volume vs. temperature curve. A Schematic illustration of this curve is shown in Figure 2-19. Usually glasses show a high dependency of volume and enthalpy on temperature above  $T_g$  but below this region, this dependency will considerably decrease so volume and enthalpy will become relatively constant and finally glass will solidify. A slow cooling rate which results in formation of a crystalline structure does not show any of these characteristics. The temperature where the volume separates from the equilibrium curve is controlled by the viscosity or kinetic factors. A slower cooling rate (Figure 2-19 a) allows glass to follow the equilibrium curve to a lower temperature ( $T_{ga}$ ) while a faster cooling rate (Figure 2-19 b) results in a higher transition temperature ( $T_{gb}$ ). Annealing of a fast cooled glass allows the volume to accommodate itself with the equilibrium

curve and hence, the glass transition temperature decreases to the appropriate transition temperature of the equilibrium condition [13, 36, 38].

Endothermic peak mentioned in Figure 2-18 at  $T_{gi}=550^{\circ}\text{C}$  is followed by a glass-in-glass phase separation at  $T_s=570^{\circ}\text{C}$ . This means that the glass is no longer homogeneous but rather consists of two immiscible phases. Another exothermic peak begins at  $T_{ci}=610^{\circ}\text{C}$ . The formation of phosphate rich area during the glass-in-glass phase separation at  $550\text{-}570^{\circ}\text{C}$  should have a catalytic effect on the nucleation of major crystalline phase at  $610^{\circ}\text{C}$  (i.e. combeite). A second small endothermic effect which relates to crystallization of phosphate rich phase is observed at  $T_{g2}=850^{\circ}\text{C}$ . Finally melting takes place in the  $1070\text{-}1278^{\circ}\text{C}$  range. Two endothermic peaks may be attributed to the melting of two different crystalline phases [13].

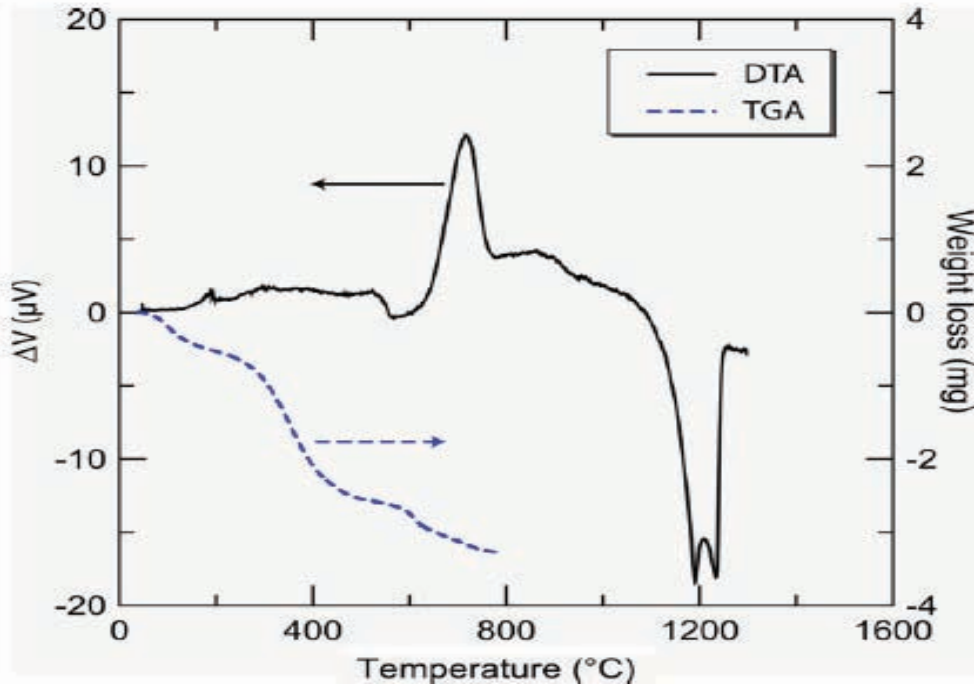


Figure 2-18 TGA-TDA of 45S5 bioglass [13]

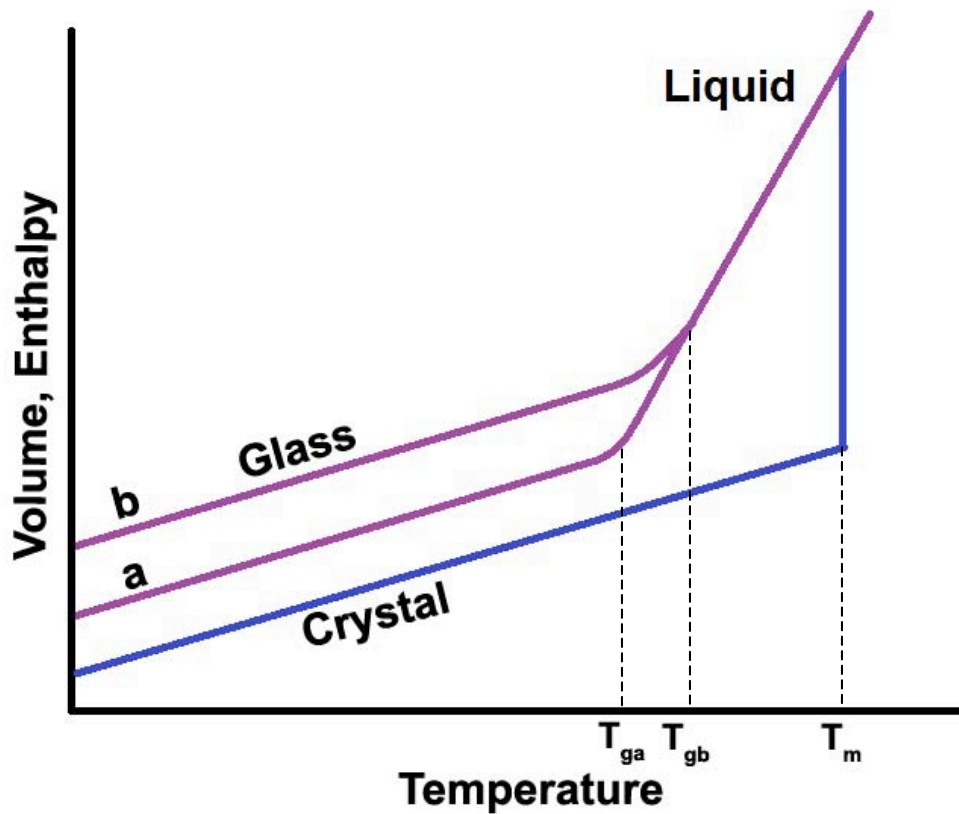


Figure 2-19 Effect of temperature on volume of a crystal and a glass cooled with two cooling rates a. slow b. fast [39].

## 2.8 Preparation of crystalline 45S5 by the sol-gel method

Production of bioactive glass 45S5 by the sol-gel method has not been studied thoroughly because of the presence of sodium in the composition. Most bioglasses produced by the sol-gel synthesis method, do not contain sodium. The presence of sodium has two important effects, in the sol-gel technique: (1) Sodium will react with nitrogen (which is in the form of nitric acid as catalyst) to form sodium nitrite. So, relatively high stabilization temperature is needed for decomposing this compound and removing it from the sample ( $\sim 600^{\circ}\text{C}$ ). (2) Presence of sodium is necessary for crystalline phase  $\text{Na}_2\text{Ca}_2\text{Si}_3\text{O}_9$  (combeite) formation at temperatures around  $600^{\circ}\text{C}$ . Therefore, since high stabilizing temperature is needed and it will overlap with crystallization temperature, 45S5 with 24.5 wt%  $\text{Na}_2\text{O}$  in composition will have crystalline structure after

preparation by the sol-gel method. Previous studies demonstrate that crystalline bioactive material shows less bioactivity in compared with amorphous structure of same composition. So, generally it could be expressed that although the presence of sodium in bioglass as a network modifier enhances precipitation and crystallization of HA, the final crystalline structure of gel-derived biomaterial leads to the formation of crystalline structure and glass-ceramic instead of glass.

As mentioned before, the main advantage of sol-gel technique for synthesis of bioglasses is production of a sample with a high specific surface area. High surface area leads to faster reaction of the implant with body fluid and it is expected that HA formation rate rises by using sol-gel method for material preparation. This advantage might overcome the poor dissolution rate of crystalline samples, which results in formation of crystalline biomaterial with a high dissolution rate.

## ***2.9 In vitro test***

As mentioned before, in this research the formation of HA will be studied while the proliferation and differentiation of stem cell of prepared HA needs to be further studied by *in vivo* tests and animal experiments.

There are many methods to study formation of hydroxyapatite on the surface of a biomaterial. In 1991 Kokubo proposed that the essential requirement for an external implant to bond to living bone is the formation of apatite on its surface when implanted in the living body. He showed this apatite formation could be tested in simulated body fluid (SBF) with ion concentrations near to human blood plasma. By immersing a biomaterial in SBF, HA formation and could be studied [40, 41].

It should be noted that preparation of clear SBF with no precipitation due to highly supersaturated solution and with respect to apatite is not easy and needs careful preparation to prevent precipitation.

The first SBF used by Kokubo *et al.* [40, 42] and Hench *et al.* [40, 43] lacks the  $\text{SO}_4^{2+}$  ions contained in human blood plasma as shown in Table 2-3 . This was corrected later by Kokubo *et al.* [40, 44]. It can be seen in that corrected SBF is still richer in  $\text{Cl}^-$  ion and poorer in  $\text{HCO}_3^-$  than human blood plasma. Subsequently in 2003, Oyane *et al.* tried to correct this difference by preparing revised SBF in which the concentrations of all ions were reached nearer to human blood plasma [40, 45]. Also in 2004, Takadama *et al.* proposed a newly improved SBF in which the concentration of  $\text{HCO}_3^-$  was same as corrected SBF is illustrated in Table 2-3 [40]. Corrected SBF is the solution which used for following *in vitro* tests.

**Table 2-3 [40]**  
Ion concentrations of SBFs and human blood plasma

	Ion concentration (mM)							
	$\text{Na}^+$	$\text{K}^+$	$\text{Mg}^{2+}$	$\text{Ca}^{2+}$	$\text{Cl}^-$	$\text{HCO}_3^-$	$\text{HPO}_4^{2-}$	$\text{SO}_4^{2-}$
Human blood plasma [15]	142.0	5.0	1.5	2.5	103.0	27.0	1.0	0.5
Original SBF	142.0	5.0	1.5	2.5	148.8	4.2	1.0	0
Corrected SBF (c-SBF)	142.0	5.0	1.5	2.5	147.8	4.2	1.0	0.5
Revised SBF (r-SBF)	142.0	5.0	1.5	2.5	103.0	27.0	1.0	0.5
Newly improved SBF (n-SBF)	142.0	5.0	1.5	2.5	103.0	4.2	1.0	0.5

## 2.10 Summary

1. The sol-gel method has many advantages such as higher surface area and interfacial reaction, over melt- cast preparation of bioglasses.
2. 45S5 is a commercialized bioglass widely used in medical applications.
3. 45S5 shows high apatite formation rate because of the presence of sodium as network modifier.
4. The presence of sodium in 45S5 leads to crystal formation during using the sol-gel method for manufacturing.
5. The effect of crystallization is still studying. It is believed that bioglass-ceramics show better mechanical properties and lower dissolution rate compared with bioglasses.
6. Effect of sodium content, crystallization and morphology all together has not been studied thoroughly.

### 3 Experimental procedure

Objectives	Experiments	Anticipated outcomes
<p>Characterization of produced biomaterials</p>	<ul style="list-style-type: none"> <li>-Sol-gel method</li> <li>-DSC, TGA</li>   <li>-XRD</li>   <li>-FTIR</li> <li>-SEM</li> <li>-BET</li> <li>-PSD</li> <li>-EDS</li> </ul>	<ul style="list-style-type: none"> <li>-Porous biomaterial</li> <li>-Phase transformations, removing undesired compounds</li>   <li>-Determining the crystals as function of <math>T_{stab}</math></li>   <li>-Identification of bonds</li> <li>-Morphology of powder and HA</li> <li>-Specific surface area</li> <li>-Particle size</li> <li>-Semi-quantitative analysis of HA formation</li> </ul>
<p>In vitro tests</p>	<ul style="list-style-type: none"> <li>-Immersion in SBF</li> <li>-XRD</li> <li>-FTIR</li> <li>-SEM</li> <li>-EDS</li> </ul>	<ul style="list-style-type: none"> <li>-HA formation</li> <li>-HA crystal progression</li> <li>-Evolutions during dissolution</li> <li>- HA morphology</li> <li>-Semi-quantitative analysis</li> </ul>

### 3.1 Materials

The composition of bioactive glass 45S5 used in this study is: 46.1% SiO<sub>2</sub>, 24.4% Na<sub>2</sub>O, 26% CaO, and 2.6 P<sub>2</sub>O<sub>5</sub> in molar percentage.

The melt-derived 45S5 powder with less than 20 μm size was supplied by Mo-Sci Corporation (Rolla, US).

20 grams of gel-derived 45S5 were prepared as follows:

*Hydrolysis and condensation:* Initially 0.15 mol (33.5 ml) Tetraethylorthosilicate (TEOS, 99%, Sigma Aldrich, US) was added to 1M nitric acid with H<sub>2</sub>O: TEOS molar ratio equal to 18 in 250ml size Teflon beaker (Fisher scientific). For preparation of 20 grams powder, 2.25 ml pure nitric acid was added to 48.6 ml water. Consumed nitric acid was 69%, therefore 3.26 ml of 69% nitric acid was added to 47.6 ml of water to achieve 1M nitric acid solution. The mixture was allowed to react for 60 min for hydrolysis of precursor during stirring at room temperature. After that, the following reagents were allowed to react for 45 min during stirring in the following sequence: 0.017 mol (2.9 ml) triethylphosphate (TEP, 98%, Sigma Aldrich, US), 0.085 mol (20.13 grams) calcium nitrate tetrahydrate (99%, Sigma Aldrich, US), and 0.16 mol (13.52 grams) sodium nitrate (99%, Sigma Aldrich, US). Most of hydrolysis and condensation reactions were accomplished after stirring for 45 minutes. After this stage a transparent sol was achieved.

*Gelation:* The sol was then stored in a sealed Teflon container for five days at ambient temperature to form the gel. Sealing was necessary for prohibiting the water evaporation since water is needed for continuing hydrolysis of the gel. Figure 3-1 shows the gel formed after 5 days.

*Aging:* The formed gel was aged in a sealed container for 1 day at 70°C. The result was a shrunken gel surrounded by liquid.

*Drying:* The aged gel was dried by heating at 120°C for 1 day. A white porous solid mass like material remained after this stage, as shown in figure 3-2.

*Stabilization:* The dried sample was stabilized at 700°C for 1 day to remove residual nitrates, silanols and other undesired compounds.

Finally the prepared powder was wet-ground by planetary ball-milling (Retsch PM 100) at 500 rpm for 10 min. The size of most particles was between 5-15 $\mu\text{m}$  (same as melt-cast powder) and for 10 grams of powder about 30 media were used. In this procedure the dried sample was immersed in methanol and spherical zirconia media (2mm diameter) were used to have the least amount of abrasion. The mill was left to stand for 10 minutes in the machine. Eventually the product was heated for 30 minutes at 120 $^{\circ}\text{C}$  to evaporate all the alcohol. Eventually fine powders with size of around 10 $\mu\text{m}$  were achieved.

Production of 45S5 by melt casting and sol-gel method are briefly illustrated in Figure 3-3.

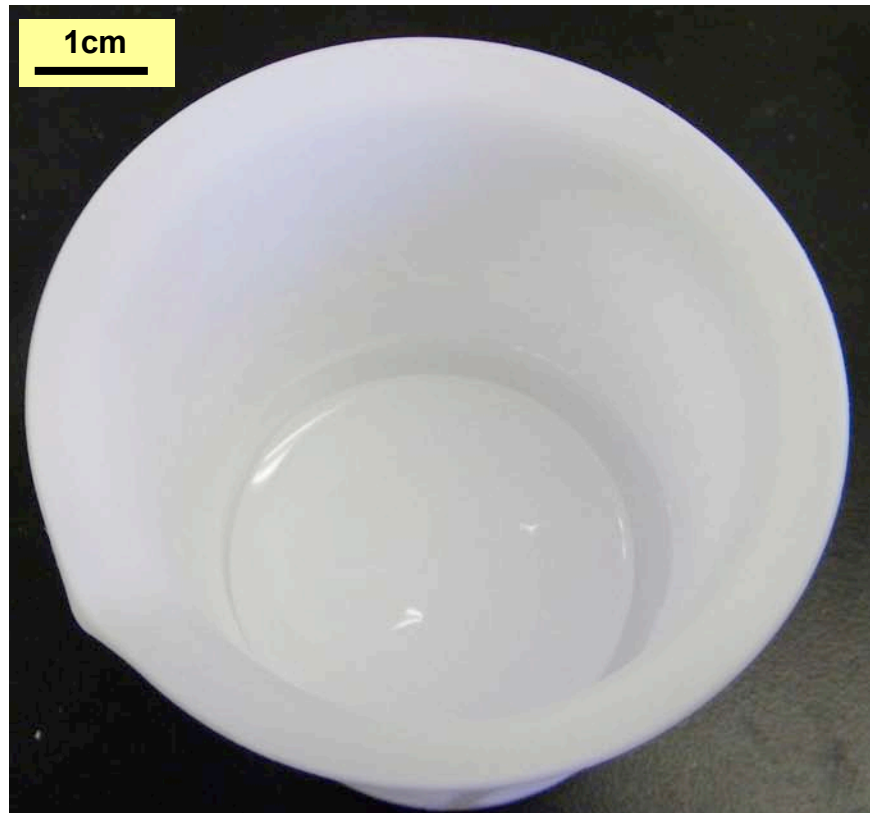


**Figure 3-1 45S5 gel which formed after keeping sol for 5 days at room temperature.**



Figure 3-2 45S5 dried gel which formed after keeping sol for 1 day at 120°C temperature.

### 3.2 *In vitro* bioactivity testing

Corrected simulated body fluid (SBF) was used to evaluate bioactivity of both bioglasses. This solution has an ionic composition similar to that of human blood plasma which was discussed before and is widely used for testing the dissolution rate of bioactive materials. Reaction of SBF with body fluid forms HA or HCA on glass surfaces which are essential for osteoproduction. Bioactive glass powders were immersed in SBF for various times up to 21 days with powder: SBF ratio of 0.002 gml<sup>-1</sup> at body temperature (36.5°C) in petri dish (50ml volume). SBF buffer solution was changed every three days to have fresh reactive ions always present reacting with powder. Finally the powders were rinsed with deionized ultra-filtered water (DIUF, Fisher) to prevent further reaction and then dried in oven at 120°C for one day.

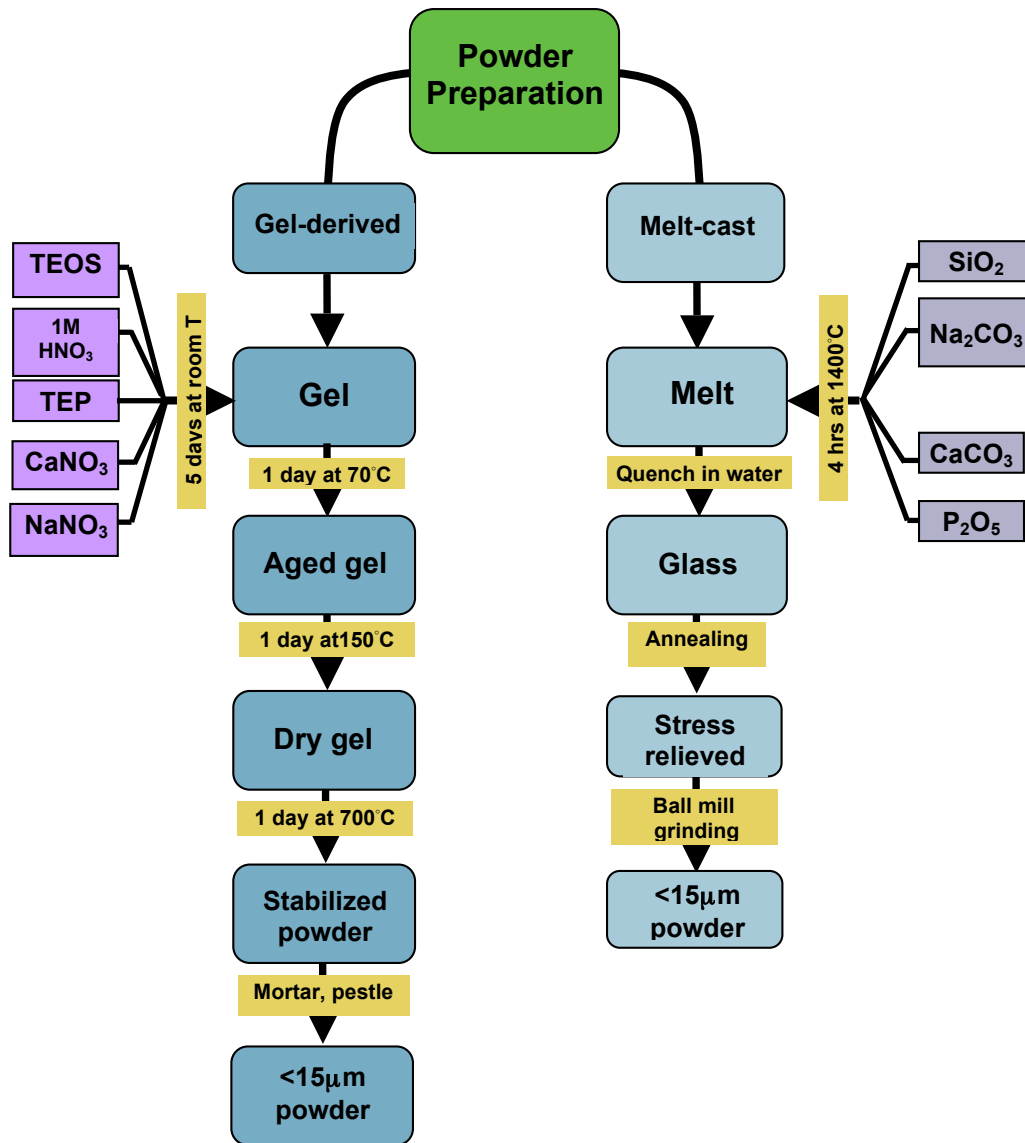


Figure 3-3 Flow chart of bioactive glass 45S5 preparation techniques

### 3.3 Characterization

#### 3.3.1 Particle size distribution (PSDA)

Particle size distribution was carried out by laser diffraction technique (Mastersizer 2000). In this method the particles are suspended in a liquid like alcohol or water and after that passed through a laser beam which scatters light in an angle related to the particle size. Scattered light form a series of concentric rings with different intensities. Generally larger particles scatter strongly and at

lower angles. Figure 3-4 shows the relation of particle size and scattered angle of anatase (titanium oxide mineral) in water. By having this knowledge and the assumption of spherical particle morphology, the distribution of particle size can be obtained. The main result for this test is  $d(0.5)$  –the volume median diameter which shows that 50% of the distribution is above and 50% is below this value.

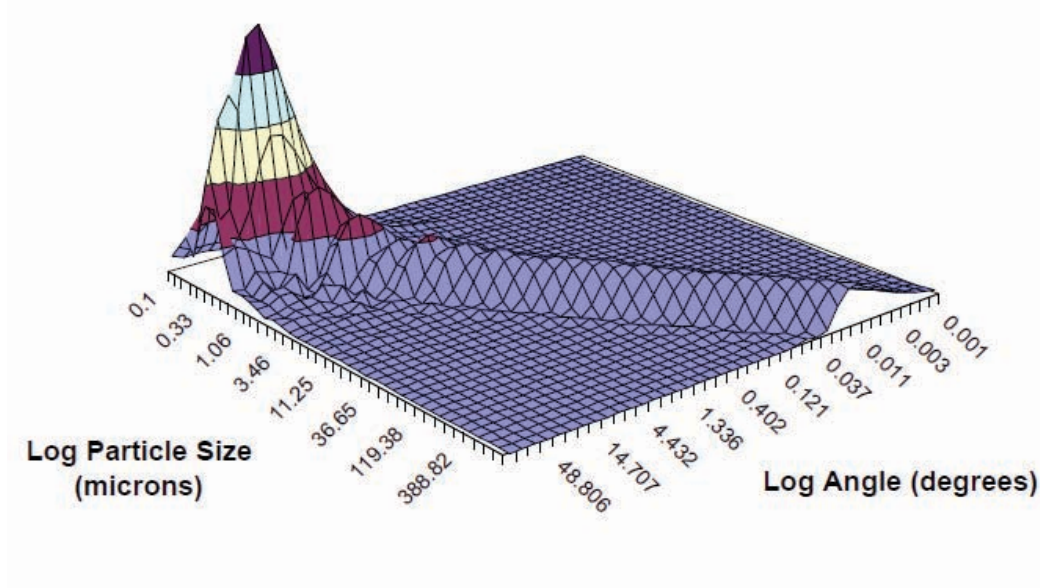


Figure 3-4 Light scattering energy as function of particle size and observation angle [46].

### 3.3.2 BET

BET is a familiar method for measuring specific surface area of particles, which is based on the theory stated by Brunauer, Emmett and Teller. In this method the sample is initially heated while simultaneously under vacuum to remove adsorbed gasses from the sample. After that it will be cooled by liquid nitrogen (73K). By introducing an inert gas (like nitrogen) over the surface of the cooled sample, gas will be adsorbed. Since the process temperature and the volume of chamber is constant, by varying the gas pressure, the pressure that adsorption and desorption of gas is isotherm can be found due to the ideal gas law:

$$PV=nRT$$

Where  $P$  is absolute pressure,  $V$  is volume,  $n$  is number of atoms,  $R$  is the gas constant ( $8.13 \text{ J/K.mol}$ ) and  $T$  is absolute temperature of gas.

By this technique the number of atoms absorbed on surface can be measured. Knowing the area occupied by the adsorbate molecule (e.g. for nitrogen:  $16.2 \text{ \AA}^2$ ), the total surface area can be determined.

To analyze the surface area of the bioglasses a Quantachrome Autosorb 1 MP automatic gas adsorption system was used. The system is dedicated to standard measurements of nanostructured materials by nitrogen sorption isotherms at  $77 \text{ K}$ . Multipoint BET surface area measurement was done using ASIWin, version 1.5, software which supports the BET data reduction algorithm. Samples were degassed at  $500^\circ\text{C}$  under vacuum.

### **3.3.3 DSC-TGA**

Differential scanning calorimetry (DSC) and thermogravimetric analysis (TGA, TA instrument SDT Q600) were carried out on sol-gel powder before stabilization to understand the transformations and temperatures of interest including weight loss up to  $1400^\circ\text{C}$  with a heating rate of  $5^\circ\text{Cmin}^{-1}$ .

DSC is a thermal analysis technique used to measure changes in heat flows associated with thermal material transformations. This measurement provides data on endothermic and exothermic processes occurring in the sample. It is typically used to find glass transition temperature, crystallization temperature and other transitions such as melting happened in glasses. In this test the material is weighed and placed into DSC sample cup. The sample cup and an empty reference cup are put into the DSC apparatus. Then the cups are heated at the same controlled rates. The differential heat flow between sample and reference are monitored and subsequently the obtained heat flow can demonstrate transformations as a function of temperature. The heat flow at any temperature is related to the difference in the heat flow of the reference and the sample. The area under the heat flow curve represents the enthalpy change associated with the thermal transition.

TGA shows the weight loss of the sample as function of temperature at a uniform heating rate and specific environment. In this test the sample is weighed carefully and placed in the cup. There will be a balance which reports the weight change of sample while the temperature is increased. Finally the TGA curve shows the weight change during increasing temperature.

### **3.3.4 XRD**

X-ray diffraction (XRD) technique (Rigaku Rotaflex) was used to analyze the crystalline phases and structures present in samples before and after immersion in SBF. The diffractometer was operated at 40KV and 110mA at  $2\theta$  range of  $10-110^\circ$  with step size of  $0.02^\circ$  by using copper anode as target.

This technique operates with respect to the wave nature of X-rays which are diffracted by the lattice of the crystal. The diffraction obeys Bragg's relationship:

$$n\lambda=2d\sin\theta$$

where  $n$  is number of planes,  $\lambda$  is wavelength of X-rays,  $d$  is distance between two planes in crystal lattice and  $\theta$  is diffraction angle.

This equation shows that for a specific crystal structure, there is a specific diffraction angle and attained angles are characteristics of specific phases which can be found by comparing patterns with reference cards. The detector moves around the sample and collects all the diffracted waves in different angles. Comparing the resultant pattern with standards one can identify of different crystalline structures.

### **3.3.5 FTIR**

Surface reactions due to immersion in SBF and formation of an apatite layer was studied with Fourier transform infrared spectroscopy (FTIR, Nicolet Magna 750) in the range of  $3600-400\text{cm}^{-1}$  using KBr pellet as background. Spectra were collected in absorbance mode. FTIR was also helpful in understanding the amorphous phases which were not detectable in XRD.

FTIR relies on the fact that atomic bonds vibrate at characteristic frequencies which produces a unique identification of that bond. Bonds absorb, transmit, and reflect the incident infrared energies at their characteristic frequencies. After that the infrared transmittance and absorbance at different frequencies will be translated and transformed to an x-y plot by Fourier transformation which is called FTIR spectra.

### **3.3.6 SEM-EDS**

Scanning electron microscopy (SEM) and energy dispersive X-ray analysis (EDS) techniques (JEOL 6301F) were used to understand the morphology and size of particles and apatite layers formed on their surfaces, and compositional change after immersion in SBF. Samples were chromium coated to increase conductivity (Edwards XE200 Xenosput). 20KV accelerating voltage was used for EDS analysis and 5 KV for SEM images to reduce charging of powder specimens. EDS was helpful to study the surface layer composition of particles in order to quantify the composition trends between gel-derived and melt-cast samples.

In SEM, electrons are used to form an image instead of light. Penetration of electrons into the conductive material can represent contrast in atomic weight (backscatter electron mode) and topography (secondary electron mode). The resultant electrons will be collected by the detector to form an image. Images were taken by using secondary electrons.

EDS is a chemical microanalysis technique used in conjunction with SEM. In this method, the x-rays emitted from sample, due to the high energy electron beams are detected. When the sample is bombarded by electrons, electrons will be ejected from atoms. This will result in filling these empty places by electrons at higher states and emitting x-rays to balance the energy difference between the two electron states. The energy of the emitted x-ray is the characteristic of atom and will be collected by detector and forms a peak in the spectrum. Resolution of this method depends on interactions volume and depth of penetration of electrons in the sample which is usually around 1-3 $\mu\text{m}$  [47]. This method is usually known as

a non-accurate technique for measuring composition of elements. It was shown that there might be a relative error of  $\pm 6$  of the amount present, which can change due to atomic weight and concentration of that element [48]. Therefore it is needed to analyze EDS results beside other results achieved by other techniques such as XRD. Each sample was tested once.

Another parameter that reduces the accuracy of EDS mapping in this research, relates to the surface roughness of powder. It is advised to use the surface as flat as possible for impacting the electrons. This will help to reduce the effect of topography on the results. Thus, the mentioned error might increase while using EDS on powders and it is needed to use other techniques to confirm EDS results.

#### **3.3.6.1 EDS mapping**

EDS mapping is a technique used for studying the elements which are present in a field of view in a particular SEM micrograph. In this test, the dispersion of a specific element on the surface will be studied by using EDS on whole surface represented in SEM. The concentration of elements is shown by marking dots on the micrograph. Therefore, the higher the number of dots means the higher the concentration of element on that region. Using EDS for mapping is not as accurate as other methods such as Auger electron spectroscopy or XPS, so this technique is needed to be used just as a proof of other experiments. As, mentioned before, large error bars of EDS technique leads to less accuracy of results achieved in mapping.

## 4 Results and discussion

### 4.1 *Crystallization and stabilization of gel-derived 45S5*

As discussed before, stabilization is essential for removing compounds related to sol-gel processing and silanols out of the dried gel. DSC-TGA, XRD and FTIR test were performed to understand the best stabilization temperature and final structure.

#### 4.1.1 *DSC-TGA*

Figure 4-1 represents DSC-TGA curves of dried gel up to 1400°C. By analyzing both graphs, the physiochemical processes which occurred on the sample can be characterized. Table 4-1 briefly explains transformations occurred during heating.

TGA data shows more than 50% weight loss, by rising temperature up to 700°C. Also DSC curve illustrates some endothermic and some exothermic peaks related to phase transformation and mass loss. First peak is a small endothermic one at around 60-150°C. From the TGA graph, about 8% weight loss could be emphasized by removal of absorbed water and other liquids. The other peak at 230°C with 12% weight loss refers to removing water from further condensation of precursors and catalyst out of sample. These two peaks are endothermic because heat is needed to overcome the latent heat of evaporation. As mentioned before, the stabilization temperature needs to be more than 400°C so that removing trapped water becomes irreversible. So, if heating be stopped at 230°C, it is possible that the powder could reabsorb water and other liquids again. Endothermic peaks at ~1300°C correspond to melting of glass (heat of melting).

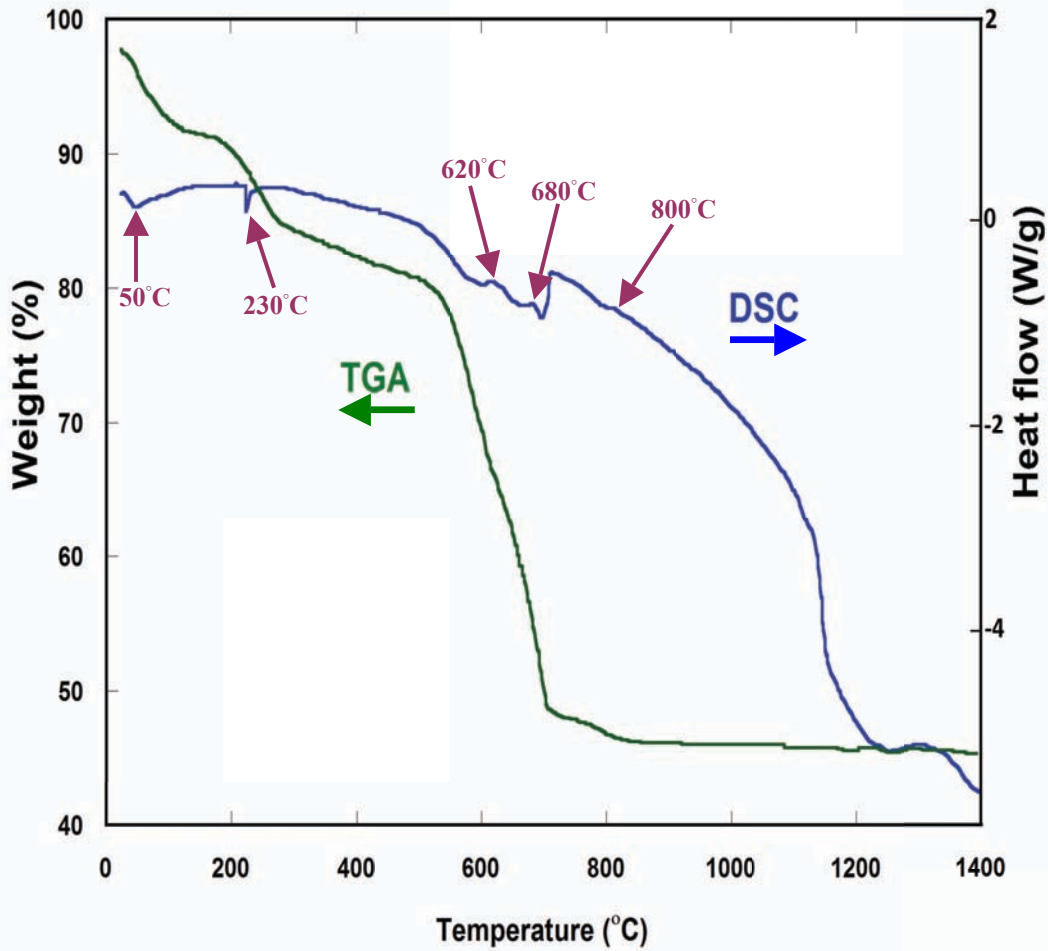


Figure 4-1 DSC-TGA of unsterilized 45S5 prepared by sol gel method.

Table 4-1 Brief explanation of DSC-TGA curve of gel-derived 45S5

Temperature (°C)	% wt. loss	Event
60- 150	8	Free water evaporation
230	12	Bound water removed
600-750	30	-Nitrogen compounds removed - Silanols removed -Combeite crystal formed
800	0	Phosphate rich crystal formed
1300	0	Melt

Figure 4-1 also exhibits one vast endothermic and two exothermic peaks at 600-750°C range which play a great role on the crystallinity of gel-derived 45S5. The TGA curve shows a high amount of weight loss (~30%) around this temperature range. The TGA graph shows no weight loss after 700°C which means stabilization of gel-derived 45S5 is finished at 700°C (for a heating rate of 5°C/min). Also phase transformation and crystal formation are indicated by exothermic peaks at 620°C and 680°C. This graph shows that crystallization and the nitrate release temperature overlap. DSC-TGA curves illustrate that stabilization temperature of more than 650°C is needed to remove all nitrogen rich compounds and silanols out of the sample. Nitrogen content compositions are removed concerning to the mentioned endothermic peak and TGA curve (~30% weight loss discussed before).

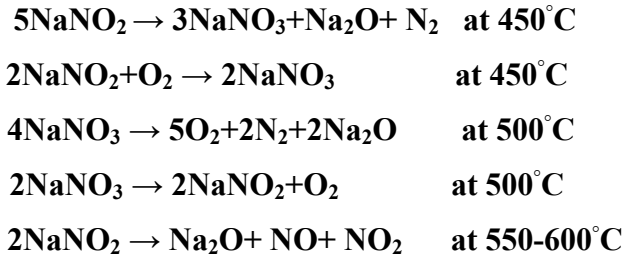
In addition, there is a small exothermic peak at 800°C which might be related to the crystallization of a phosphate rich phase in 45S5. As discussed before, this crystallization occurs at temperatures more than 800°C after a long time [11]. A potential reason why this peak is small might be related to the heating rate and lack of time for crystallization.

#### **4.1.2 XRD**

XRD was performed to understand the crystals which form in gel-derived samples, before and after stabilization. Figure 4-2 shows XRD patterns of gel-derived samples with various stabilization temperatures after a heating rate of 1°Cmin<sup>-1</sup> and a dwell of 1 day at the stabilization temperature.

XRD patterns show that the nitrate phase which formed during sol-gel processing is sodium nitrate (NaNO<sub>3</sub>). This phase is present in the sample, before stabilizing and at temperatures up to 600°C. The temperature required for removing this phase is lower than what was shown in DSC curve and this is because of higher heating rate of sample tested by DSC (5 °C/min vs. 1 °C/min) . But the sample which was tested by XRD was kept for 1 day at the stabilization

temperature and there was enough time for nitrates to escape from the sample. A sequence of probable reactions which occurred and resulted in decomposition of sodium nitrate is:



These reactions help to explain the DSC-TGA results and demonstrate that nitrogen leaves the sample in the form of NO and NO<sub>2</sub>.

At 600°C, crystalline phase combeite Na<sub>2</sub>Ca<sub>2</sub>Si<sub>3</sub>O<sub>9</sub> (PDF#075-1687), starts to form and consequently leaves amorphous phosphorous rich phase in the matrix. Combeite has the hexagonal structure as shown by Fischer *et al.* [49]. A maximum amount of crystalline combeite (~80mol %) will form at 700°C due to depleted CaO. The remaining 20% of the structure should include an amorphous phosphorous rich matrix with no calcium. Since complete crystallization of combeite overlaps with formation of another phase and crystallization rate of combeite slows with time due to less available calcium, it was not possible to form a 100% combeite structure. Figure 4-3 refers to other heat treatments performed on raw sample at lower temperatures and stabilization time. As could be seen, although the intensity of sodium nitrate decreased during this procedure, combeite is formed and it is possible to detect both phases in one sample.

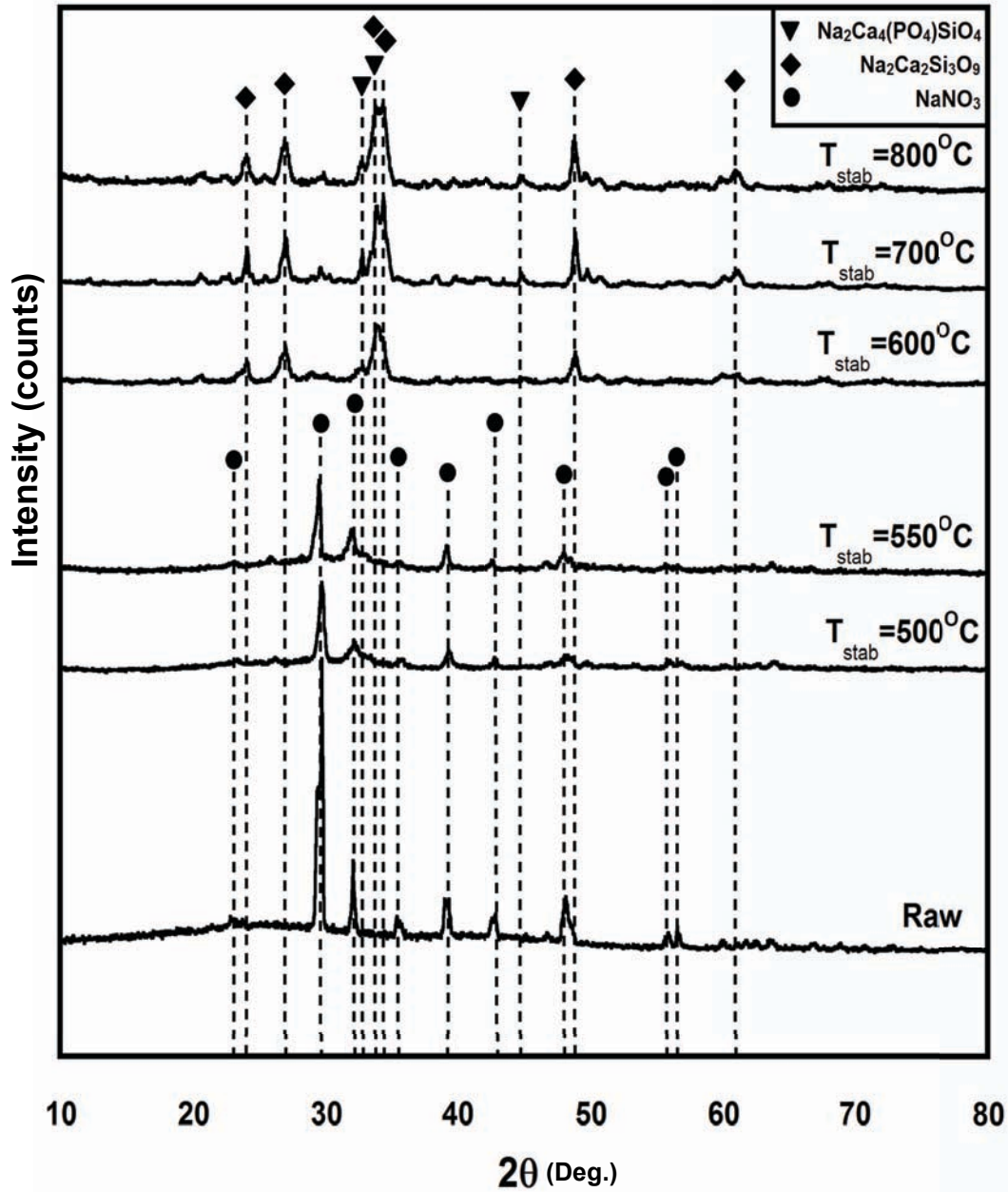


Figure 4-2 X-ray diffraction pattern of 45S5 prepared by the sol-gel method as function of stabilization temperature.

Placing the sample at temperatures more than 800°C for long time leads to formation of crystalline apatite-like phase as discussed before. It is expected that the high temperature crystal phase be phosphate base due to the phosphorous rich glass which remains after crystallization of combeite. The main problem of detecting the newly formed crystals is related to their low amount and difficulty in

detecting it in XRD due to low intensity of peaks. Silicorhenanite  $\text{Na}_2\text{Ca}_4(\text{PO}_4)_2\text{SiO}_4$  (PDF# 032-1053) was the best match found for the crystalline phase at  $800^\circ\text{C}$ . It has hexagonal structure which is represented by Kapralik *et al.* [50]. As mentioned before, after combeite formation, there should be no calcium present in the amorphous phosphorous rich phase. The presence of calcium in the higher temperature crystalline phase might be because there was not enough time for full crystallization of combeite. For better assessment of this transformation, raw powder was kept at  $550^\circ\text{C}$  for phase separation of silicon and phosphorous rich regions and then immediately heated to  $900^\circ\text{C}$  for 12hrs. The idea was to not give enough time for combeite formation. The result is shown in Figure 4-4. The main difference from the sample stabilized at  $800^\circ\text{C}$  with slow heating rate was the separation of two main peaks at around  $33^\circ$ . Lefebvre *et al.* [11] stated that this is due to a variation of lattice parameter rather than to phase change. They showed that  $a$  decreases with temperature while  $c$  increases. This change in lattice parameter is due to the formation of silicorhenanite at  $800^\circ\text{C}$ . This phase is isostructural to apatite (combeite) and after nucleation of this phosphate rich crystal it will lead to expansion of combeite in  $c$  axis while the other direction will contract. Lefebvre *et al.* [11] showed that 75% of phosphorous ions are in the crystalline phosphate phase which is an orthophosphate ( $\text{PO}_4^{3-}$ ). It indicates that at around  $800^\circ\text{C}$ , orthophosphates will migrate into silica network and they will replace  $\text{SiO}_4$  groups. So, the mentioned expansion is attributed to a larger size of orthophosphate rather than silica. Therefore it could be concluded that this peak separation is another proof of phosphate rich crystal formation at higher temperatures.

Other kinds of tests like FTIR might help to achieve more information about the secondary phases formed during 45S5 crystallization.

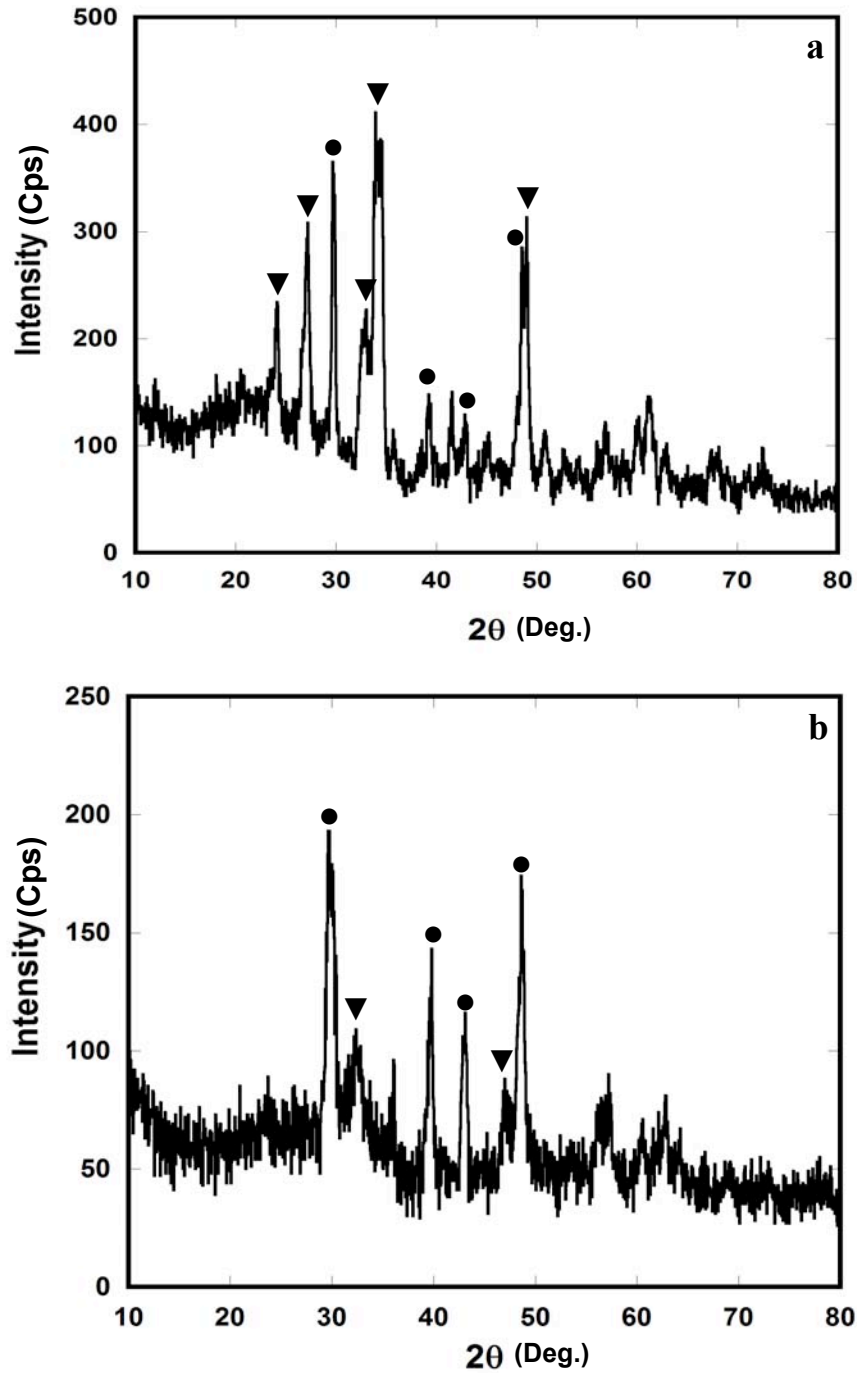


Figure 4-3 XRD pattern of raw 45S5 stabilized: a. 6 hrs at 600°C b. 18hrs at 500°C and 6 hrs at 500°C. b shows lower intensity of peaks but still formation of combeite could be seen (▼ : combeite and ● : nitrate)

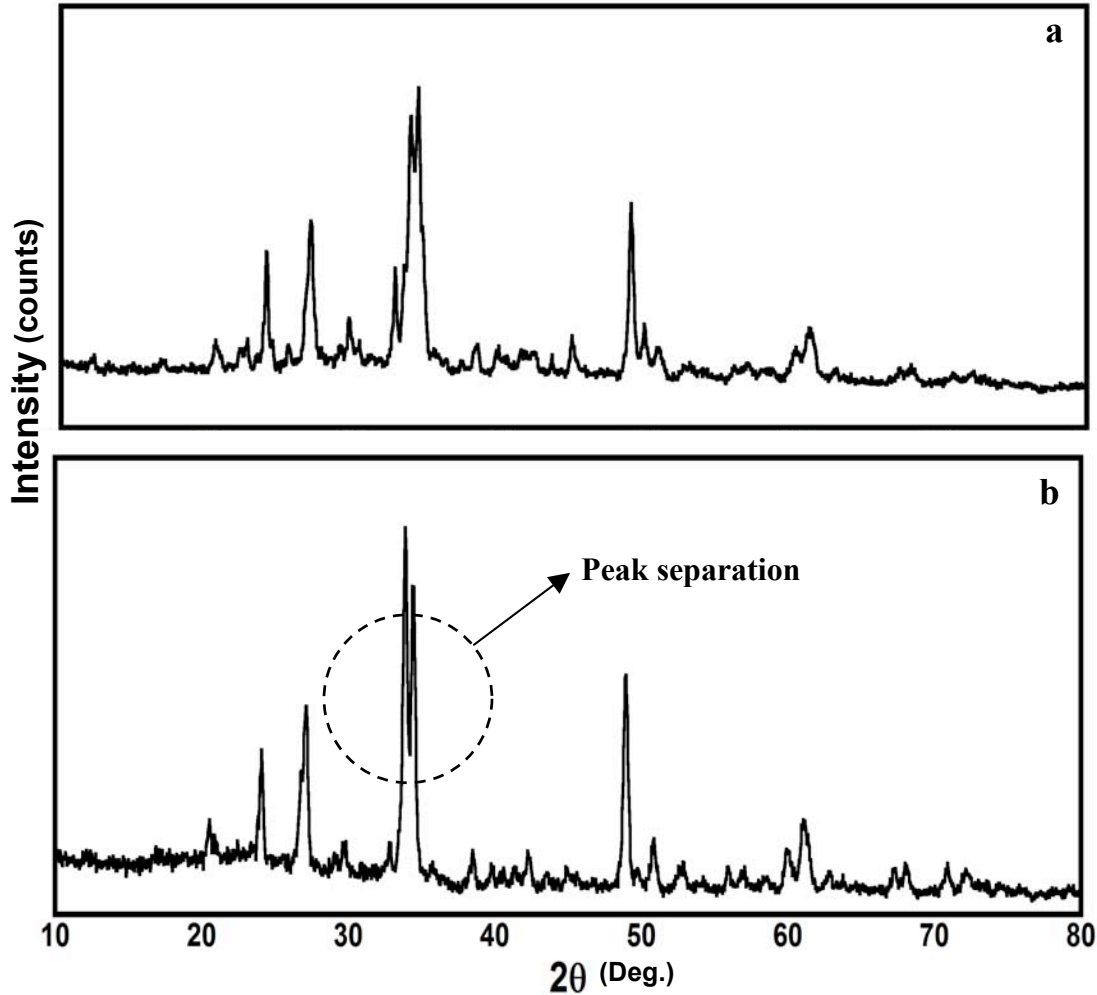


Figure 4-4 XRD of gel-derived 45S5, a. stabilized at 700°C b. stabilized 12hrs at 550°C for phase separation and then kept at 900°C for 12hrs. Peaks are related to combeite phase.

### 4.1.3 FTIR

Figure 4-5 shows the FTIR result of sample stabilized at 800°C where the presence of peaks with 520, 580 and 620  $\text{cm}^{-1}$  wave numbers correspond to crystalline bonds of P-O bending [10, 13]. The presence of these Si-O peaks which are related to combeite, confirm XRD results.

The peak at 880  $\text{cm}^{-1}$  corresponds to the Si-O stretch which is attributed to the silicon bond of phosphorous rich phase [13]. This phase hardly could be detected in 700°C stabilized sample which was supposed to be crystallizing with just combeite. In contrast to the work of Li et al. [36], which stated that the apatite

phase that form at 800°C is  $\text{Ca}_{10}(\text{PO}_4)_6$ , the 880  $\text{cm}^{-1}$  peak and XRD results show that the formed apatite contains silicate. Two small peaks at 696 and 729  $\text{cm}^{-1}$  are related to stretch Si-O bonds which attribute presence of crystalline silicate in the structure [51].

Finally the high intensity peak at 926  $\text{cm}^{-1}$  is attributed to the Si-O bond with non-bonding oxygen. High intensity of this peak is due to the crystallization of combeite [13].

Reports show that phosphor in solid solution has higher effect on dissolution rate, so formation of this apatite-like phase reduces bioactivity [11]. To avoid this apatite phase formation or reducing this crystallization, stabilization temperature should be decreased.

Assessing all results from DSC-TGA, XRD and FTIR show that best stabilization temperature, with highest apatite formation rate and removing all nitrogen content compositions should be around 700°C.

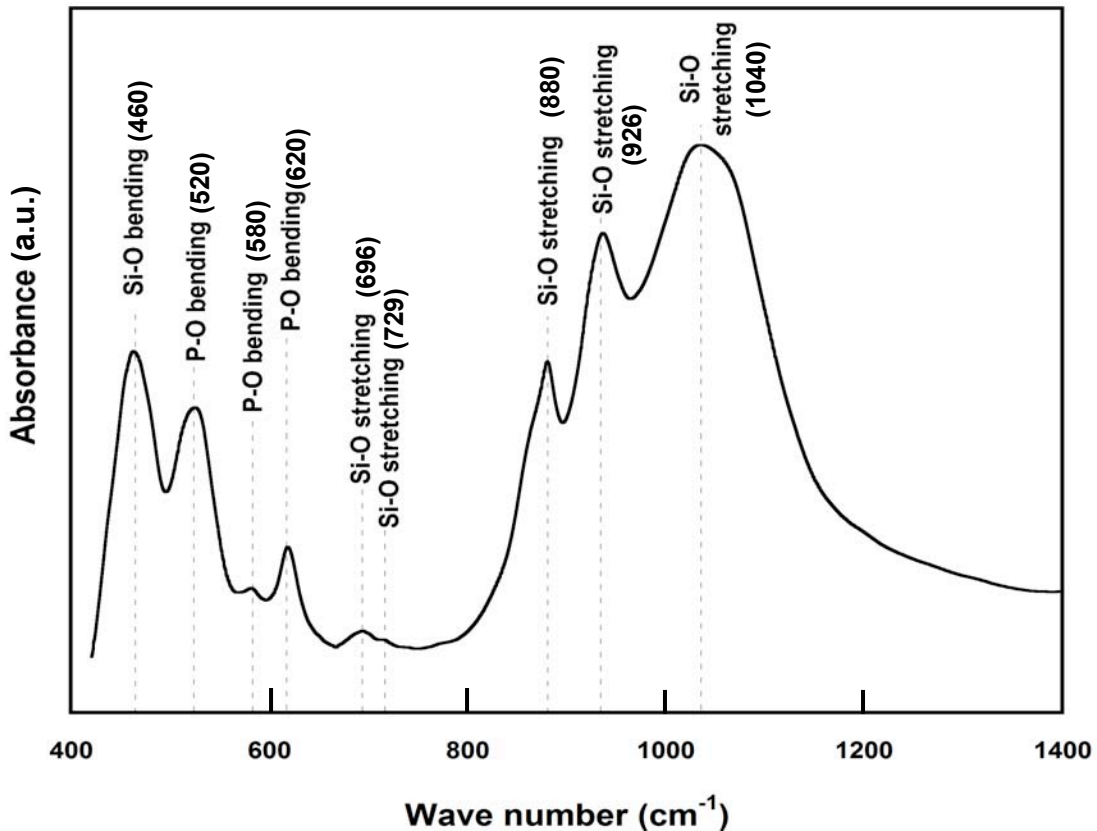


Figure 4-5 FTIR spectra of gel-derived 45S5 with  $T_{\text{stab}}=800^\circ\text{C}$ .

#### 4.1.4 EDS mapping

EDS mapping was carried out to study the elemental distribution after manufacturing crystalline 45S5. The main point of this test was to determine the composition of amorphous phase which remains after formation of crystalline combeite in 45S5. As discussed before, low accuracy of this method only allows for semi-quantitative analysis and is best interpreted when combined with other test methods to determine trends.

It is expected that in the region which phosphorous is concentrated, there would be no calcium as discussed in previous section, and probably no silicon. Figure 4-6 shows the map of a specific region in gel-derived 45S5. As could be seen there are some regions which the concentration of phosphorous is much higher, which could be related to the amorphous region. EDS mapping also shows that in the phosphorous rich regions, there is no calcium (as expected) and also no silicon; all the calcium and silicon was consumed for crystallization of combeite and the amorphous phase contains phosphorous and sodium, which is supports theoretical predictions mentioned before about the compositional changes following 45S5 crystallization. Li *et al.* [36] stated that the dissolution of crystalline 45S5 does not occur in the phosphorous rich region. It was also shown by Nychka *et al.* that elements not involved in the formation of combeite, such as phosphorous, could migrate to grain boundaries and alter dissolution, i.e., dissolution could preferentially occur near the grain boundary due to compositional changes. The slight increase in density after crystallization, which leads to development of some residual tensile stress around the grain boundary, could also contribute to dissolution; tensile stresses enhance dissolution of bioglass while compressive stresses reduce dissolution. Thus, it is expected to observe first stages of interfacial reaction around the phosphorous rich regions (grain boundaries) [52].

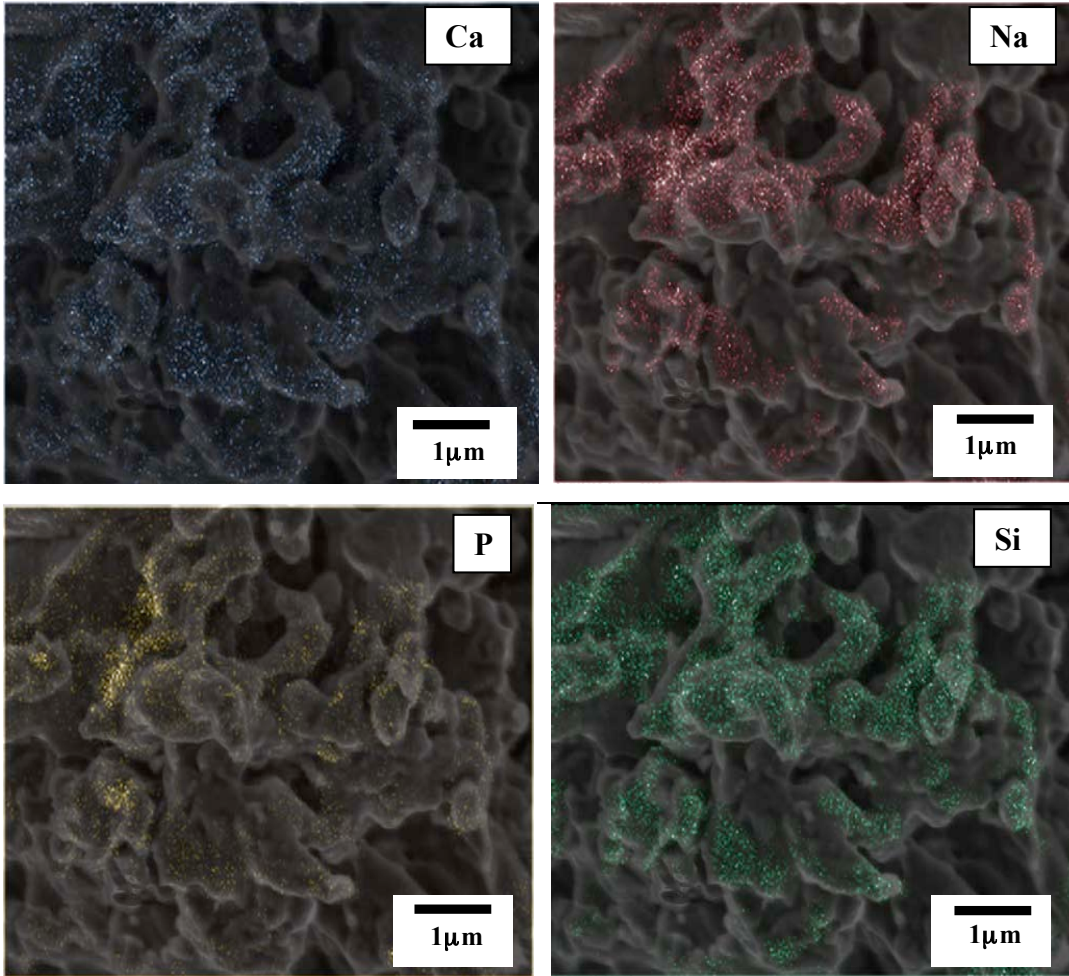


Figure 4-6 EDS mapping of gel-derived 45S5. Color points are related to elements. Calcium and silicon were not detected in phosphorous rich regions.

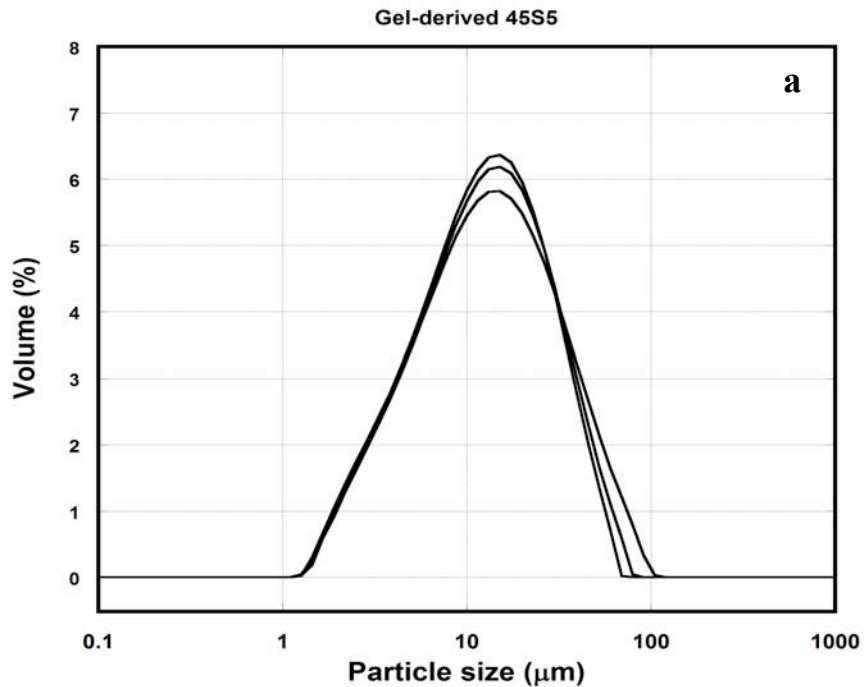
## 4.2 Particle size distribution

Ground gel-derived and melt-cast powder size distributions were measured by assuming particles are spherical. This assumption might not be accurate for melt-cast 45S5 as will be shown later, but since it is the universal method for measuring particle sizes, it was used to measure particle size of powders. The SEM images which will be shown in next section indicate that the PSDA results are close to reality. The main purpose of this test was to be sure that the size of tested powders had equivalent size. This test was performed 3 times for each sample and the results are shown in Figure 4-7. The detailed results are shown in

Error! Not a valid bookmark self-reference.. Generally it could be expressed that the particle size of all tested samples were close (particle size around 10  $\mu\text{m}$ ) and could be tested under similar conditions.

**Table 4-2 Particle size distribution analysis of 45S5 and 58S bioactive glasses**

Sample	Median particle size d (0.5) ( $\mu\text{m}$ )			Average median particle size ( $\mu\text{m}$ )	Standard deviation
Gel-derived 45S5	12.2	11.8	11.4	11.8	0.4
Melt-cast 45S5	8.4	7.8	7.8	8.0	0.3
Gel-derived 58S	7.9	8.0	7.6	7.8	0.2



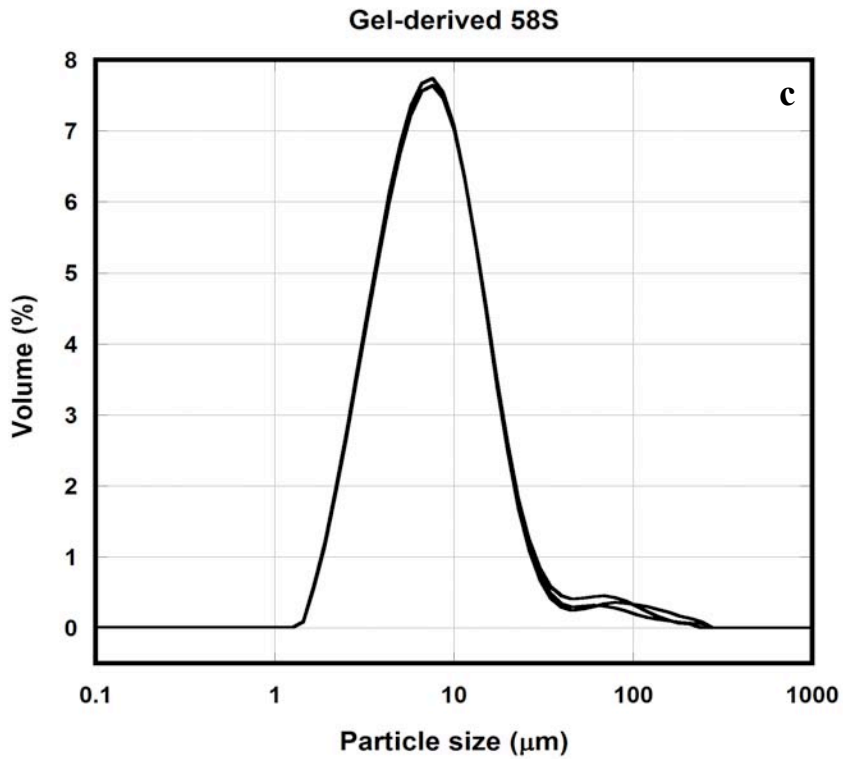
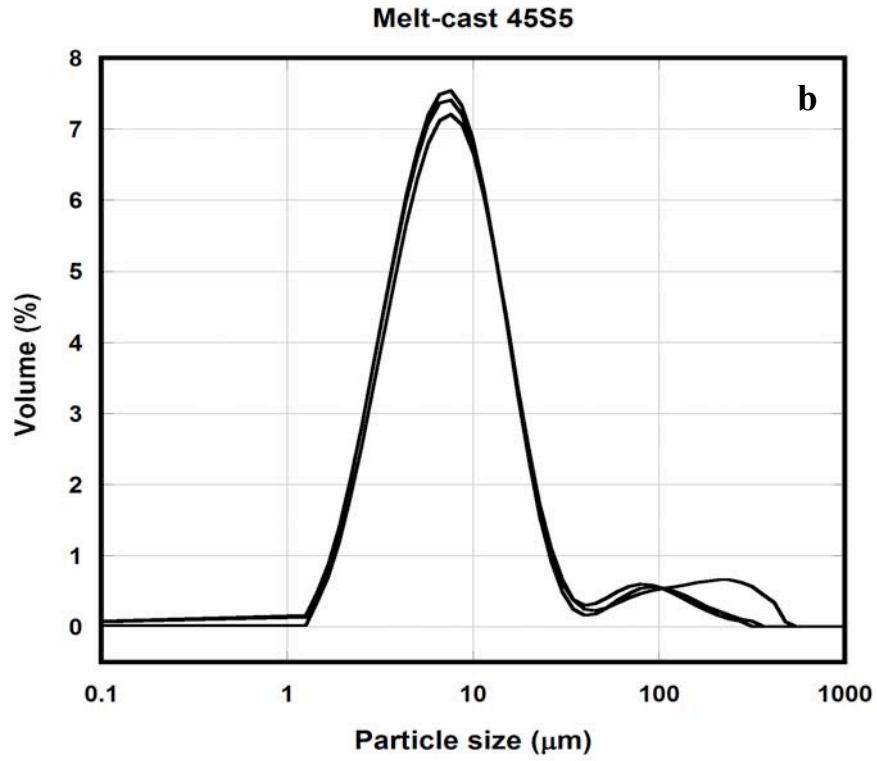


Figure 4-7 Particle size distribution of a. gel and b. cast derived 45S5 and c. gel-derived 58S.

#### 4.2.1 SEM

Figure 4-8 illustrates the SEM image of the powder particle size distributions at low magnification. As shown by particle size distribution analysis, most particle sizes of gel-derived powder are around 10  $\mu\text{m}$  (8-12  $\mu\text{m}$ ) while melt cast powder shows various particle sizes. Some particles are around 1  $\mu\text{m}$  but some are larger than 10  $\mu\text{m}$ , but as discussed before the average is around 10  $\mu\text{m}$ . Besides gel-derived powder seems to be spherical while in melt-cast powder different shapes of particles could be found.

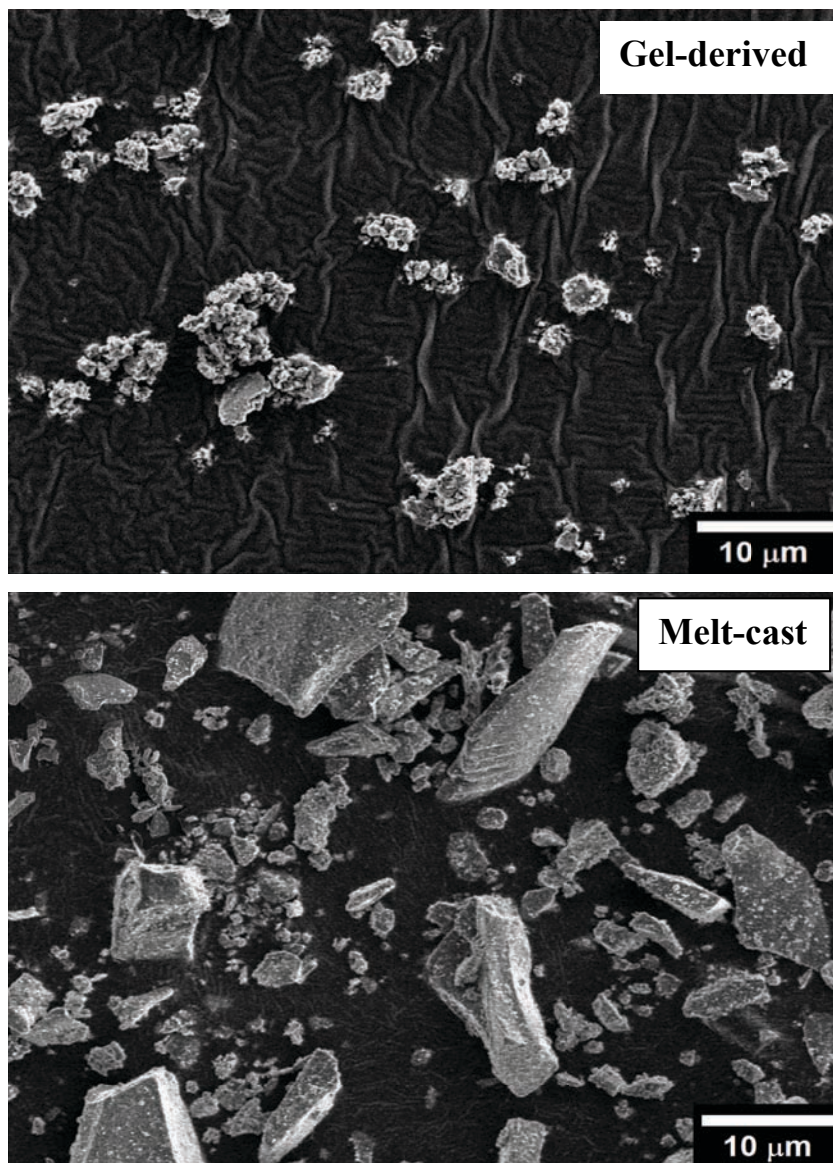


Figure 4-8 SEM micrograph of particle distribution of gel and melt-derived 45S5 powders.

### **4.3 Surface area**

#### **4.3.1 BET**

BET test is usually carried out to determine the specific surface area of specimens. The specific surface area of melt-cast 45S5 was measured and it was  $3.7 \text{ g/m}^2$ . As discussed in the experimental chapter, before taking the test, the sample needs to be heated up to high temperatures to remove impurities from the surface of the powder (degassing). This procedure takes about two hours.

Since the gel-derived 45S5 powder has a much higher surface area, it is expected that degassing time will be higher than the melt-cast powder. The sample was kept in a vacuum chamber for more than 8 hours but still degassing was continuing, and due to lack of time, and subsequent lack of equipment access, it was not possible to measure the specific surface area of the gel-derived 45S5. Previous researches of gel-derived bioglasses showed that the specific surface area of the powder should be around  $100\text{-}300 \text{ g/m}^2$  which is *much* higher than the melt-cast powders [53].

#### **4.3.2 SEM**

Figure 2-1 illustrates the SEM image of the melt and gel-derived bioglass, which shows the difference in the surface area of the product. It clearly shows the surface area of the gel-derived 45S5 is much higher than the melt-cast 45S5.

### **4.4 In vitro test**

*In vitro* tests and dissolution rate of samples were carried out by immersing cast and gel derived powders in SBF for 12, 18 hrs, 1, 3, 7, 14, 18 and 21 days. Bioactivity assessment was achieved by understanding the dissolution rate. XRD, FTIR and SEM-EDS were executed on immersed powders to understand the reactions occurring on sample during immersion. Comparison of HA formation and the rate of reaction in two samples were used to compare dissolution rate.

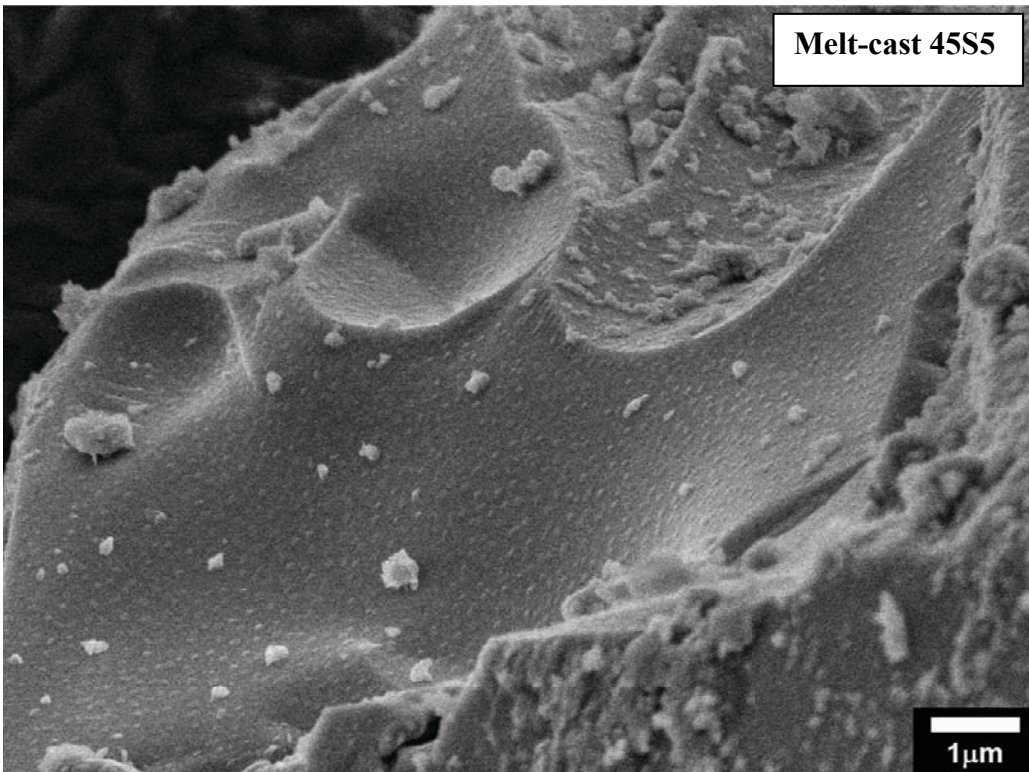
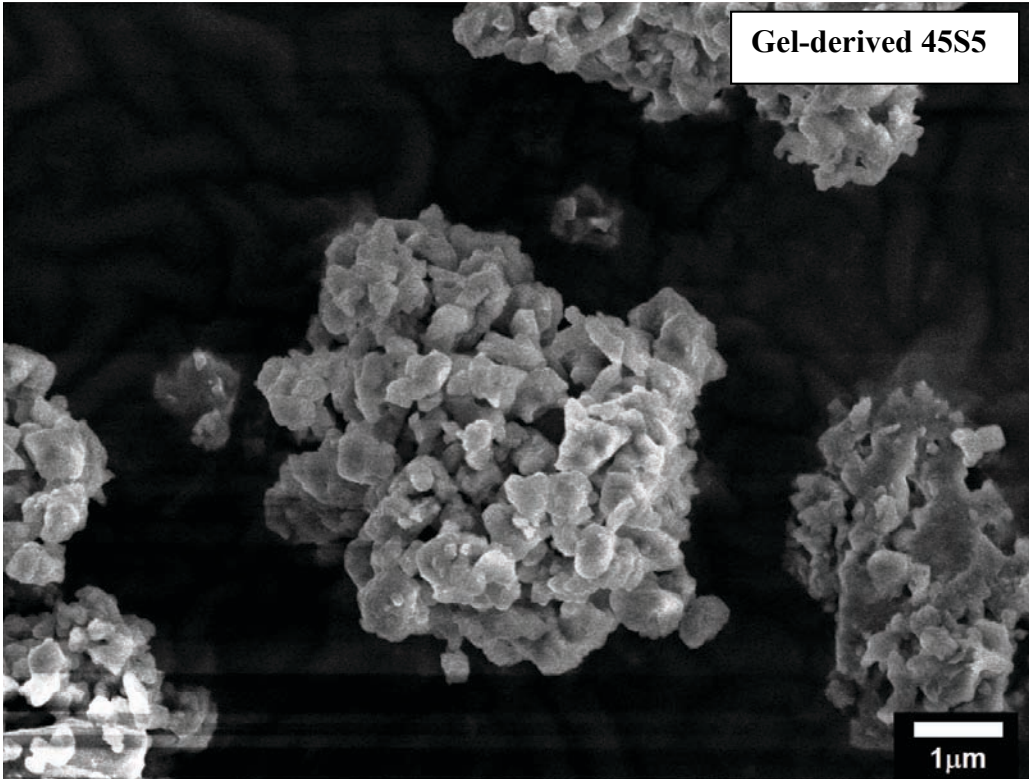


Figure 4-9 SEM micrograph of gel-derived and melt-cast 45S5 before immersion in SBF.

## 4.4.1 XRD

### 4.4.1.1 Melt-cast and gel derived 45S5

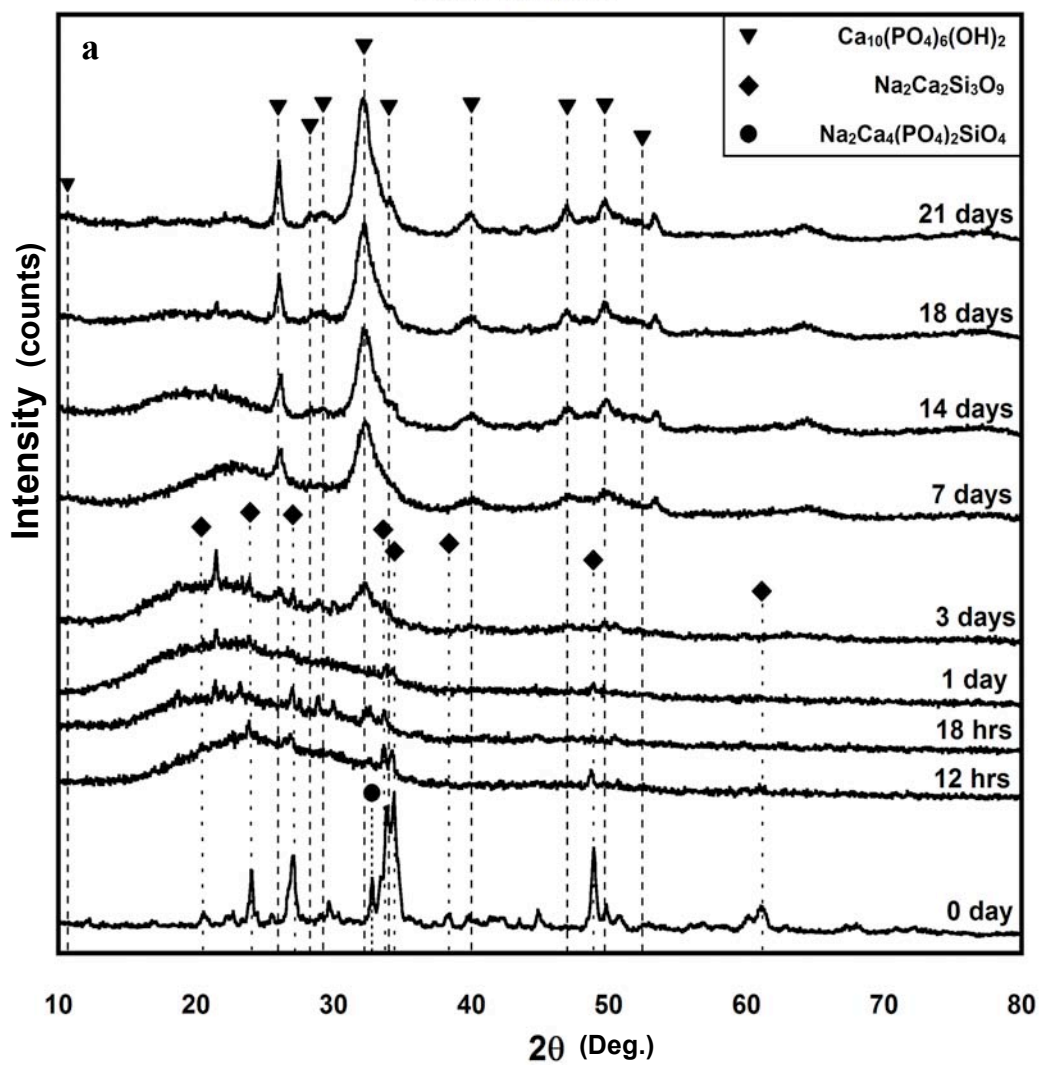
XRD results of both samples immersed in SBF for various days are displayed in Figure 4-10. Figure 4-11 represents comparison of HA formation in both samples in a smaller scale so it could be compared more easily.

Gel-derived powder shows crystal peaks of  $\text{Na}_2\text{Ca}_2\text{Si}_3\text{O}_9$  (Combeite) before immersion in SBF; this crystalline phase could be detected after 3 days of immersion. After HA covered the surface, no combeite peak could be detected.

Also in 3 days,  $\text{Ca}_{10}(\text{PO}_4)_6(\text{OH})_2$  hydroxyapatite (PDF#086-0740) starts to form and results in the growth of the main peak at  $2\theta$  around  $32^\circ$ , which indicates that HA is growing on the surface of the biomaterial. Finally after 18 days the surface was covered with HA, such that no other crystalline phases could be detected. This means that after 18 days, the thickness of hydroxyapatite is thick enough that no other glassy phases could be detected by XRD.

No strong crystalline peak could be detected in the melt cast 45S5 before immersion due to the amorphous structure, as expected. So the XRD spectra just showed a wide peak related to amorphous background. This broad peak is related to the irregular arrangement of atoms and various atomic bond lengths in glasses. This leads to detection of x-ray in different  $2\theta$ s but without detectable peaks related to the structure of material. After immersion and within 3 days the HA peak could be found in the XRD pattern. Comparing the HA peaks in both samples show that HA formation in first days of immersion is slightly faster in the melt cast powder. Presence of a broad amorphous peak even after 14 days in gel-derived powder is proof of this, where this peak is much smaller in melt-cast powder after 14 days of immersion. After the first days of reaction, the gel derived 45S5 crystal formation rate increased and at 18 days it reached to melt-cast 45S5 formation rate. Finally after 21 days both samples show similar apatite formation rates, and their surfaces are covered with HA.

# Gel-derived



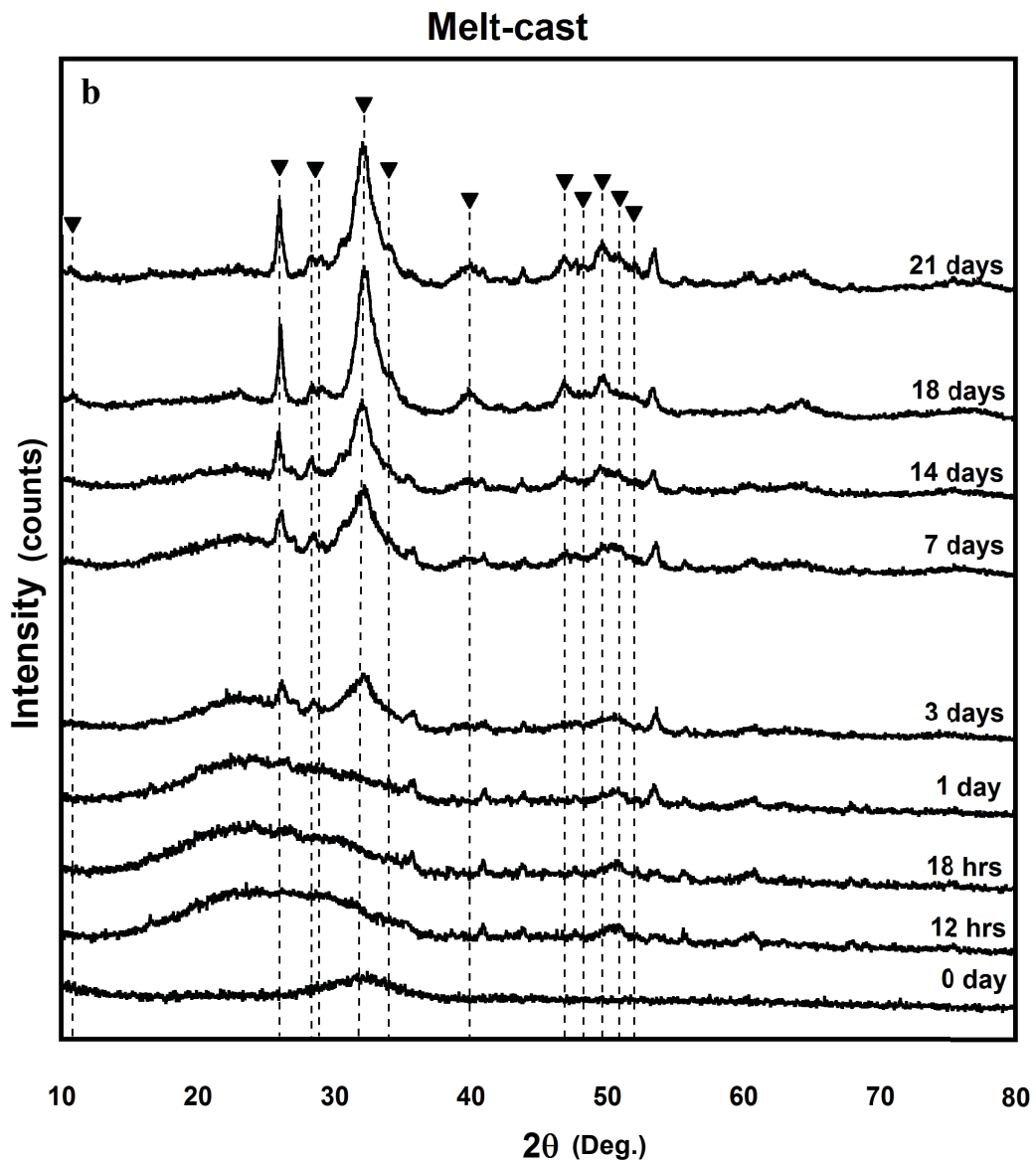
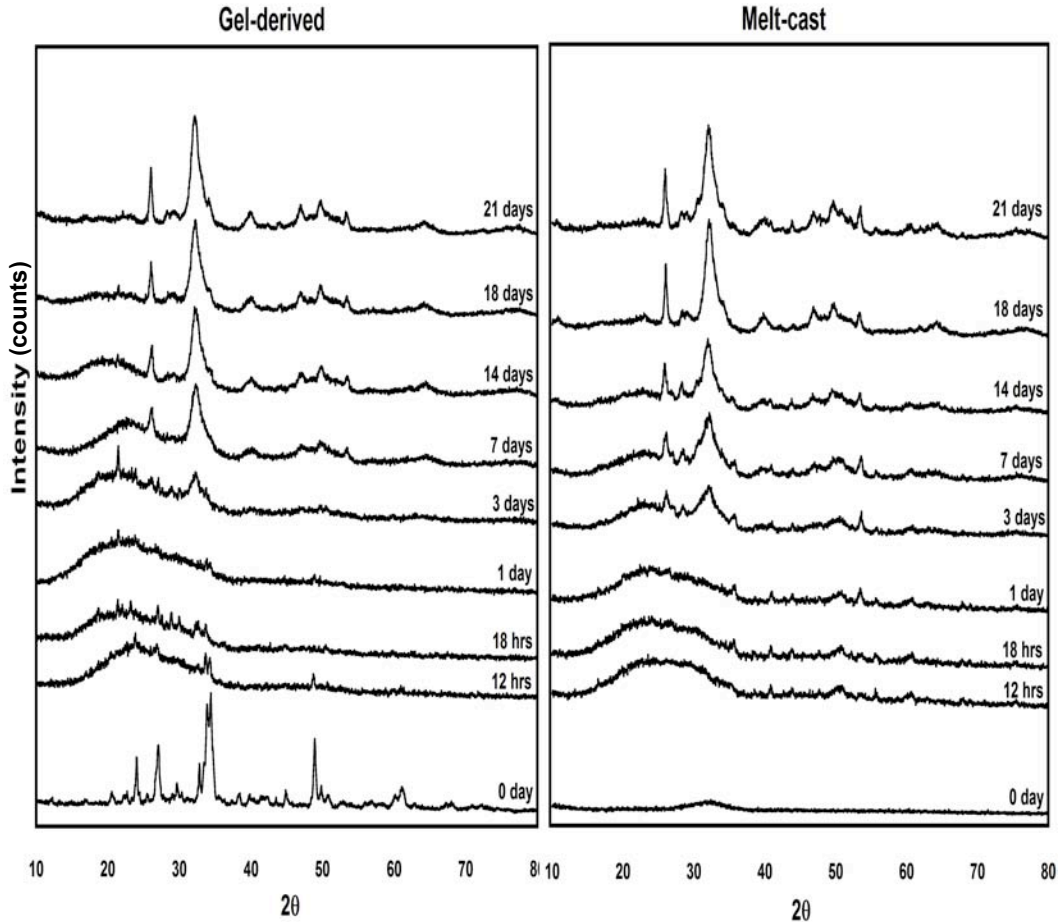


Figure 4-10 XRD spectra of immersed 45S5 prepared by a. sol-gel and b. casting in SBF as function of time.



**Figure 4-11** Brief comparison of melt and gel derived 45S5 hydroxyapatite formation rate. After one day immersion, complete peaks are not detectable in gel-derived 45S5 and after 18 days both samples show similar amount of apatite formation.

#### 4.4.1.2 Gel-derived 58S

The 58S sample was immersed in SBF as the function of time. Since this bioglass was widely tested before, in this study it will be briefly studied to compare apatite formation rate with 45S5 in the same immersion condition.

As displayed in Figure 4-12, unlike 45S5, it was possible to prepare amorphous 58S by sol-gel method. Comparison of the XRD results of 58S with 45S5 shows that just after 1 day HA peaks are detectable in 58S, but in 45S5 HA peaks could be detected after 3 days. After 14 days immersion, it seems that the surface reaction in 58S is somehow stopped and even after 21 days, amorphous background could be detected in XRD patterns.

### Gel-derived 58S

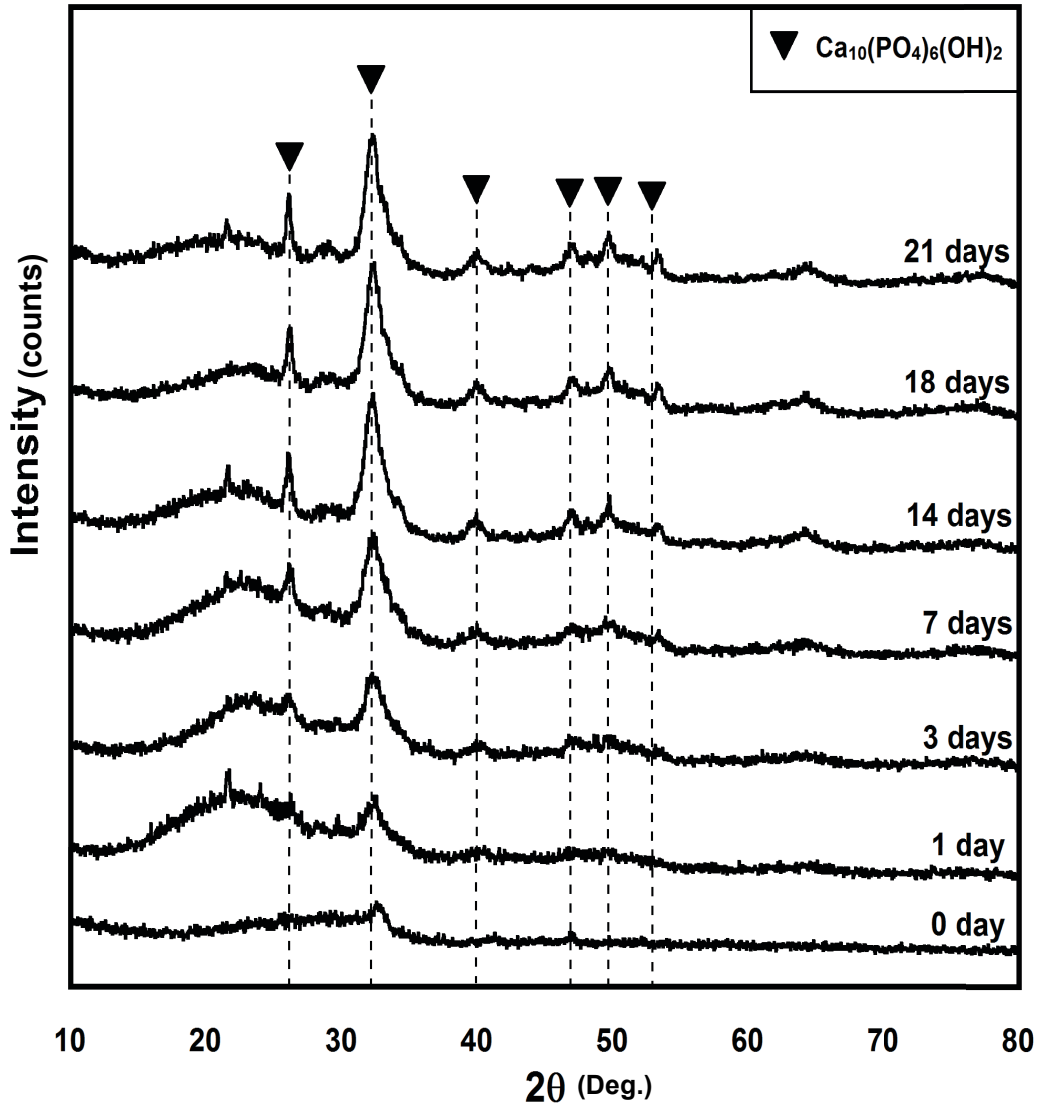


Figure 4-12 XRD spectra of gel-derived 58S, immersed in SBF as function of time.

#### 4.4.2 FTIR

FTIR spectroscopy was performed for verifying XRD results and studying amorphous structure more specifically. The results are illustrated in absorbance mode in Figure 4-13. Table 4-3 briefly explains the peaks which could be identified in FTIR spectra.

**Table 4-3 Correlation of energy peaks achieved by FTIR**

	<b>Peak (cm<sup>-1</sup>)</b>	<b>Correlation</b>
<b>Amorphous glass</b>	470	Si-O bending [10, 18]
	926	Si-O stretching [10, 18]
	~1024	Si-O stretching [10, 18]
	935	Si-O stretching [18, 27]
	1040	Si-O stretching [18, 27]
<b>Crystalline phases</b>	460	Si-O bending [18, 27]
	575	P-O bending [10, 13]
	620	P-O bending [10, 13]
	880	Si-O stretching [13]
	926	Si-O stretching [10, 18]
<b>Surface minerals</b>	800	Si-O stretching (silanols) [54]
	~1100	P-O stretching (CaP) [10]
	560	P-O bending [55]
	604	P-O bending [55]
	870	C-O stretching [10]

The main absorption bands that represent amorphous 45S5 are the Si-O bending modes at 470cm<sup>-1</sup> and 1024 cm<sup>-1</sup>. The Si-O stretch at 926 cm<sup>-1</sup> is related to non-bridging (NBO) oxygen which is present in both amorphous and crystalline structures but is expected to show higher intensity in crystalline specimen [10, 18, 51]. These peaks are shown in melt-cast powder before immersion, in Figure 4-13. The three aforementioned peaks confirm presence of silicate bonds in 45S5 glass.

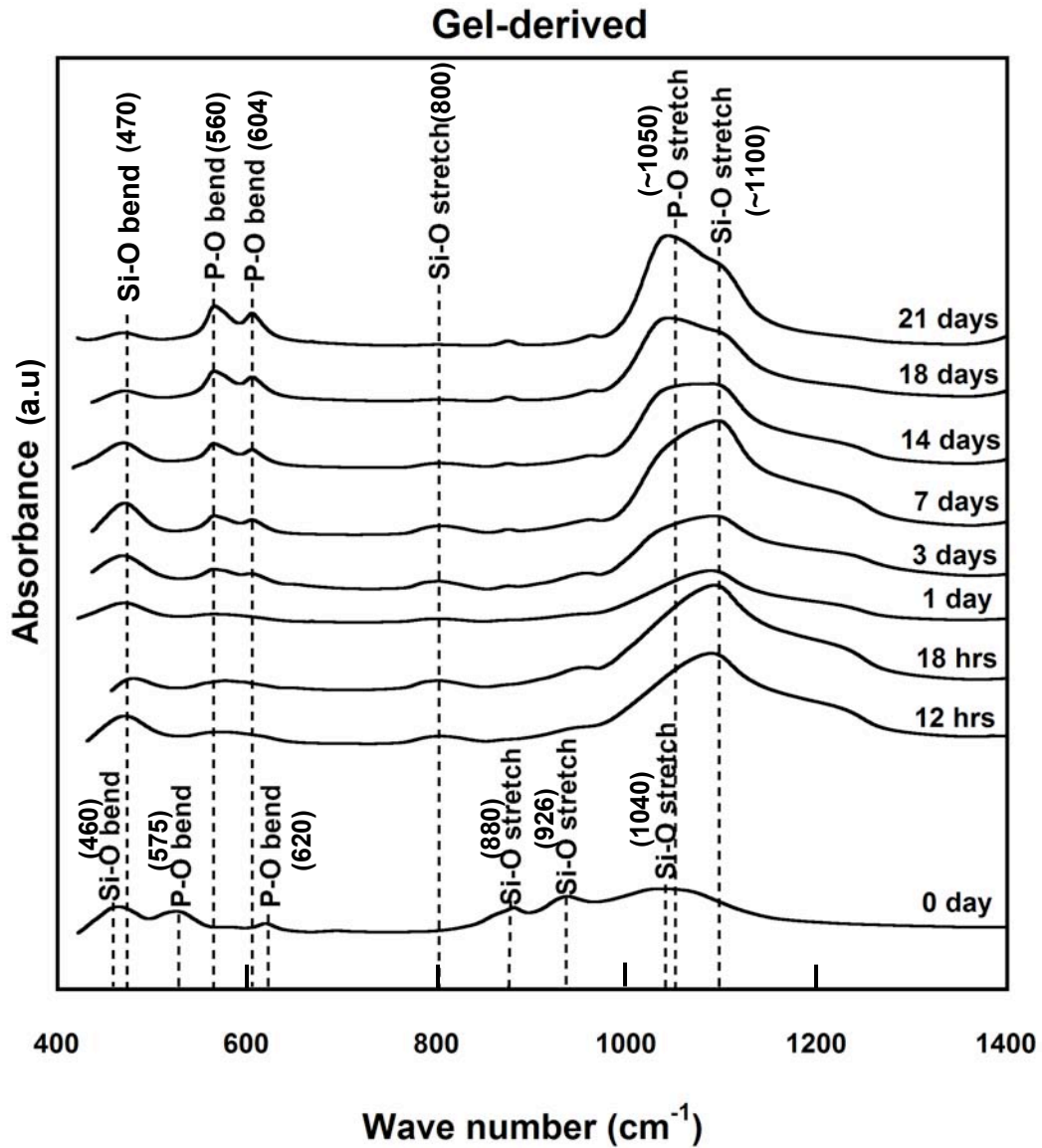
The gel-derived powder before immersion shows some other peaks which are mostly related to crystalline structure. The peak at  $460\text{ cm}^{-1}$  [18, 27, 56] refers to Si-O bending bonds of developed crystals and peaks at  $575\text{ cm}^{-1}$   $620\text{ cm}^{-1}$  [10, 13] refer to P-O bonds which show small amount of crystalline phosphate rich phase at  $700^\circ\text{C}$  with less intensity than at  $800^\circ\text{C}$ . Besides the Si-O stretch peak  $880\text{ cm}^{-1}$  presented for gel-derived samples with  $800^\circ\text{C}$  stabilization temperature is so small and hardly detectable in the  $700^\circ\text{C}$  sample (recall Figure 4-5). These results show that crystallization of apatite-like phosphorous rich phase occurs at  $700^\circ\text{C}$  but in much lower amounts. Also in comparison with melt-cast samples the peak at  $1024\text{ cm}^{-1}$  is split into two bands due to combination of isolated tetrahedral Si in combeite [13]. Furthermore, two small double peaks at  $696$  and  $729\text{ cm}^{-1}$  are attributed to symmetric stretch Si-O-Si in crystalline combeite [51]. Finally the peaks at  $935$  and  $1040\text{ cm}^{-1}$  are attributed to the stretch bond between Si and NBO spectrum and imply the occurrence of crystallization in gel-derived 45S5 [18, 27, 28, 51]. These peaks show that most of Si-O groups contain at least one NBO as is expected to see in presence of combeite.

Within the period of 12 hrs and 7 days of immersion, a small peak at  $800\text{ cm}^{-1}$  forms which represents Si-O bond stretch [54]. This bond corresponds to formation of amorphous Si-OH silanols in the second and third stage of interfacial reaction. After 7 days this peak disappears due to the crystallization of combeite on the surface.

At stage 4 of interfacial reaction,  $\text{Ca}^{2+}$  and  $\text{PO}_4^{3-}$  will migrate through the silica-rich layer causing growth of amorphous calcium phosphate [10]. The wide FTIR peak around  $1100\text{ cm}^{-1}$  demonstrates stretch P-O bond which shows the formation of calcium phosphate.

After immersion in SBF, the main peaks that should be noticed are P-O bonds that represent HA ( $\text{Ca}_{10}(\text{PO}_4)_6(\text{OH})_2$ ) crystallization. Three peaks at  $560$ ,  $604$  and around  $1100\text{ cm}^{-1}$  that grow after immersion, relate to P-O bonds. Since the P-O bond stretching at  $1100\text{ cm}^{-1}$  (mentioned before) is superimposed on the Si-O stretching bonds corresponding to biomaterial, it is difficult to discriminate P-O stretching bond. So growth of two P-O bending peaks at  $560$  and  $604\text{ cm}^{-1}$

are the peaks used for characterizing HA layer [10, 18, 55, 56]. The growth of these two peaks is obvious after 3 days immersion and become sharper with increasing time.



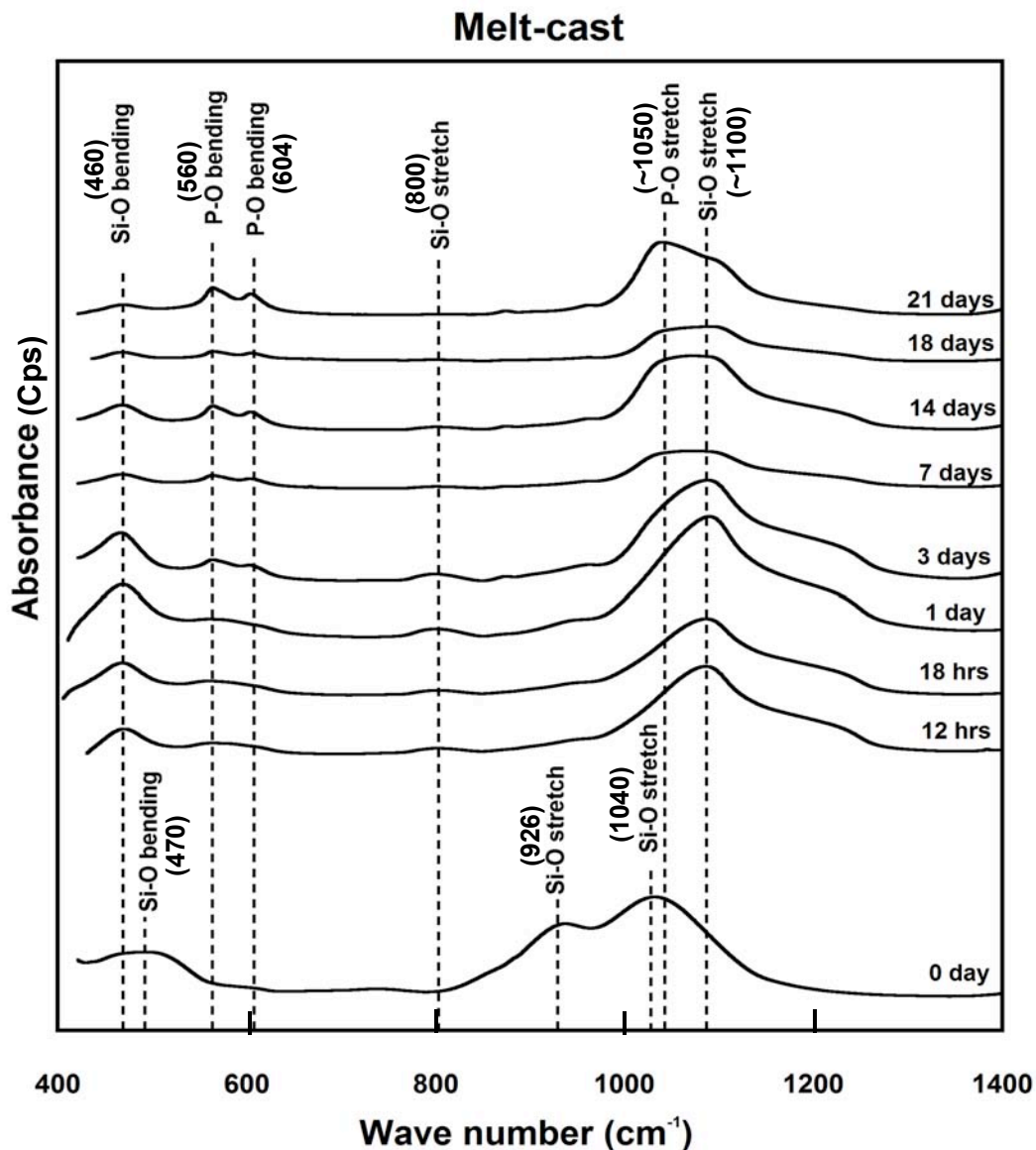


Figure 4-13 FTIR spectra for gel and melt derived 45S5 after immersion in SBF for various times.

Better assessment of the reaction kinetics was achieved by measuring the ratio of P-O bond intensity with the intensity of a stable peak during reaction as a reference. The best peak which was present in both samples and showed relatively steady state was Si-O bending with  $\sim 470 \text{ cm}^{-1}$  wave number. Table 4-4 shows the ratio of the intensity first P-O bending peak ( $560 \text{ cm}^{-1}$ ) over the intensity of high energy Si-O bending. As could be seen, it is obvious that this ratio is relatively getting constant after 18 days in gel-derived sample, while this occurs in melt-cast

powder after 21 days. This can be a good sign to show that the HA formation reaction is slightly higher in the gel-derived 45S5 since the formation of P-O bonds -which is attributed to HA formation- is faster.

**Table 4-4 Absorbance Intensity ratio of P-O bending at 560 cm<sup>-1</sup> over Si-O bending at 470 cm<sup>-1</sup>.**

<b>Days in SBF \ Specimen</b>	<b>Gel-derived*</b>	<b>Melt-cast*</b>
<b>3</b>	0.60 (0.16/0.28)	0.45 (0.19/0.42)
<b>14</b>	1.00 (0.22/0.22)	0.95 (0.22/0.21)
<b>18</b>	2.85 (0.26/0.90)	1.13 (0.08/0.09)
<b>21</b>	3.00 (0.36/0.12)	2.68 (0.24/0.09)

\* Numbers in parentheses indicate intensities used in calculation of absorbance intensity ratio

#### 4.4.3 SEM

##### 4.4.3.1 Melt-cast and gel-derived 45S5

Scanning electron microscopy is a practical method for understanding the morphology of gel-derived and melt-cast powders and HA which forms after immersion. After immersing powders in SBF, it is expected that 5 stages of surface reaction mentioned before, occur on the sample. Figure 4-14 shows the SEM image of 45S5 prepared by casting and immersion in SBF for 12 hrs. The EDS analysis result of this particle is shown in Table 4-5 which shows that the surface is covered with silicon and oxygen and small amounts of P, Ca and Na. This proves that the first two stages of the surface reaction happened on the powder after 12 hrs of immersion in SBF and that the powder is enclosed within amorphous silanol Si-OH gel.

**Table 4-5 EDS analysis of melt cast powder immersed in SBF for 12 hrs.**

<b>Element</b>	<b>Si</b>	<b>P</b>	<b>Ca</b>	<b>Na</b>	<b>O</b>
wt%	40.57	0.90	3.82	4.31	50.40
Atomic%	29.44	0.59	1.94	3.82	64.21

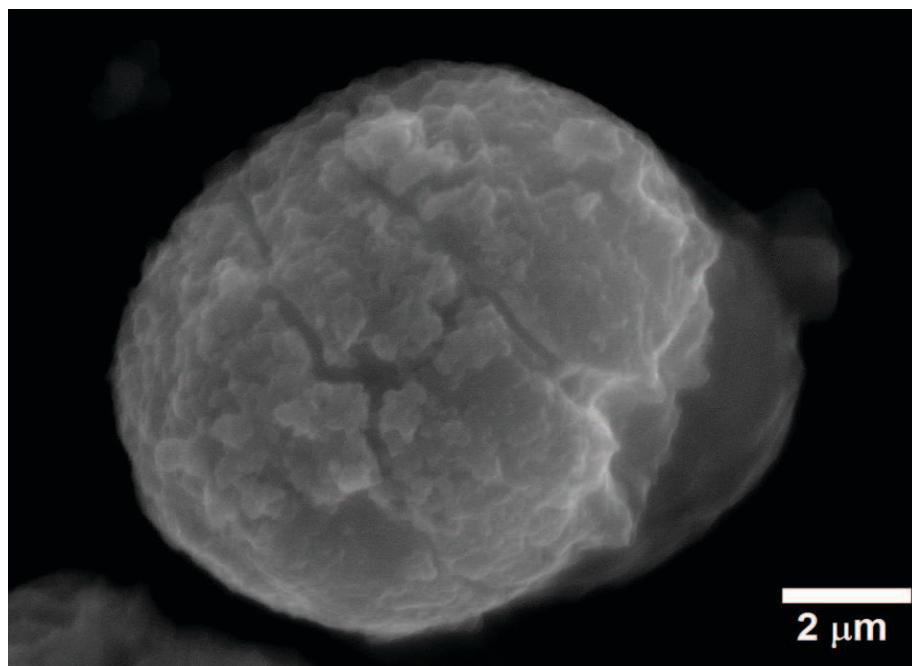


**Figure 4-14 Melt-cast 45S5 immersed in SBF for 12 hrs.**

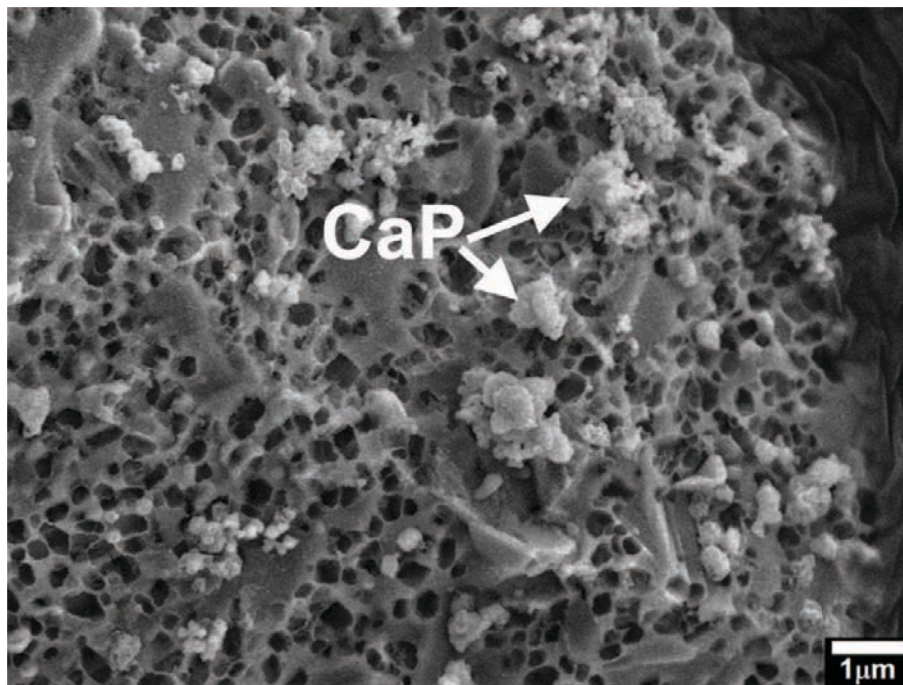
As discussed before, the high porosity and surface area of the gel derived 45S5, plays a major role in the reactions of the powder with SBF. Figure 4-15 represents the porous structure of the gel-derived 45S5 after 1 day immersion in SBF. A small nucleus of calcium phosphate could be detected on the surface. The porous structure makes interfacial reactions easier, even though the powder is crystalline.

Figure 4-16 a illustrates the gel-derived sample immersed in SFB for 7 days, showing some of the HAs coating has spalled. Presence of HA was confirmed by carrying out EDS on the area shown. Figure 4-16 a shows that the thickness of HA after 7 days is around 300nm. Also in Figure 4-16 b, deformation and scratches of the powder at the removed HA region due to unintentional mechanical force could clearly be detected. Figure 4-16 shows that even after 7 days the surface of the powder is covered with HA. But since the thickness of hydroxyapatite is small, XRD still can detect the composition under HA.

Immersion of the melt and gel-derived powder in SBF resulted in the formation of hydroxyapatite after 3 weeks, as discussed by XRD and FTIR results. SEM micrographs of 45S5 prepared by sol-gel and casting techniques, and comparison of HA formation of their surface is demonstrated in Figure 4-17.

Figure 4-17 a shows that nuclei (~200-500 nm; large white particles) form after 1 day of immersion in SBF on both specimen types. These nuclei are likely related to amorphous calcium phosphate which forms in the fourth stage of interfacial reaction. EDS spectra taken from these particles show a higher calcium and phosphorous content than the bioactive glass powder, but HA and calcium phosphate have similar composition (HA is a hydroxylated calcium phosphate), so it is impossible to distinguish between these phases from EDS probes. Moreover, XRD and FTIR after 1 day immersion could not have indicated HA or calcium phosphate because the volume of the observed particles was too small. It should be mentioned that FTIR is the main method to distinguish between calcium phosphates and HA because of the presence of the hydroxyl peaks in HA, provided there is enough to detect. However, the morphology and also theoretical basis of interfacial reaction could be a clue for showing that particles are calcium phosphate. By focusing on Figure 4-17 a (gel-derived), small needle like hydroxyapatites could be detected all over the surface. Therefore it could be stated that hydroxyapatites form in two modes: 1) calcium phosphate nuclei form on the bioglass, and after that hydroxyapatites form on the surface of calcium phosphates, which implies that the first four stages of interfacial reaction happen together and then hydroxyapatites forms on calcium phosphates; 2) hydroxyapatite crystals nucleate directly on the surface of bioactive glass powder. Previous work has shown that hydroxyapatite can form on many different compositions of calcium phosphate, and that the morphology of such hydroxyapatite crystals is needlelike [57, 58]. It was not possible to assess the sequence of these reactions, but it seems that second case occurs more on the surface of rougher powder which is gel-derived 45S5. Therefore, small HA particles were not detected on the surface of melt-cast 45S5. It should be noticed that the image shown the melt-cast powder was prepared by sintering therefore the surface is not flat as expected in melt cast powders. This image is used just to show that HA nuclei form on the surfaces of both samples, but for other tests such as XRD and FTIR, and also SEM for more days of immersion, the flat sample which was grounded from the bulk glass was tested.

After 14 days the entire surface is covered with HA and new bunches of HA nuclei on the surface of gel-derived powder could be detected as illustrated in Figure 4-17 b. Figure 4-17 c demonstrates that new HA forms on the surface of previous hydroxyapatites. It can also be seen that HA forming on the surface of the gel-derived powder is much finer than the melt-cast. The thickness of HA platelets on the gel-derived 45S5 was measured around 10 nm while in the melt-cast powder it was approximately 30 nm by using Image J software. This indicates that finer hydroxyapatite platelets could be achieved by using 45S5 prepared by the sol-gel method.



**Figure 4-15 High porosity structure of gel derived 45S5 after 1 day immersion in SBF.**

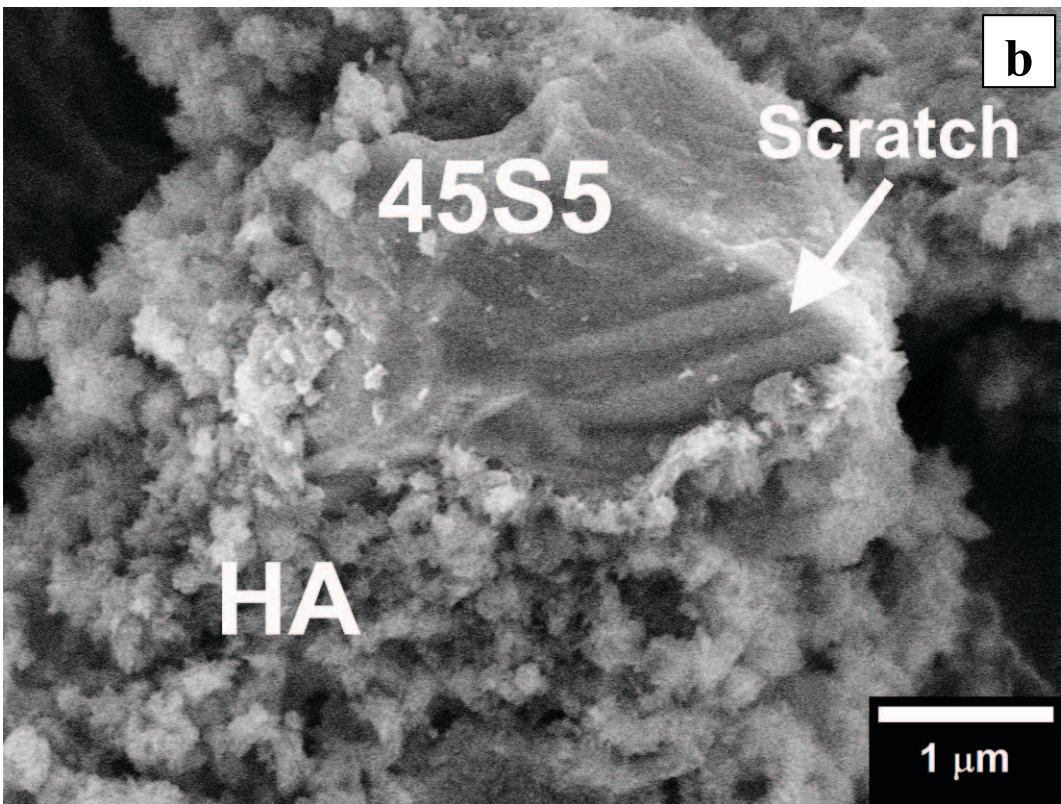
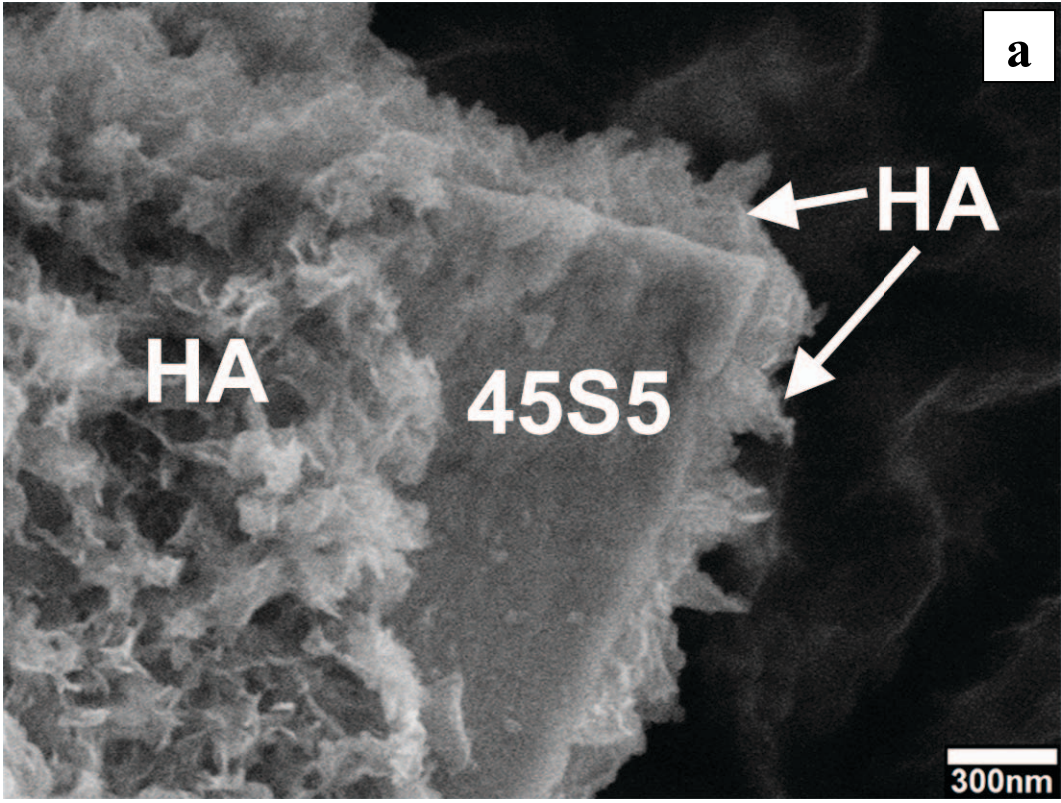


Figure 4-16 SEM micrograph of gel derived 45S5 immersed in SBF for 7 days

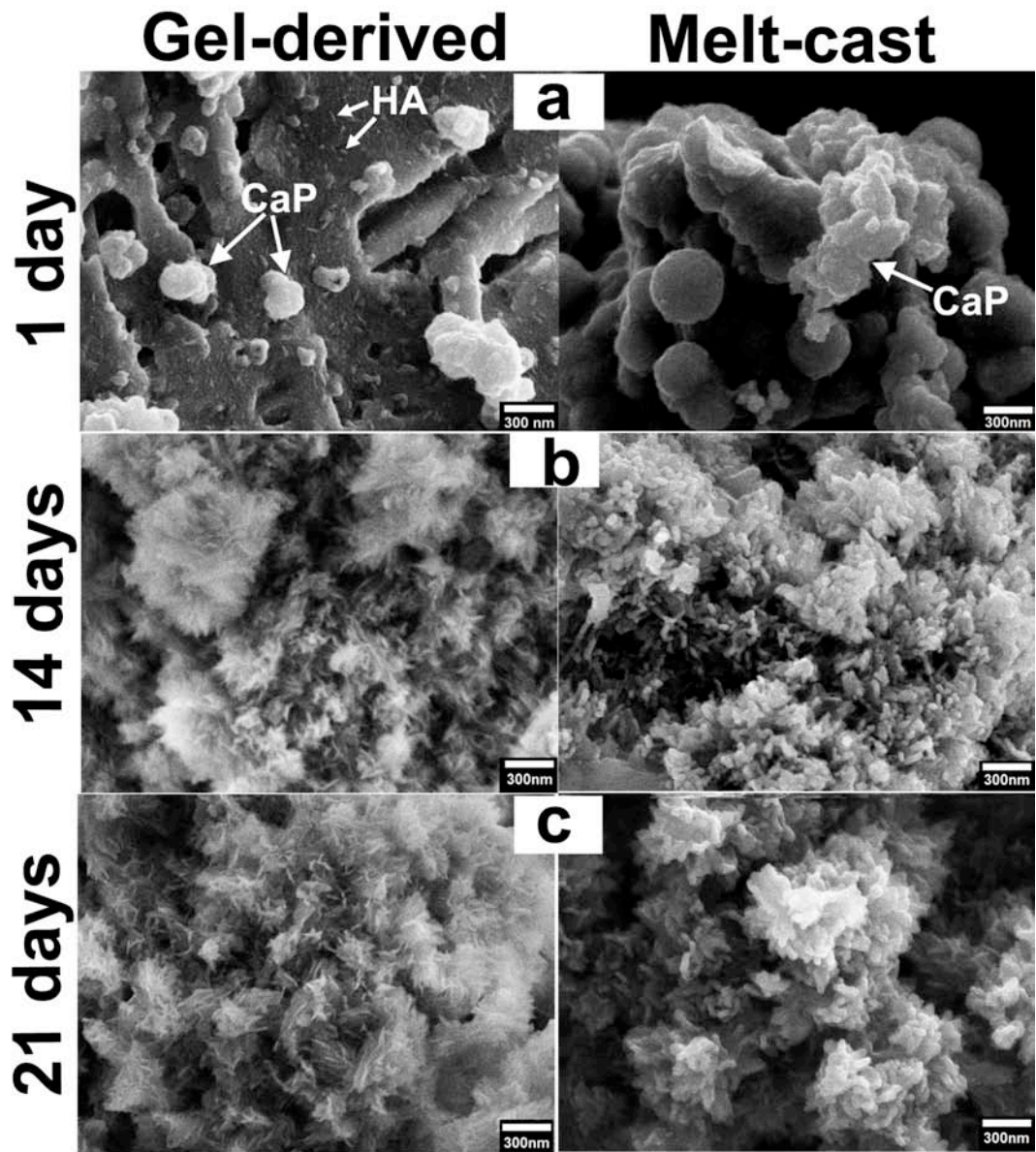


Figure 4-17 SEM micrograph of gel-derived and melt-cast 45S5 after a. 1 day b. 14 days c. 21 days immersion in simulated body fluid.

#### 4.4.3.2 Gel-derived 58S

The scanning electron microscopy images of 58S bioglass prepared by the sol-gel method are shown in Figure 4-18. It shows that after 1 day small particles of HA start to form and after 7 days the porous surface is covered with HA. By measuring the size of HA after 21 days immersion, the thickness of particles was found to be around 20-25 nm.

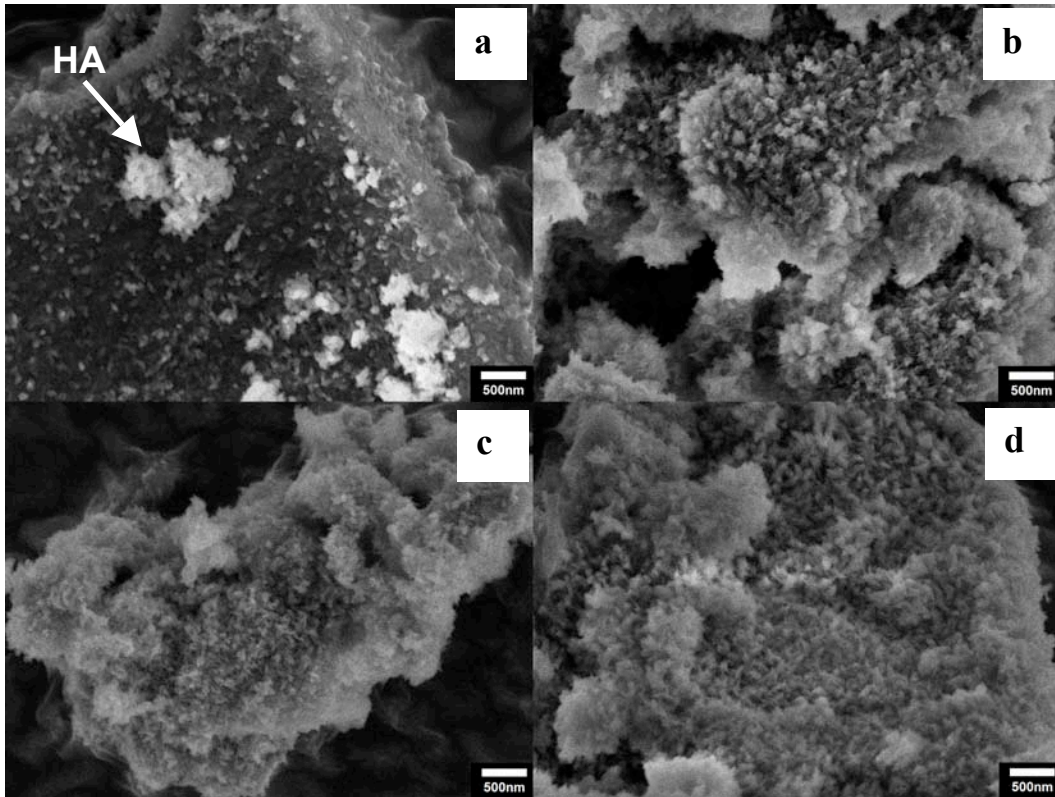


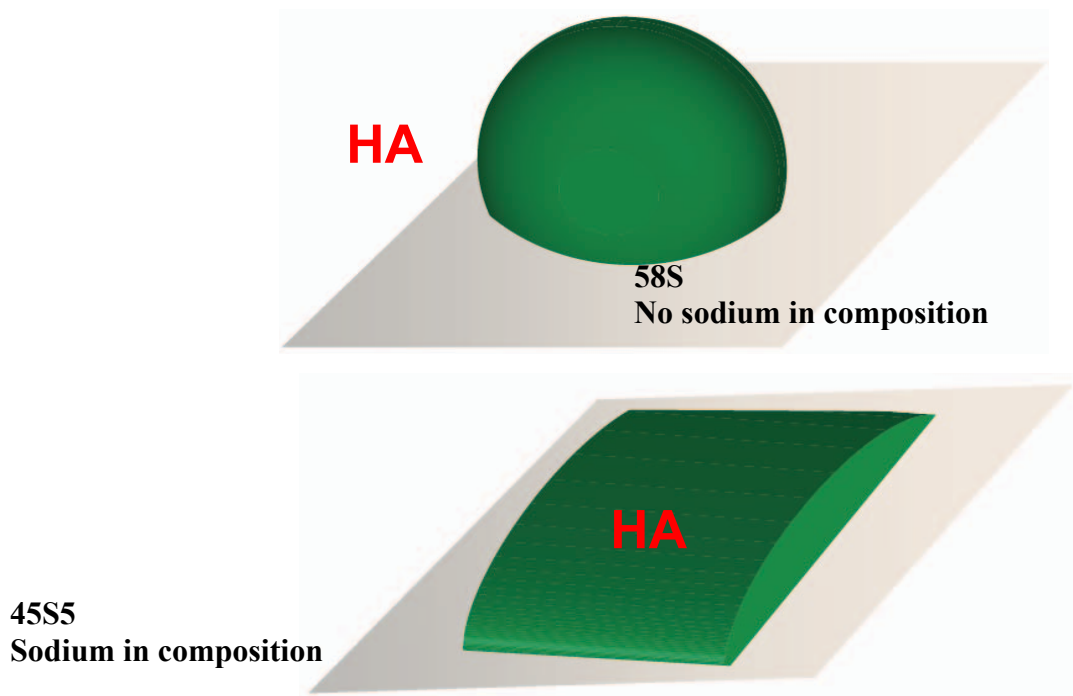
Figure 4-18 SEM micrograph of gel-derived 58S after a. 1 day b. 7 days c. 14 days and d. 21 days immersion in SBF.

Figure 4-18 represents that the HA particles have a smaller aspect ratio compared to the HA formed on the surface of the gel-derived 45S5 which was more acicular. The main reason may be attributed to the presence of sodium as a modifier in 45S5. Sodium is an important element which enhances HA nucleation rate. This element enhances the reaction of bioglass with body fluid due to increasing NBO bonds. When the surfaces of bioactive glasses contain sodium,

more surface is available to react (more surface reaction) which leads to the formation of an HA morphology with higher surface area (e.g., platelets). In 58S, there is less interest of a surface reaction, therefore HA desires to form more on itself than the surface of bioglass, compared with 45S5 as shown in Figure 4-19. This lead to have more volume to surface ratio in HA formed on surface of 58S.

HA morphology has been reported to change with temperature and solution concentration (e.g., NaCl) [57], however in this research the temperature and solution concentration (i.e., SBF) were held constant, so the HA morphology differences observed are believed to be due to powder composition, surface area, and structure.

As discussed before, more surface area makes the kinetics of the reaction higher. So the reason of lower HA rate formation after 14 days of immersion in 58S, could be related to the stable shape of apatite. It also means that the effect of HA morphology on reaction interest was more than the thickness of the particle (melt-cast 45S5 vs. gel-derived).



**Figure 4-19 Schematic illustration of the effect of presence of sodium on the morphology of bioglass, HA forms on itself more in 58S than 45S5.**

#### 4.4.4 EDS

Quantitative data about the sequence of interfacial reactions and the amount of elemental changes are represented by EDS in Table 4-6 and Table 4-7. The theoretical elemental composition of 45S5 is: 16.30% Si, 1.77% P, 9.51% Ca, 17.26% Na and 55.16% O in mol%. EDS results show compositions close to expected the slightly higher amount of sodium might be due to less accuracy of lighter elements detection in EDS. Hydroxyapatite ( $\text{Ca}_{10}(\text{PO}_4)_6(\text{OH})_2$ ) forms after immersion of 45S5 in SBF, due to the interfacial reactions mentioned before [40]. The composition of HA is: 22.73% Ca, 13.64% P, 59.10% O and 4.54% H (molar %). So, EDS results should show, increase in Ca, and P elements and decrease in Na and Si. EDS results show that after 1 day immersion in SBF, as anticipated, 45S5 shows increase in Ca and P and considerable decrease in Na. There no significant change in silicon value because, silicon is needed at first stages of interfacial reaction to form amorphous silanols. So it could be concluded that after 1 day, the first two stages of reaction are almost accomplished. Melt cast powder shows higher rate of reaction after 1 day immersion. It shows around 3 % decrease in silicon and also higher increase in Ca and P. After 14 days immersion, EDS results of gel-derived and melt cast powder represent relatively similar values. This means that, although at first days of immersion melt-cast powder shows faster dissolution, later and after 14 days, gel-derived powder reactions get faster and match that of melt-cast powder. Both types of sample still show noticeable amount of silicon due to amorphous silanol. The XRD results and the presence of a Si-OH peak at  $800\text{ cm}^{-1}$  in FTIR, after 14 days immersion confirm the EDS results. Finally after 21 days, a small amount of silicon and sodium and large amount of Ca and P could be detected by EDS test. Stoichiometric value of Ca/P which is expected for HA is 1.67. This value for gel-derived and melt-cast powder is 1.58 and 1.90 respectively. It shows that stoichiometric ratio achieved by gel-derived 45S5 is close to the expected value.

**Table 4-6 EDS results of immersed 45S5 prepared by sol-gel method in SBF (mol%).**

<b>Days in SBF</b>	<b>0</b>	<b>1</b>	<b>14</b>	<b>21</b>
<b>Si</b>	15.81	15.11	8.34	2.20
<b>P</b>	1.41	7.50	12.54	14.48
<b>Ca</b>	8.00	13.28	17.02	22.88
<b>Na</b>	20.68	2.55	0.71	1.29
<b>O</b>	53.85	62.32	63.40	61.63

**Table 4-7 EDS results of immersed 45S5 prepared by melt-casting technique in SBF (mol%).**

<b>Days in SBF</b>	<b>0</b>	<b>1</b>	<b>14</b>	<b>21</b>
<b>Si</b>	15.12	12.05	9.77	0.42
<b>P</b>	1.56	9.33	11.11	13.25
<b>Ca</b>	8.00	14.13	15.80	25.27
<b>Na</b>	22.37	1.95	1.09	1.22
<b>O</b>	53.60	62.52	62.95	59.84

Another way to show elemental change and EDS results of gel-derived and melt-cast 45S5 after immersion in SBF is illustrated in Figure 4-20. It shows the trend of decrease in Na and Si and increase in Ca and P values. Furthermore, higher rate of melt-cast reaction in first day of immersion can be seen.

EDS results can be a helpful method to roughly determine the thickness of HA. As shown in Figure 4-21, the interaction volume of electrons which penetrate in the sample shows how much dept of sample is detected by EDS. Interaction

volume is roughly around  $2\mu\text{m}$  [47] which means whenever elements related to substrate could not be detected, the thickness of HA has reached  $\sim 2\mu\text{m}$ .

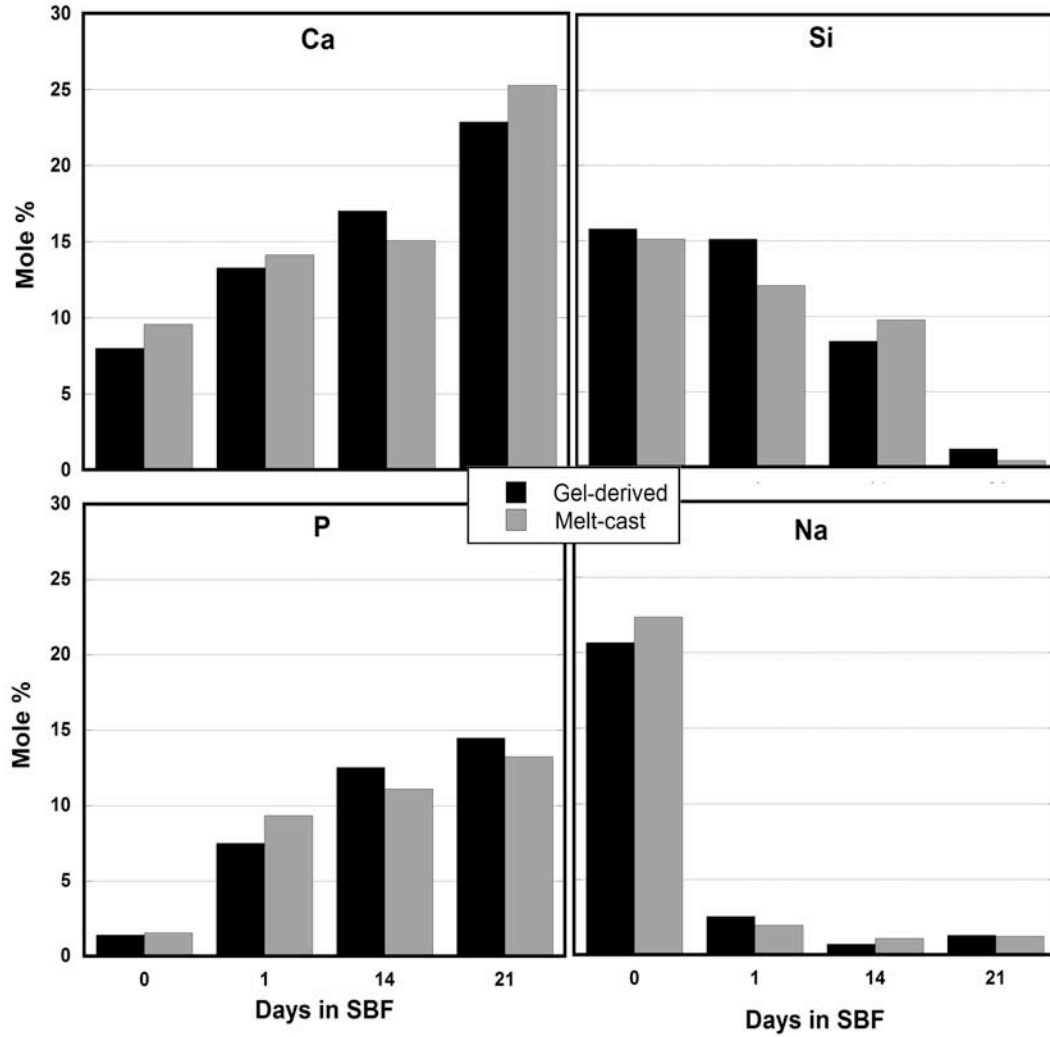


Figure 4-20 EDS analysis of melt-cast and gel-derived 45S5.

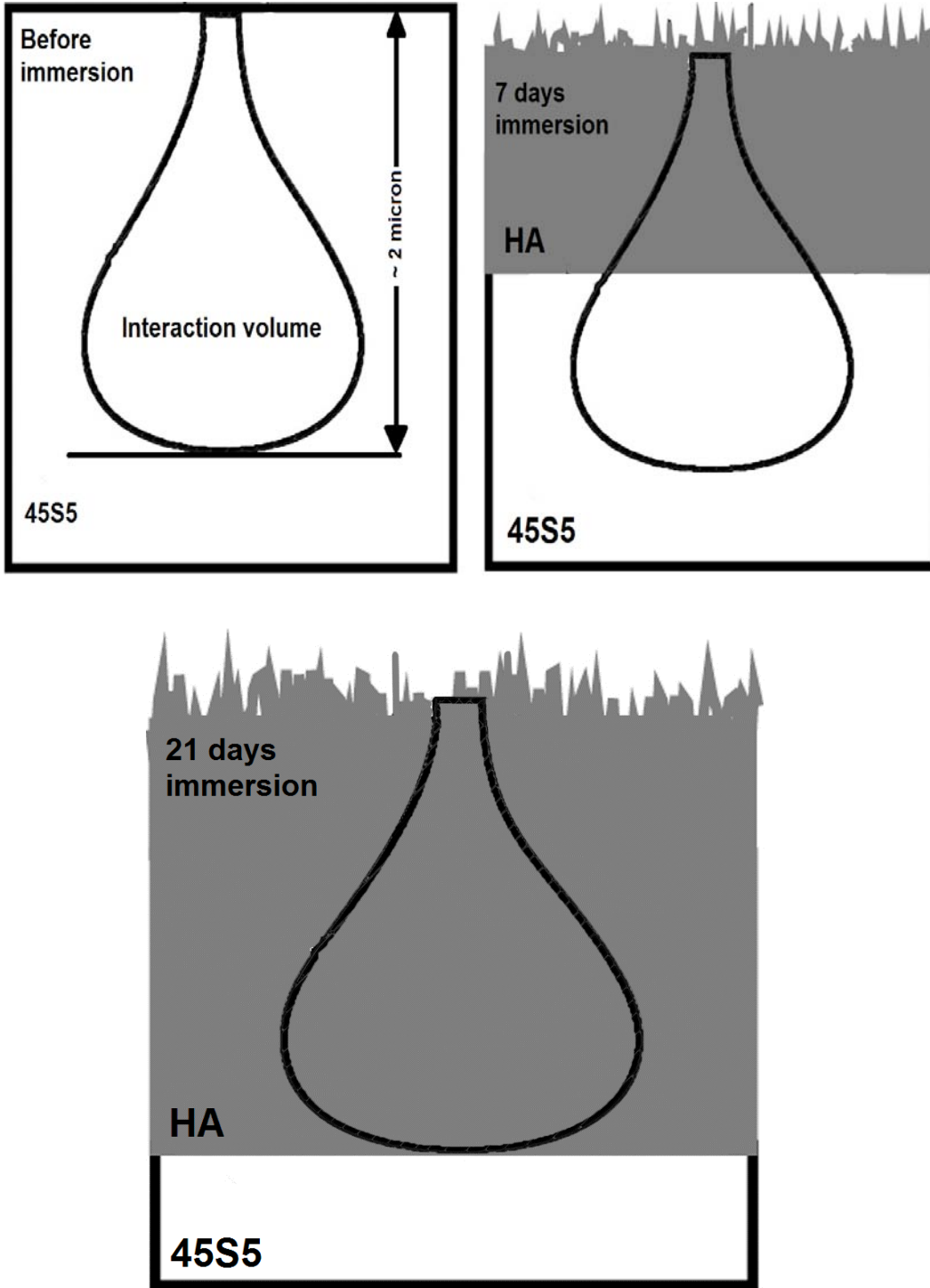


Figure 4-21 Schematic illustration of the dept of electrons could be detected. Before immersion, interaction volume just detect 45S5 as expected, after 7 days both 45S5 and HA will be detected and finally after 21 days, the thickness of HA will be as thick as interaction volume that only HA could be detected.

EDS, XRD and FTIR help in comparing the reactions rate of specimens during immersion. Results show that the reaction is slightly faster during the first days of immersion of the melt-cast powder, but after 3 days the gel-derived samples show a higher rate of reaction. A simple reason might be explained via the morphology and structure of the samples. As shown in the XRD spectra, combeite crystal peaks are present up until 3 days of immersion for the gel-derived powder. This phenomenon indicates that the lower dissolution rate in the first days of immersion is related to the presence of stable crystalline combeite which makes dissolution more difficult. In general, crystalline ceramics have the most stable structure compared with ceramic glasses (i.e., crystals have a lower Gibbs free energy). Materials, including glasses, change their state by transforming to the structure with the lowest energy, which is why glasses crystallize upon heating at sufficiently high temperatures and long times to allow for diffusion. Being more energetically stable, crystalline structures do not have as high a cation release as glasses, so the first stages of interfacial reaction are thermodynamically more difficult in crystals. However, in the amorphous structure, since the structure is metastable compared with crystals, ion release can occur more easily. Therefore, interfacial reaction is more favorable on the surface of amorphous bioglass than crystalline or partially crystalline glass-ceramics, but the reason that there is not that much of a difference in reaction after HA covered the surface relates to effect of porosity and roughness of the gel-derived powder on the kinetics of interfacial reaction. The increased surface area of sol-gel derived powders was found to overcome thermodynamic limitations of structure mediated dissolution by achieving enhanced kinetics, due to increase in the available surface area for reaction and increased aspect ratio of the apatite crystals. The rougher surface helped the reaction to occur more quickly because there were more reaction sites. Generally it could be concluded that there are three parameters which affect surface reactions before HA covers the surface of the gel-derived 45S5: 1) atomic structure of the powder: crystalline vs. amorphous; 2) the specific surface area: high vs. low; 3) composition: sodium vs. sodium free. The latter is slightly more dominant, which helps to explain the lower reaction rate of

the 58S compared to the 45S5 powder (independent of crystallinity) within 3 days of reaction.

As mentioned before, during first days of immersion, hydroxyapatites form on the surface of bioglass in two ways. Melt-cast bioglasses shows apatite formation more, by the first mechanism (production of HA on surface of calcium phosphate) and it is probably difficult to find apatite which formed by the second way (as could be seen in Figure 4-17 a) [17, 37]. But in gel-derived biomaterial the other mode of apatite formation happens more. This might be related to high roughness which is expected to see on the surface of the gel-derived material. High roughness makes the major part of interfacial reactions occur on the edges of small roughness (which is not detectable in SEM micrograph and probably will be ~10 nm due to the size of particles formed by sol-gel method). Larger edges which could be detected in SEM micrographs make first mode of reaction available.

Within 3 days the first layers of HA start to form on the surface of gel-derived powder. This means that the connection between the surface of the glass ceramic and body fluid probably decreases, and the structure of the powder has no effect on the rate of the reaction. In melt-cast powder after formation of calcium phosphate on the surface this connection is lost. Therefore, the reaction rate is just related to the formed apatite and its morphology. XRD and FTIR results represent that both samples surfaces are covered with hydroxyapatite ( $\text{Ca}_{10}(\text{PO}_4)_6(\text{OH})_2$ ). So, the only parameter that might affect the surface reaction after the apatite formation on the surface is HA morphology itself. As mentioned before, and shown in Figure 4-17c, the hydroxyapatites which formed on the surface of the gel-derived 45S5 are much finer than HA formed on the melt-cast bioglass. Higher surface area and the roughness of the gel-derived particles might be the reason of the finer hydroxyapatite platelets in the gel-derived sample as compared with the melt-cast powder. It is expected that apatite which form individually, become finer since they form on rougher nucleation sites. The surface of amorphous calcium phosphate could not be as rough as surface of gel-derived 45S5. As shown in Figure 4-22, rough surface shows more nucleation sites, thus

finer particles will form on surface of rougher powder. It is easier for HAs to nucleate on corners because of the higher surface area. As a result finer platelets will be formed in comparison with the melt-cast 45S5, where apatite forms on the surface of calcium phosphate rich glass. Many reports show that subsequent layers of HA form on the surface of previous HA [17]. As the platelets of HA appear finer for the gel-derived powder, the next layers will form faster due to a higher nucleation surface. Round fine clusters which could be seen in Figure 4-17c are related to these new hydroxyapatites.

Eventually after 21 days of immersion in SBF, the dissolution rate of 45S5 prepared by sol-gel method, even though the structure is crystalline (and of slightly different composition locally), becomes higher than the amorphous cast-derived bioglass. It could be expected that the next stages of interfacial reaction between interface and body fluid will be faster in the gel-derived powder due to finer morphology. Besides, previous research has shown that finer hydroxyapatite will make the surface rougher so the connection with the body will become easier and mechanical attachment will improve as well [59-61].

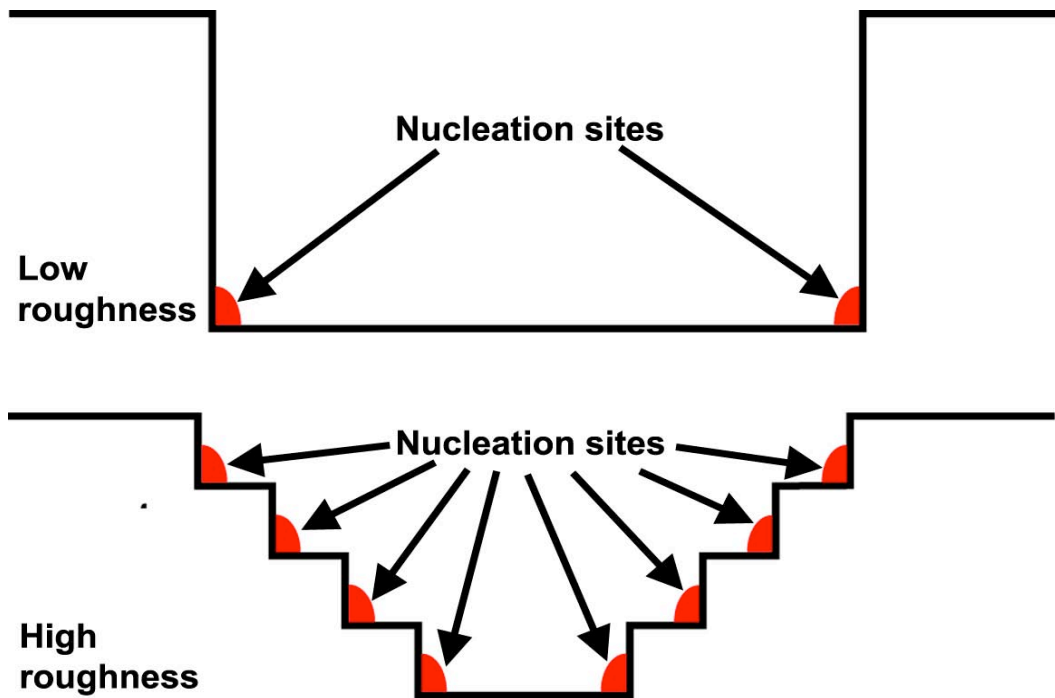


Figure 4-22 Schematic illustration of Surface with low roughness which shows less nucleation sites than surface with more roughness

## 5 Conclusions

In this research the apatite formation rate of three bioactive glasses was compared. Comparison of traditional compositions (used in medical applications) of melt cast bioglass 45S5, with gel-derived glass-ceramic 45S5 and gel-derived bioglass 58S (45S5 without sodium oxide in composition) were carried out by immersion in simulated body fluid (SBF). The rate of hydroxyapatite (HA) formation during immersion in SBF was used as an appropriate sign to correlate the bioactivity of the materials.

1. Since preparation of amorphous 45S5 by sol-gel method was not possible due to crystallization, it was first expected to have a lower apatite formation rate because of the stable crystalline structure. This means that crystalline structure thermodynamically showed less favor to form apatite, than amorphous bioglass. However the high surface area of sol-gel powders helped to increase the kinetics of HA formation therefore, increased the rate of apatite formation.
2. Immersing gel-derived 45S5 powder in SBF showed similar HA formation rate compared with melt cast 45S5. This occurred because of the higher roughness and surface area of 45S5 prepared by sol-gel method, despite its crystalline structure.
3. Specific surface area, which indirectly changes surface roughness of the powder, is the likely determinant in affecting the morphology of observed HA; it was shown that finer HA platelets formed on gel-derived samples.
4. The presence of sodium in 45S5 was a major factor leading to formation of crystal structure when using the sol-gel method; compositions without sodium did not crystallize after stabilizing heat treatments.
5. The kinetics of interfacial reaction for gel-derived 58S was faster than for gel-derived and melt-cast 45S5 in the first days of immersion, which is related to the high surface area *and* amorphous structure of 58S.
6. After 7 days of immersion, the rate of reaction became slower in 58S. It might be related to the morphology of the formed HA. Although the size

of HA was relatively small, the spherical shape of it could have lead to lower formation rate of HA. This morphology had much less surface area compared with acicular HA particles formed in gel-derived 45S5. This is because of less aspect ratio which leads to have less surface area, in a constant volume. Therefore, the reaction became slower after the first layers of HA covered the surface.

***Future work:***

Mechanical properties and *in vivo* studying of melt-cast 45S5 and gel-derived 58S have been explored by previous researchers. Gel-derived 45S5 has not been tested in living tissues. There is high potential of this material to show characteristics for use as bone filling therapy. As mentioned before, it is expected to have better mechanical properties in comparison with amorphous 45S5. So, many kinds of tests such as nano-indentation could be carried out on powder to study the hardness of particles. Since the gel-derived 45S5 has a crystalline structure it would be feasible to sinter it at high temperatures to form a bulk sample. This could help to study other mechanical properties such as fracture toughness, stress, and elastic modulus. It is important to perform *in vivo* tests on such samples to achieve better assessment about the true bioactivity of crystalline gel-derived 45S5. Finally, testing mechanical properties and the effect of finer HA layers in gel-derived powder on the nature and strength of the interface between implant and bone could be useful.

## Bibliography

- [1] Hench LL. The story of Bioglass (R). *J Mater Sci-Mater Med* 2006;17: 967-78.
- [2] Hench LL. Sol-gel materials for bioceramic applications. *Current Opinion in Solid State & Materials Science* 1997;2: 604-10.
- [3] Hench LL. Bioceramics. *J Am Ceram Soc* 1998;81: 1705-28.
- [4] Hench LL, Wilson J. An Introduction to bioceramics. World scientific publishing co 1999.
- [5] Hench LL, Polak JM, Xynos ID, Buttery LDK. Bioactive materials to control cell cycle. *Mater Res Innov* 2000;3: 313-23.
- [6] Kokubo T, Kim HM, Kawashita M. Novel bioactive materials with different mechanical properties. *Biomaterials* 2003;24: 2161-75.
- [7] Hench LL, Jones JR, Sepulveda P. Bioactive materials for tissue engineering scaffolds.
- [8] Wopenka B, Pasteris JD. A mineralogical perspective on the apatite in bone. *Mater Sci Eng C-Biomimetic Supramol Syst* 2005;25: 131-43.
- [9] Hench LL, Wheeler DL, Greenspan DC. Molecular control of bioactivity in sol-gel glasses. *J Sol-Gel Sci Technol* 1998;13: 245-50.
- [10] Peitl O, LaTorre GP, Hench LL. Effect of crystallization on apatite-layer formation of bioactive glass 45S5. *J Biomed Mater Res* 1996;30: 509-14.
- [11] Peitl O, Zanotto ED, Hench LL. Highly bioactive P2O5-Na2O-CaO-SiO2 glass-ceramics. *J Non-Cryst Solids* 2001;292: 115-26.
- [12] Hench LL. Bioceramics - from Concept to Clinic. *J Am Ceram Soc* 1991;74: 1487-510.
- [13] Lefebvre L, Chevalier J, Gremillard L, Zenati R, Thollet G, Bernache-Assolant D, Govin A. Structural transformations of bioactive glass 45S5 with thermal treatments. *Acta Mater* 2007;55: 3305-13.
- [14] Li R, Clark AE, Hench LL. An Investigation of Bioactive Glass Powders by Sol-Gel Processing. *J Appl Biomater* 1991;2: 231-9.
- [15] Chen QZ, Rezwan K, Armitage D, Nazhat SN, Boccaccini AR. The surface functionalization of 45S5 Bioglass (R)-based glass-ceramic scaffolds and its impact on bioactivity. *J Mater Sci-Mater Med* 2006;17: 979-87.
- [16] Kim HM, Himeno T, Kokubo T, Nakamura T. Process and kinetics of bonelike apatite formation on sintered hydroxyapatite in a simulated body fluid. *Biomaterials* 2005;26: 4366-73.
- [17] Li P, Ohtsuki C, Kokubo T, Nakanishi K, Soga N, Nakamura T, Yamamuro T. Process of Formation of Bone-Like Apatite Layer on Silica-Gel. *J Mater Sci-Mater Med* 1993;4: 127-31.
- [18] Aguiar H, Serra J, Gonzalez P, Leon B. Structural study of sol-gel silicate glasses by IR and Raman spectroscopies. *J Non-Cryst Solids* 2009;355: 475-80.
- [19] Malavasi G, Menziani MC, Pedone A, Civalleri B, Corno M, Ugliengo P. A computational multiscale strategy to the study of amorphous materials. *Theor Chem Acc* 2007;117: 933-42.

- [20] Lin S, Ionescu C, Pike KJ, Smith ME, Jones JR. Nanostructure evolution and calcium distribution in sol-gel derived bioactive glass. *J Mater Chem* 2009;19: 1276-82.
- [21] Jun IK, Koh YH, Kim HE. Fabrication of a highly porous bioactive glass-ceramic scaffold with a high surface area and strength. *J Am Ceram Soc* 2006;89: 391-4.
- [22] Bonding Mechanisms at the Interface of Ceramic Prosthetic Materials.
- [23] Sakka S. Handbook of Sol–Gel science and technology. Kluwer Academic Publishers.
- [24] Brinker CJ. Sol-gel science: the physics and chemistry of sol-gel processing. Academic Press Inc 1990.
- [25] Gil-Albarova J, Garrido-Lahiguera R, Salinas AJ, Roman J, Bueno-Lozano A, Gil-Albarova R, Vallet-Regi M. The in vivo performance of a sol-gel glass and a glass-ceramic in the treatment of limited bone defects. *Biomaterials* 2004;25: 4639-45.
- [26] Fathi MH, Doostmohammadi A. Bioactive glass nanopowder and bioglass coating for biocompatibility improvement of metallic implant. *J Mater Process Technol* 2009;209: 1385-91.
- [27] Pappas GS, Liatsi P, Kartsonakis IA, Danilidis I, Kordas G. Synthesis and characterization of new SiO<sub>2</sub>-CaO hollow nanospheres by sol-gel method: Bioactivity of the new system. *J Non-Cryst Solids* 2008;354: 755-60.
- [28] Balamurugan A, Sockalingum G, Michel J, Faure J, Banchet V, Wortham L, Bouthors S, Laurent-Maquin D, Balossier G. Synthesis and characterisation of sol gel derived bioactive glass for biomedical applications. *Mater Lett* 2006;60: 3752-7.
- [29] Saboori A, Rabiee M, Mutarzadeh F, Sheikhi M, Tahriri M, Karimi M. Synthesis, characterization and in vitro bioactivity of sol-gel-derived SiO<sub>2</sub>-CaO-P<sub>2</sub>O<sub>5</sub>-MgO bioglass. *Mater Sci Eng C-Biomimetic Supramol Syst* 2009;29: 335-40.
- [30] Hench LL, West JK. The Sol-Gel Process. *Chem Rev* 1990;90: 33-72.
- [31] Wright JD, Sommerdijk NAJM. Sol-gel materials chemistry and applications. Gordon and breach science publishers 2001.
- [32] Jones RW. Fundamental principles of sol-gel technology. The Institute of Metals 1989.
- [33] Aelion R, Loebel A, Eirich F. Hydrolysis of Ethyl Silicate. *J Am Chem Soc* 1950;72: 5705-12.
- [34] Davis PJ, Brinker CJ, Smith DM. Pore Structure Evolution in Silica-Gel During Aging Drying .1. Temporal and Thermal Aging. *J Non-Cryst Solids* 1992;142: 189-96.
- [35] Lefebvre L, Gremillard L, Chevalier J, Bernache-Assolant D. Sintering behavior of 45S5 Bioglass (R). In: Daculsi G, Layrolle P, editors. *Bioceramics*, Vol 20, Pts 1 and 2, vol. 361-363. Stafa-Zurich: Trans Tech Publications Ltd, 2008. p.265-8.
- [36] Li P, Yang Q, Zhang F, Kokubo T. The Effect of Residual Glassy Phase in a Bioactive Glass-Ceramic on the Formation of Its Surface Apatite Layer In vitro. *J Mater Sci-Mater Med* 1992;3: 452-6.

- [37] Chen QZZ, Thompson ID, Boccaccini AR. 45S5 Bioglass (R)-derived glass-ceramic scaffolds for bone tissue engineering. *Biomaterials* 2006;27: 2414-25.
- [38] Shelby JE. *Introduction to glass science and technology. Advancing the Chemical Sciences* 2005.
- [39] Kingery WD, Bowen HK, Uhlmann DR. *Introduction to Ceramics*. 1976.
- [40] Kokubo T, Takadama H. How useful is SBF in predicting in vivo bone bioactivity? *Biomaterials* 2006;27: 2907-15.
- [41] Kokubo T. *Bioactive Glass-Ceramics - Properties and Applications*. *Biomaterials* 1991;12: 155-63.
- [42] Kokubo T, Kushitani H, Sakka S, Kitsugi T, Yamamuro T. Solutions Able to Reproduce In vivo Surface-Structure Changes in Bioactive Glass-Ceramic a-W3. *J Biomed Mater Res* 1990;24: 721-34.
- [43] Filgueiras MR, Latorre G, Hench LL. Solution Effects on the Surface-Reactions of a Bioactive Glass. *J Biomed Mater Res* 1993;27: 445-53.
- [44] Ohtsuki C, Kushitani H, Kokubo T, Kotani S, Yamamuro T. Apatite Formation on the Surface of Ceravital-Type Glass-Ceramic in the Body. *J Biomed Mater Res* 1991;25: 1363-70.
- [45] Oyane A, Kim HM, Furuya T, Kokubo T, Miyazaki T, Nakamura T. Preparation and assessment of revised simulated body fluids. *J Biomed Mater Res Part A* 2003;65A: 188-95.
- [46] Wedd MW. *Determination of Particle Size Distributions Using Laser Diffraction*. 2003.
- [47] Goldstein J, Newbury DE, Joy DC. *Scanning electron microscopy and x-ray microanalysis: Volume 1* 2003.
- [48] Beaman DR, Solosky LF. Accuracy of Quantitative Electron-Probe Microanalysis with Energy Dispersive Spectrometers. *Anal Chem* 1972;44: 1598-&.
- [49] Fischer RX, Tillmanns E. Die Kristallstrukturen von natürlichem Na<sub>2</sub>Ca<sub>2</sub>Si<sub>3</sub>O<sub>9</sub> vom Mt. Shahreru (Zaire) und aus dem Mayener Feld (Eifel) *Neues Jahrb Mineral Monatsh* 1983;1983: 49.
- [50] Kapralik I, Hanic F. Polymorphism and Solid-Solutions in System 2cao.Sio<sub>2</sub>-2cao.Na<sub>2</sub>o.P<sub>2</sub>o<sub>5</sub>. *Transactions and Journal of the British Ceramic Society* 1977;76: 126-33.
- [51] Qian JM, Kang YH, Wei ZL, Zhang W. Fabrication and characterization of biomorphic 45S5 bioglass scaffold from sugarcane. *Mater Sci Eng C-Biomimetic Supramol Syst* 2009;29: 1361-4.
- [52] Nychka JA, Mazur SLR, Kashyap S, Li D, Yang FQ. Dissolution of bioactive glasses: The effects of crystallinity coupled with stress. *Jom* 2009;61: 45-51.
- [53] Chen XF, Meng YC, Li YL, Zhao NR. Investigation on bio-mineralization of melt and sol-gel derived bioactive glasses. *Appl Surf Sci* 2008;255: 562-4.
- [54] Oki A, Parveen B, Hossain S, Adeniji S, Donahue H. Preparation and in vitro bioactivity of zinc containing sol-gel-derived bioglass materials. *J Biomed Mater Res Part A* 2004;69A: 216-21.

- [55] Nottingher I, Jones JR, Verrier S, Bisson I, Embanga P, Edwards P, Polak JM, Hench LL. Application of FTIR and Raman spectroscopy to characterisation of bioactive materials and living cells. *Spectr-Int J* 2003;17: 275-88.
- [56] Andrade AL, Valerio P, Goes AM, Leite MD, Domingues RZ. Influence of morphology on in vitro compatibility of bioactive glasses. *J Non-Cryst Solids* 2006;352: 3508-11.
- [57] Brown PW, Fulmer M. Kinetics of Hydroxyapatite Formation at Low-Temperature. *J Am Ceram Soc* 1991;74: 934-40.
- [58] Brown PW, Hocker N, Hoyle S. Variations in Solution Chemistry During the Low-Temperature Formation of Hydroxyapatite. *J Am Ceram Soc* 1991;74: 1848-54.
- [59] Murugan R, Ramakrishna S, Rao KP. Nanoporous hydroxy-carbonate apatite scaffold made of natural bone. *Mater Lett* 2006;60: 2844-7.
- [60] Xia W, Chang J. Preparation and characterization of nano-bioactive-glasses (NBG) by a quick alkali-mediated sol-gel method. *Mater Lett* 2007;61: 3251-3.
- [61] Chun YW, Webster TJ. The Role of Nanomedicine in Growing Tissues. *Ann Biomed Eng* 2009;37: 2034-47.